APPLICATIONS OF ORGANIZED MEDIA IN CHROMATOGRAPHY AND FLOW INJECTION ANALYSIS

BY

STEPHEN HOUGHTON BROOKS

A DISSERTATION PRESENTED TO THE GRADUATE SCHOOL
OF THE UNIVERSITY OF FLORIDA IN PARTIAL FULFILLMENT
OF THE REQUIREMENTS FOR THE DEGREE OF
DOCTOR OF PHILOSOPHY

UNIVERSITY OF FLORIDA

1988

This dissertation is dedicated to my grandfather,

Alvin Newman Dugar,

whose love and direction were such important factors

in the completion of this work.

Nemo vir magnus sine aliquo adflatu divino umquam fuit.

(No man was ever great without some portion of divine inspiration.)

Cicero

De Natura Deorum

Book ii, Chapter 66, Section 167

To Maruja:

There is much satisfaction in work well done;

praise is sweet;

but there can be no happiness equal to the joy

of finding a heart that understands.

Victor Robinson

William Godwin, The Truth Seeker

6 January, 1906

ACKNOWLEDGMENTS

There are so many people whom I need to thank for making this achievement possible. Most immediately, I wish to thank my mentor, John Gordon Dorsey, for his patience, direction, insight and exquisite taste in food and wine. They have all greatly contributed to my educational experience. My only regrets at the end of my tenure are that John still insists upon pledging his allegiance to that semblance of a baseball team which calls Fulton County Stadium its home and that despite substantial trial and error (certainly the trials have far outweighed the errors), he was unable to eclipse the NBS Depth Charge standard of 1985 points. I did, however, have the privilege of witnessing a 1948 (bringing to mind an ancient Chinese proverb) and certainly, MGK once again breathes a sigh of relief.

Professionally, I wish to thank Alain Berthod, María A. Hernández Torres, Dan Leff, Rick Williams and Barbara Kirsch for their contributions to this dissertation and wish them continued success in their lives (especially Maruja!). Thank you goes to my typist, Cindy Zimmerman, for her prompt and accurate preparation of this work. Special thanks go to Danny Coffman for his outstanding draftsmanship throughout the years.

I feel that this accomplishment would have been impossible without the guidance and contribution of Mr. Sibson, Mr. Parr, Mr. Boothby, Mr. Bolduc, Mr. Pinette, Mr. Thibault, Mr. Sharp,

Mr. Jackson, Mr. Weatherbie and the rest of the outstanding public high school teachers who provide the foundation for achievements such as this.

Special thanks are offered to the Dorsey group members, those associated with the Analytical Division, residents of the Thunderdome, Florida Pest Control, Dub Thomas, Stranger, Dorian Gray, Scarlet, the Purple Porpoise, the Gator Sports programs, Jack Hairston, Skeeter's flying biscuits, bouncing babies, warm winters, air conditioning, and Walt Disney for making my four years in Gainesville a thoroughly enjoyable experience.

Thanks go to Maruja for her love and support during these years. Thanks go to all the members of my family who were so instrumental in my continued perserverance, Gertrude Dugar, Bertha Brooks, Rich, Kathy, Aunt Betty, Uncle Bill and Aunt Mary.

In keeping with tradition, I have chosen to save the greatest thanks for last. I wish to thank my parents, Mr. and Mrs. Richard H. Brooks, for their tireless contribution to my health and welfare from day one until the present. In an everchanging world, all too often dominated by things beyond our control, it has always been uplifting to realize that there was the constancy of their love and support for me to lean on.

TABLE OF CONTENTS

LIST OF TABLES

LIST OF FIGURES

Abstract of Dissertation Presented to the Graduate School
of the University of Florida in Partial Fulfillment of the
Requirements for the Degree of Doctor of Philosophy

APPLICATIONS OF ORGANIZED MEDIA IN
CHROMATOGRAPHY AND FLOW INJECTION ANALYSIS

BY

STEPHEN HOUGHTON BROOKS

August, 1988

Chair: John G. Dorsey
Major Department: Chemistry

The precision, speed and instrumental simplicity of a flow injection analysis (FIA) system are combined with a gradient chamber and flow-through conductance and absorbance detection to produce a system for the rapid, accurate determination of the critical micelle concentrations (CMCs) of ionic and nonionic surfactants. The theoretical basis of the method is presented and the validity of the technique is verified by a determination of the CMC values for both ionic (CTAB, CTAC, SDS) and nonionic (Brij 35, Brij 56, Brij 99, Triton X-100) surfactants.

The application of surfactant solutions as carrier streams in flow injection analysis is examined. The reaction rates are determined for the base catalyzed hydrolysis of acetylsalicylic acid in aqueous, micellar and microemulsion solutions. The performance of an aqueous and microemulsion carrier stream is compared. The loss in

relative sensitivity when employing the microemulsion can be traced to the increased dispersion in the more viscous carrier stream.

Dispersion (D) is the most popular peak descriptor in FIA. Unfortunately, D yields no direct information describing peak shape and no information in the time domain. Using previously derived equations, we examine the second moment (variance) of FIA peaks and use this as a fundamental descriptor of the FIA response curves. Unlike dispersion, the second moment is shown to obey a linear relationship with respect to flow rate and to yield valuable information in the presence of a chemical reaction.

The effects of the addition of 3% medium chain length (propanol-hexanol) normal alcohols to SDS micellar mobile phases upon chromatographic efficiency (N) and solvent strength (ε^{o}) are investigated. The solutes examined indicate that n-butanol and n-pentanol are far superior as mobile phase additives with respect to both N and ε^{o} when compared to n-propanol. The validity of the pseudophase retention model of micellar liquid chromatography is addressed and is employed for a direct examination of changes in physicochemical properties (binding constants, partition coefficients) with variation of alcohol chain length. Application of the random walk model yields solute adsorption/desorption rate constants across the stationary phase-mobile phase interface and confirms that inefficient mass transfer across this interface is responsible for decreased efficiencies observed in micellar liquid chromatography.

CHAPTER I
INTRODUCTION

Surface Active Agents

A surface active agent or surfactant is an amphiphilic molecule, containing distinct hydrophobic and hydrophilic regions. When surfactant is present in a system, it adsorbs on surfaces or interfaces of the system. An interface is defined (Rosen, 1978) as a boundary between any two immiscible phases while a surface specifically refers to a boundary where one phase is gaseous, in most cases the gaseous phase is air. Interfacially adsorbed surfactants thus have the ability to change the free energies of surfaces and change the minimum work required to create or expand interfaces. Measurement of the surface tension of surfactant containing solutions allows the determination of the interfacial free energy per unit area of a system. Most commonly, the interfacial free energy of a system is decreased by the addition of surfactants.

Surfactants are generally classified as ionic or nonionic, according to the nature of the hydrophilic headgroup. In general the hydrophobic portion of the surfactant displays much less structural variation than the polar headgroup. However, the nonpolar tail may be a straight or branched alkyl chain, may contain unsaturated or aromatic portions and may include perfluorinated or polysiloxane groups (Rosen, 1978). Typically, the hydrophobic tail contains eight

to twenty hydrocarbon units in length. Shorter chain lengths are too soluble to display surface activity while chain lengths of greater than twenty carbon units are too insoluble for aqueous use. Table I provides a list of common surfactants categorized by charge type. Ionic surfactants can be further classified by headgroup as cationic, anionic or zwitterionic.

Cationic surfactants have the general formula $R_nX^+Y^-$, with R representing the hydrocarbon chain. Nitrogen containing surfactants ($R_nN^+Y^-$) are the most common cationic surfactants, due to their ease of preparation and long term stability. Cationic surfactants represented approximately 63% of the total 1985 U.S. output of 5.4 billion pounds (Chem. Eng. News, 1987).

The most common anionic surfactants are alkali or alkaline earth metal salts of carboxylic, phosphoric, sulfonic or sulfuric acids containing a saturated or unsaturated hydrocarbon moiety. These surfactants have the general formula $R_nX^-Y^+$ and are typically manufactured by the hydrolysis of fats followed by neutralization with a hydroxide to form the desired salt. Anionic surfactants accounted for 8% of the 1985 U.S. output (Chem. Eng. News, 1987). Zwitterionic surfactants contain both an anionic and a cationic group on the hydrocarbon chain. Depending upon the pH of the solution and the structure of the surfactant, the hydrophobic chain can possess anionic, cationic or neutral characteristics. The most common zwitterionic surfactants are members of the alkyl betaines and alkyl sultaines which have the general structures of $R_1N^+R_2CO_2^-$ and $R_1N^+R_2SO_3^-$, respectively.

Table I. Typical surfactants with their CMC values and aggregation numbers.

Surfactant[a]	CMC (mM)	Aggregation Number
Anionic		
Sodium dodecyl sulfate (SDS) $CH_3(CH_2)_{11}OSO_3^-Na^+$	8.1	62
Potassium perfluoroheptanoate $C_7F_{15}COO^-K^+$	30	b
Cationic		
Cetyltrimethylammonium bromide (CTAB) $CH_3(CH_2)_{15}N^+(CH_3)_3Br^-$	1.3	78
Cetylpyridinium chloride[c] $C_{16}H_{33}N^+C_5H_5Cl^-$	0.12	95
Nonionic		
Polyoxyethylene(6)dodecanol $CH_3(CH_2)_{11}(OCH_2CH_2)_6OH$	0.09	400
Polyoxyethylene(23)dodecanol (Brij 35) $CH_3(CH_2)_{11}(OCH_2CH_2)_{23}OH$	0.1	40
Zwitterionic		
N,N-dimethyl-N-(carboxymethyl)octyl-ammonium salt (Octylbetaine) $C_8H_{17}N^+(CH_3)_2CH_2COO^-$	250	24
N-dodecyl-N,N-dimethylammonium-3-propane-1-sulfonic acid (SB-12) $CH_3(CH_2)_{11}N^+(CH_2)_3SO_3^-$	3	55

[a] Values for aqueous solution at 25°C.

[b] Not available.

[c] In 0.0175 M NaCl.

Nonionic surfactants accounted for approximately 29% of the 1985 U.S. commercial output (Chem. Eng. News, 1987). The most common nonionic surfactants are polyoxyethylene and polyoxypropylene derivatives. In the commercial preparation of these polymeric surfactants (Garrett, 1972), typical reactants are an alcohol and ethylene oxide. The initial reaction of the alcohol with ethylene oxide produces a small amount of the monoether of glycol:

$$R \cdot OH + H_2C\overset{O}{}CH_2 \longrightarrow R \cdot O \cdot CH_2 \cdot CH_2 \cdot OH.$$

The resulting primary alcohol from this reaction has equivalent reactivity toward additional ethylene oxide as the original alcohol, R • OH. Therefore, as the reaction proceeds, some monoalkyl diglycol, monoalkyl triglycol, etc. will be produced. As a result, the final product contains a series of monoalkyl glycols; the proportion of each present is described by the Poisson distribution series. Variations in the chain length of the final surfactant product are minimized by the choice of pH, temperature and catalyst used to decrease the activation energy of the reaction but they cannot be completely eliminated. Therefore, the number of polyoxy-n-ene units for a given nonionic surfactant represents the most commonly occurring chain length and the physicochemical properties of the surfactant will vary by batch and manufacturer.

Micelles and Micellization

When small amounts of surfactant are added to a totally aqueous solution, the surfactant molecules are predominately present in the

unassociated monomeric form, although small concentrations of dimers, trimers, etc. may be present. As the concentration of surfactant in solution is increased, the individual surfactant monomers aggregate to form structures known as micelles (from the Latin micella meaning small bit). Micellization occurs over a narrow range of concentration known as the critical micelle concentration (CMC). The continued addition of surfactant to solution above the CMC results in the formation of additional micelles, with the amount of free surfactant monomer present in solution remaining approximately constant and equivalent to the CMC. Figure 1 shows the effect of changing surfactant concentration upon the concentration of monomer and micellar aggregates present in solution. Micellar aggregates are in dynamic equilibrium with the surrounding solution; individual monomers are exchanged with the bulk solution on the microsecond to millisecond time scale, while the entire micelle is exchanged on the order of milliseconds to seconds.

In aqueous solutions at surfactant concentrations slightly above the CMC and without additives present that have the ability to solubilize within the micelle, the ionic micelle is considered to be roughly spherical (Dill and Flory, 1981) in shape. Typically the structure is 2-6 nm in diameter and contains 60-100 individual surfactant monomers. As shown in Figure 2, the hydrophobic tails of the surfactant are directed toward the interior of the structure in an attempt to minimize contact with the surrounding aqueous solution. The microviscosity of the hydrocarbon core is greater than that in pure hydrocarbons. Surrounding the interior of the micelle is a

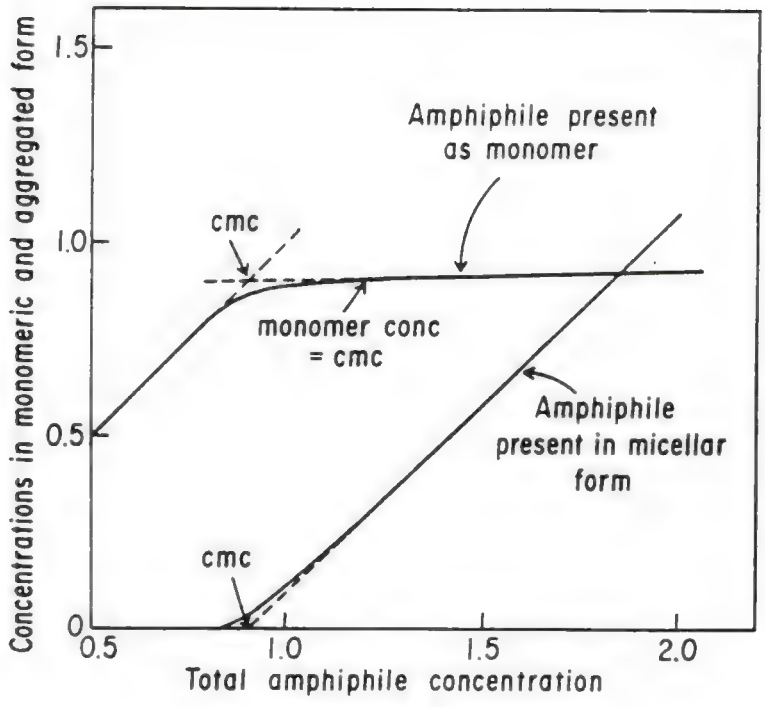

Figure 1. The relation between monomeric concentration in solution and total added concentration of surfactant with micelle formation. Dashed lines represent empirical procedures for determining the CMC; the point at which the monomer concentration is equal to the CMC is also shown (adapted from Tanford, 1980).

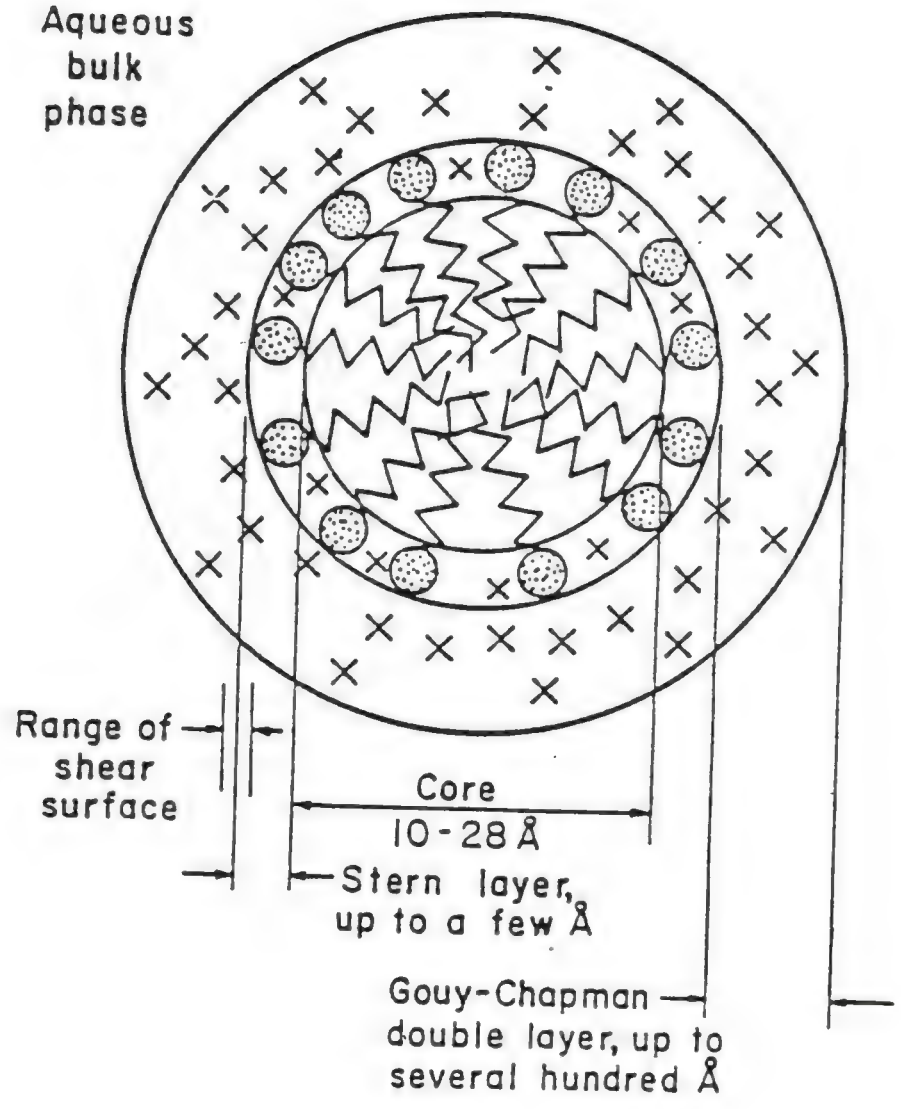

Figure 2. A two-dimensional representation of the regions of a spherical ionic micelle (adapted from Fendler and Fendler, 1975).

region several angstroms in width, the Stern layer, containing the polar headgroups, water and slightly more than one half of the counterions associated with the micelle (Rosen, 1978). The hydrocarbon chains do, however, have significant contact with the bulk solvent (Dill et al., 1984). The remainder of the counterions associated with the micelle are contained in the Gouy-Chapman portion of the electrical double layer which extends further into the bulk solution. The resulting structure can be viewed as a liquid-like hydrocarbon droplet in a pool of water.

There are three primary forces which control micellization of an ionic surfactant in aqueous solution. The hydrophobic effect or the hydrophobic repulsion between the hydrocarbon tails of the individual surfactant monomers and the surrounding aqueous medium is the dominant factor controlling micellization. The attainable size of the aggregate is limited by the charge repulsion between ionic headgroups located in the Stern layer. To a lesser degree, the micelle is stabilized by Van der Waals attraction between the alkyl chains within the structure.

At the onset of micellization, many bulk solution properties are significantly modified. Therefore, the CMC can be experimentally determined by monitoring a physicochemical property of the solution and noting the changes in that property as the concentration of the surfactant in solution is varied (Figure 3). A calibration curve of a physicochemical property vs. surfactant concentration commonly exhibits a change in slope at the CMC. Figure 4 illustrates such a

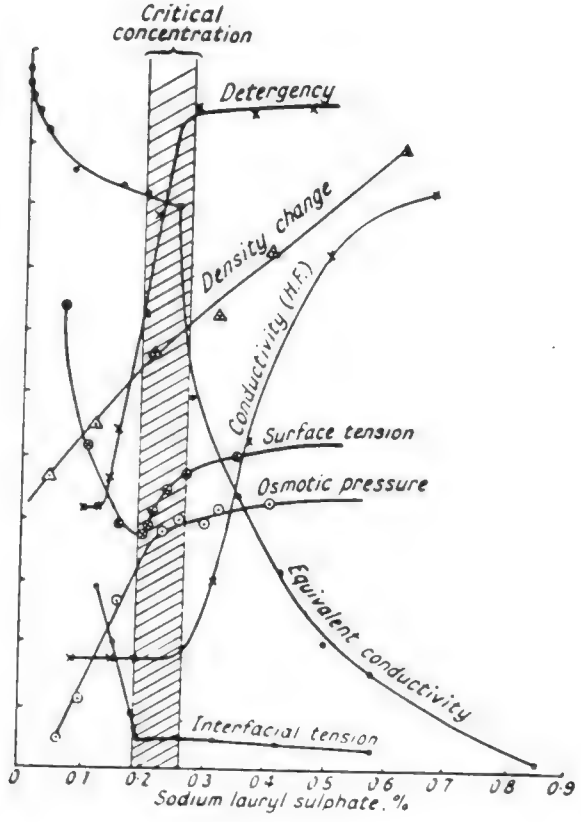

Figure 3. Changes in various physicochemical properties of an aqueous solution containing sodium dodecyl sulfate as the concentration of surfactant in solution is varied (adapted from Rosen, 1978).

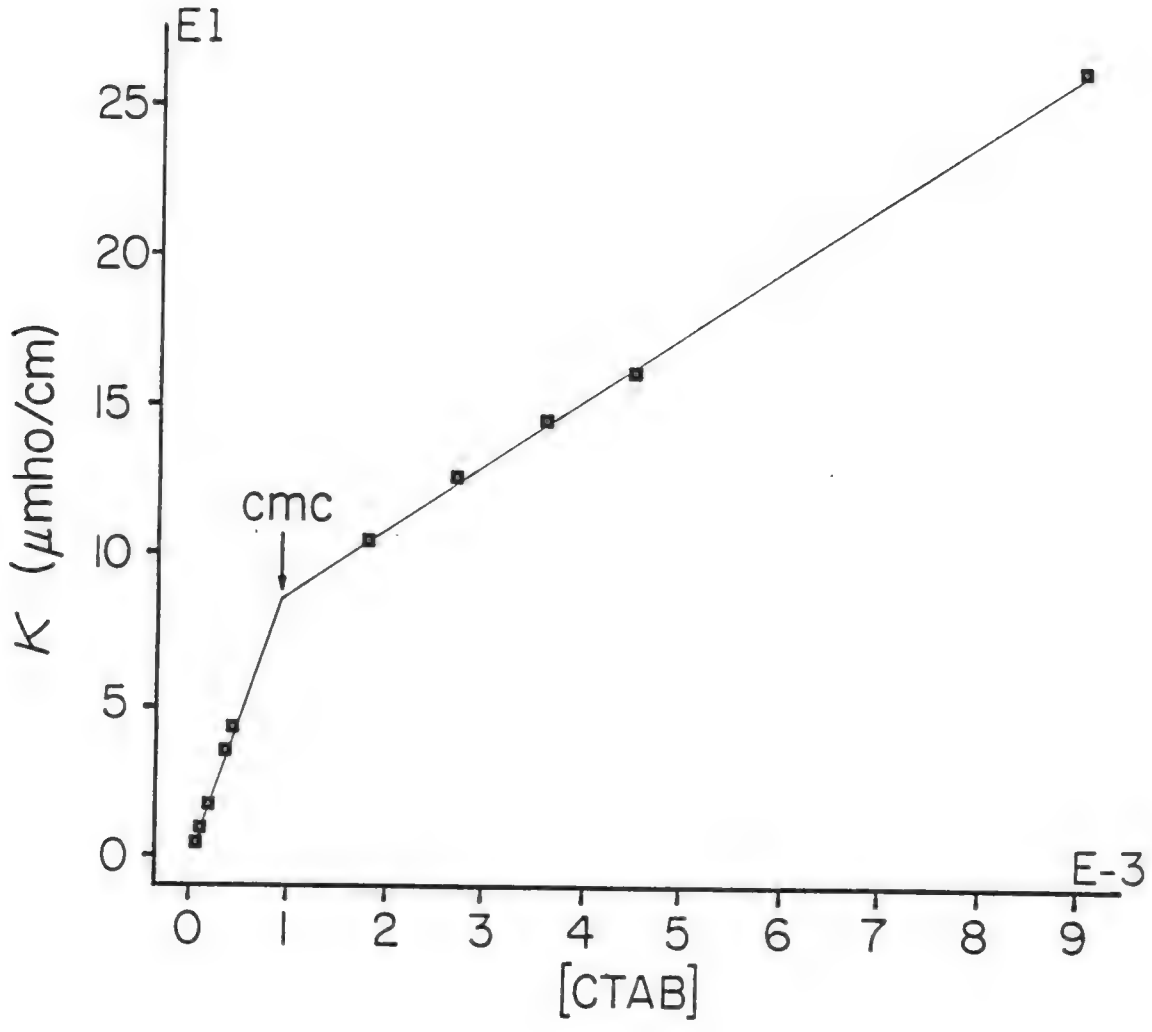

Figure 4. A calibration curve illustrating the change in slope of the conductance versus concentration curve observed at the CMC for hexadecyltrimethylammonium bromide (CTAB).

calibration curve for the determination of the CMC of hexadecyltrimethylammonium bromide in aqueous solution using conductance detection.

Changes in temperature, concentration of surfactant, additives in the bulk solution and structural groups in the surfactant may cause changes in the size, shape and aggregation number of the micelle (Berezin et al., 1973; Fisher and Oakenfull, 1977; Menger, 1979).

Analytical Applications of Surfactant Containing Solutions

Analytical applications of micellar solutions arise from the ability of the micelle to solubilize, compartmentalize and concentrate ions and molecules. The utility of micelles in analytical chemistry has been demonstrated in a variety of techniques including absorption and luminescence spectroscopy, electrochemistry and chromatography. Several reviews on the use of surfactants in analytical chemistry have appeared (Cline Love et al., 1984; Pelizzetti and Pramauro, 1985; McIntire, 1986).

Micellar aggregates have the ability to solubilize, in aqueous solution, compounds which are normally insoluble or slightly soluble. Table II shows a comparison of the solubility (Almgren et al., 1979) of some aromatic hydrocarbons in purely aqueous and aqueous micellar solutions. The observed increase in solubility can be a direct result of the hydrophobic interaction between the solute (possessing a certain degree of hydrophobic character) and the exposed hydrocarbon chains of the micelle and/or electrostatic interaction of the solute with the polar headgroups of the organized assembly.

Table II. Solubility data for arenes in water and micellar solutions.

Compound	Solubility (M)		
	Water	SDS (0.01-0.06 M)	CTAB (0.01-0.05 M)
Benzene	2.3×10^{-2}	2.5	12.3
Naphthalene	2.2×10^{-4}	0.38	1.11
Anthracene	2.2×10^{-7}	0.63×10^{-2}	3.3×10^{-2}
Pyrene	6×10^{-7}	7.0×10^{-2}	0.41

Data adapted from Almgren et al. (1979).

Solute partitioning to micelles is characterized by a partition coefficient analogous to any two-phase equilibrium. Micellar solubilization is a dynamic equilibrium process which is dependent upon temperature, nature of the solute, concentration of surfactant and the type of micellar aggregate under consideration (Berezin et al., 1973).

Micellar organization of ions and molecules on a molecular level increases the proximity of reagent(s) and analyte in solution. This may result in a modification of equilibria, acid-base and redox properties, reaction rates and chemical pathways. Additionally, micellar aggregates may change spectral distribution and/or intensities. In order to take full advantage of a micelle's ability to organize reactants it is desirable to have the species involved preferentially associate with the micelle over the bulk solvent. Using the example of accelerated reaction rates, this compartmentalization is most easily accomplished by the judicious choice of reactants which have hydrophobic character (resulting in partitioning to the micelle) and/or are electrostatically attracted to the polar headgroups of the aggregate. As a result of partitioning, the micelle concentrates the interacting species in a much reduced volume about the micelle, greatly increasing the local concentration of reactants and thus the rate of reaction.

Flow Injection Analysis

Flow injection analysis (FIA) is firmly established as a rapid, accurate, precise and versatile analytical technique. As an

indication of the growing acceptance and application of the technique, the number of FIA publications has increased exponentially (Ruzicka and Hansen, 1986) since its inception in 1975 with numerous reviews (Ruzicka and Hansen, 1978, 1986; Betteridge, 1978; Ruzicka, 1983) and several monographs (Ruzicka and Hansen, 1981; Ueno and Kina, 1983; Valcarcel and Luque de Castro, 1987) appearing.

Flow injection analysis (FIA) is based on the injection of a known, reproducible volume of a liquid sample into a moving, nonsegmented carrier stream (Ruzicka and Hansen, 1981). The injected sample forms a zone which disperses in a known, reproducible manner as it flows through the system toward eventual detection. The simplest FIA analyzer consists of a pump which propels the carrier stream, an injection port for the introduction of a precise, reproducible volume of sample and a reaction volume where the sample disperses as it advances toward a flow-through detector, producing a recorder response. The resulting FIA manifold requires no elaborate instrumentation and the strengths of the system include low cost, simplicity of operation, high sample throughput without carryover, compatibility with all conventional flow-through detectors and high precision stemming from the reproducibility of the sample injection and dispersion processes.

The major obstacle to be overcome in the development of FIA as an analytical technique was the prevention of intermixing between adjacent samples. Skeggs (1966) first introduced the concept of air segmentation in which adjacent samples were separated by air bubbles. Air segmented continuous flow analysis served as the basis

for the Technicon AutoAnalyzer, the most popular automatic analyzer ever marketed. Air segmentation, as a method to prevent sample carryover, has many drawbacks (Ruzicka and Hansen, 1981). Among the most deleterious are that the carrier stream has the tendency to pulsate, due to the compressibility of air; the air bubbles must be removed from the carrier stream prior to detection; control of the size of the air bubbles is necessary; and that the movement of the carrier cannot be instantaneously stopped or restarted (as in stopped-flow FIA methods). With the many disadvantages of segmented flow analysis as a driving force, the technique of FIA was developed by the simultaneous work of Ruzicka and Hansen (1975) in Denmark and Stewart, Beecher and Hare (1976) in the United States. The Danish group developed the nonsegmented technique by using instrumentation primarily associated with segmented flow analyzers while the Americans developed the technique employing instrumentation which is typically associated with high performance liquid chromatography (HPLC). As a result of this common historical background, the technique of flow injection analysis is often mistakenly considered as a hybrid of the two techniques.

The similarities between the two techniques are essentially limited to the instrumentation and certain operational parameters used for each method. Both techniques require the use of a pump, sample injection valve, flow-through detector and a chart recorder or data acquisition device. Additionally, injected sample volumes and flow rates in the two methods are of the same order of magnitude. This, however, is the extent of the similarities between the two techniques.

The general aim of HPLC is to separate several solutes which are present in the injected sample as it is introduced into the flowing system. The HPLC column contains two immiscible phases: the mobile phase which flows through the system and the stationary phase which consists of small diameter particles (3-20 μm) which fill the interior volume of the column. The HPLC pump typically operates at pressures in excess of 1000 psi, which is necessary to force the mobile phases through the interstitial volume of a tightly packed column. Separation of the solutes occurs due to differences in the concentration distribution coefficients (the ratio of the mole fractions of each solute in the two phases) between the various solutes. Due to the retention of solutes in a chromatographic system, the various chromatographic zones move at a velocity which is only a fraction of the mobile phase velocity.

In FIA, however, the general aim is to control the dispersion and the time allowed for a reaction to occur in the flow manifold, ensuring detectable levels of product while achieving maximum throughput (samples per hour) of the system. The peristaltic pump propels the carrier stream through short lengths (50-300 cm) of narrow, open teflon tubing (typically 0.5 mm id). Open tubing translates to low backpressure; therefore, the peristaltic pump typically operates at pressures well below 10 psi. The flow profile in FIA is essentially laminar, ensuring that the solute front moves at the same velocity as the carrier stream.

Flow injection analysis is classified as a method of continuous flow analysis, whereby the analyte concentration is continuously

monitored in a moving stream of liquid (or gas). Typically, one reactant is constantly pumped through a length of teflon tubing which constitutes the FIA reaction manifold. The other reactant is intercalated at one or more fixed points along the tubing by way of a sample injection valve. As the sample moves through the manifold toward eventual detection, it is dispersed and interacts with the carrier stream, resulting in dilution. As a result of the dispersion process, the concentration at the peak maximum is some fraction of the concentration of sample which was initially introduced into the manifold (Figure 5).

The dispersion coefficient, D, is the most common descriptor of dilution in an FIA system and is defined as the ratio of the concentration injected into the system to the concentration at peak maximum. Experimentally, the value of D is determined by introducing a standard sample of known concentration directly into the flow-through detector to obtain a steady-state response height, H_o. The FIA manifold is then operated with the carrier stream of choice and the standard is introduced into the continuously moving stream in the form of an injected sample. This ensures that the sample molecules will interact with the surrounding carrier stream, resulting in dilution of the sample and a subsequent peak height response, H_{max}. If the linear region of the calibration curve includes both C_o and C_{max} (the concentrations corresponding to H_o and H_{max}):

$$D = H_o/H_{max} \qquad \text{(eq. 1.1)}$$

Figure 5. The dispersion of a sample plug in an FIA system (adapted from Ruzicka, 1983).

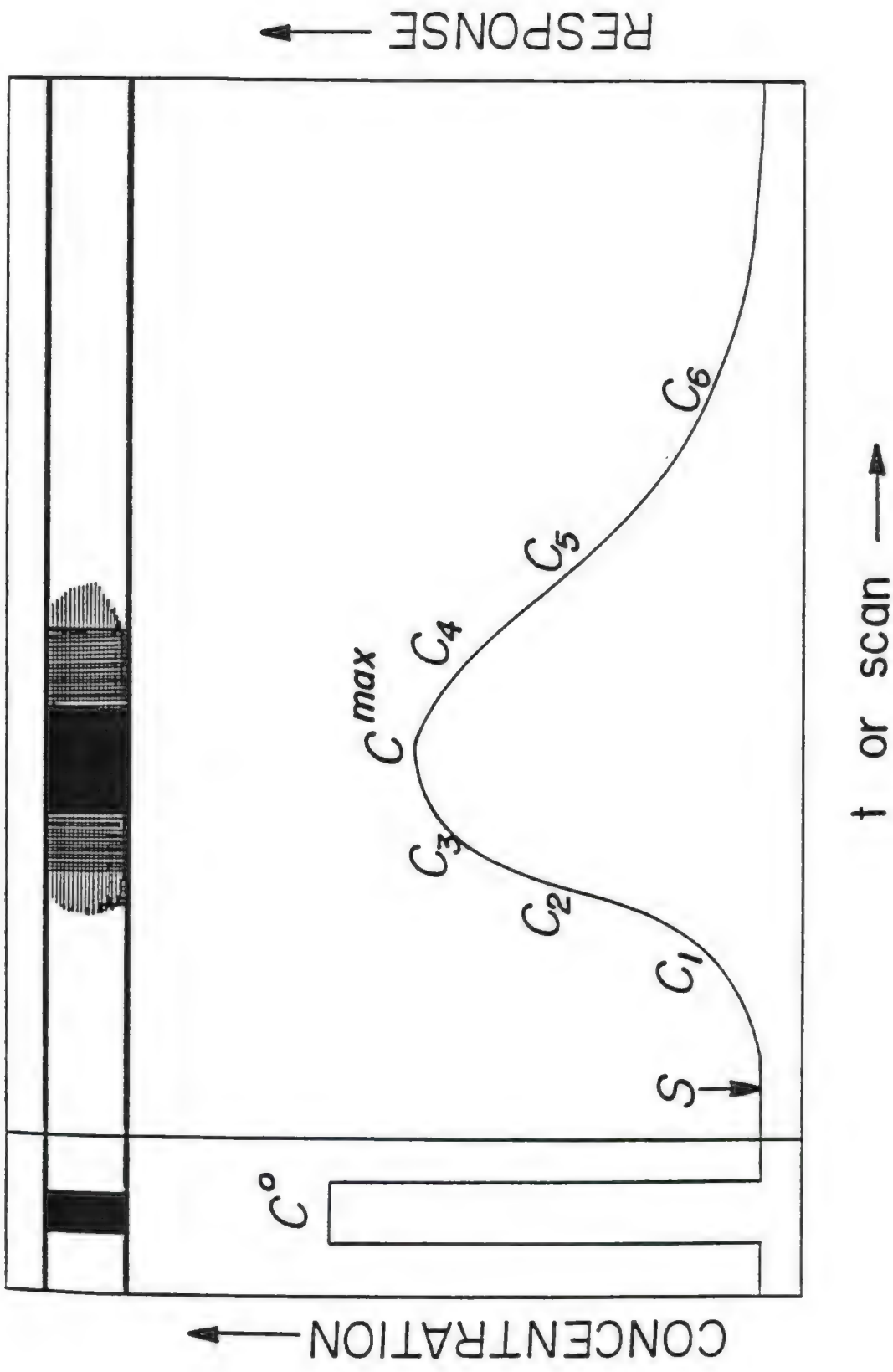
RESPONSE
CONCENTRATION
t or scan
C°
S
C1
C2
C3
C max
C4
C5
C6

and is equivalent to the dispersion of the flow injection manifold under investigation. Dispersion is generally classified as limited (D = 1-3), medium (D = 3-10) and large (D > 10) with the class of dispersion chosen being dependent upon the application. The concept of dispersion, however, is of limited utility in conveying information about the FIA system since it only accounts for dilution which affects peak height. In the presence of chemical reactions, the dispersion coefficient loses its significance, since it conveys little information related to peak width (an indication of the throughput of the system). Coiling of the tubing introduces additional mechanisms of transport which further obscure the significance of D and will be more fully considered in Chapter IV. Additionally, we will introduce an alternative measure of dispersion which gives direct information concerning the variance of the FIA peak and allows for the deconvolution of certain factors contributing to dispersion in an FIA manifold.

There are two mechanisms contributing to dispersion in an FIA system. The flow profile in FIA is essentially laminar in character (Van den Berg et al., 1980; Reijn et al., 1981b; Vanderslice et al., 1981), resulting in convective transport in the axial direction. For conditions of laminar flow, in a straight length of tubing, it is well known that molecules near the x axis (in the tube center) will move at a greater mean velocity than those at the tube wall. The velocity of any stream path, v_x, at any radial position, r_x, in a tube of radius r can be given by

$$v_x = 2v[1 - (r_x/r)^2], \qquad \text{(eq. 1.2)}$$

where v is the average flow velocity of the system;

$$v = [(P_i - P_o)r^2]/8\eta L, \qquad \text{(eq. 1.3)}$$

where P_i and P_o are the system inlet and outlet pressures, η is the viscosity (g/cm · s) of the solvent and L is the tube length in cm. Therefore, the molecules at the center of the tube will move at maximum velocity being equivalent to twice the mean velocity of the system. Theoretically, the molecules in direct contact with the tubing wall will be stationary. These flow characteristics will produce a parabolic velocity profile (Figure 6a). If laminar flow were the only factor contributing to dispersion in the system, a sample bolus introduced into the system would have an infinitely long tail (Figure 6b) resulting in carryover between adjacent samples and decreased throughput of the system. In addition to convective transport, however, there is diffusional transport in the system which is a result of concentration gradients in the convective transport regime (Figure 6c). Diffusional transport in the axial direction (Figure 6d) arises due to horizontal concentration gradients at the leading and trailing edges of the sample bolus and only minimally contributes to the overall dispersion in the system (Valcarcel and Luque de Castro, 1987). Diffusional transport in the radial direction arises from concentration gradients perpendicular to the flow vectors (Figure 6d). The overall effect of radial diffusion is that sample molecules at the tubing center diffuse toward the walls while sample

Figure 6. Velocity profiles, shape of injected sample bolus and types of transport in closed tubes: (a) laminar flow, parabolic velocity profile; (b) sample dispersion due to laminar flow without diffusion; (c) convective transport of sample molecules parallel to direction of flow; (d) diffusional transport in the axial and radial directions; (e) sample dispersion due to laminar flow with diffusion (adapted from Valcarcel and Luque de Castro, 1987).

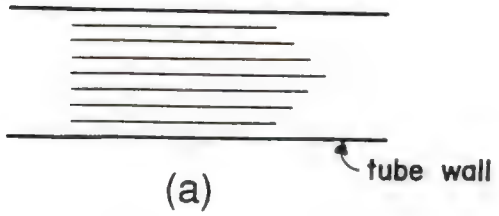

(a)

(b)

CONVECTIVE TRANSPORT

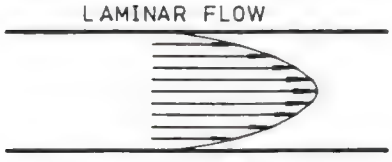

(c)

DIFFUSIONAL TRANSPORT

(d)

(e)

Velocity profiles and shapes of injected sample bolus

molecules near the walls diffuse toward the center of the tubing. In fact, this radial transport opposes convective transport in the axial direction, maintaining the integrity of the sample plug (Figure 6e). It is this radial diffusion, perpendicular to the direction of flow which eliminates the need for air bubbles in FIA, resulting in low carryover and cross contamination between adjacent samples.

Initially, application of FIA was amenable only to relative measurements with quantitation being dependent upon calibration with standards. The capability of the technique has now expanded to include absolute measurements of diffusion coefficients (Gerhardt and Adams, 1982, 1983; Betteridge et al., 1983; Vanderslice et al., 1984), solution viscosity (Betteridge and Ruzicka, 1976; Betteridge et al., 1981, 1983), reaction rates (Hungerford et al., 1985), acid constants (Fossey and Cantwell, 1985) and complex stability constants (Yoza et al., 1984a, 1984b).

Micellar Reversed Phase Liquid Chromatography

Armstrong and Henry (1980) first effectively demonstrated the use of aqueous micelles as the sole mobile phase modifier in a reversed phase liquid chromatographic system. The practical advantages of micellar mobile phases include enhanced selectivity, low cost and low toxicity when compared to typical hydro-organic mobile phases. While these benefits are certainly desirable qualities for any alternative chromatographic technique, they are not sufficiently great to cause the laboratory practitioner to abandon the time tested methods associated with hydro-organic mobile phases in HPLC. Expanded

application of micellar liquid chromatography (MLC) will result only if academic investigators continue to exploit the unique capabilities of MLC to perform separations which are not achievable with hydro-organic mobile phases. Several review articles (Armstrong, 1985; Dorsey, 1987; Khaledi, 1988) and a symposium series volume (Hinze and Armstrong, 1987) have recently appeared on the subject.

Micellar liquid chromatography incorporates secondary equilibria to adjust retention and selectivity in the chromatographic system. The "primary" equilibrium in a chromatographic system describes only the distribution of solute between the mobile phase and stationary phase. Additional equilibria which occur in the mobile phase, stationary phase or both are considered "secondary" in nature. As shown in Figure 7, the solute present in MLC partitions both to the hydrophobic environment of the micelle and to the hydrophobic stationary phase. Other examples of secondary equilibria include the use of acid-base equilibria and ion-pairing methods to provide unique chromatographic capabilities.

Potentially, MLC has a much greater range of applicability than other types of secondary equilibria. Any compound which partitions to the micelle is a candidate for micellar liquid chromatography. This includes all compounds with hydrophobic character which are preferentially solubilized in the hydrophobic environment of the micelle. Additionally, compounds which are electrostatically attracted to the surfactant polar headgroups within the micellar structure are potentially separable by MLC. As reversed phase is generally the method of choice for the separation of hydrophobic

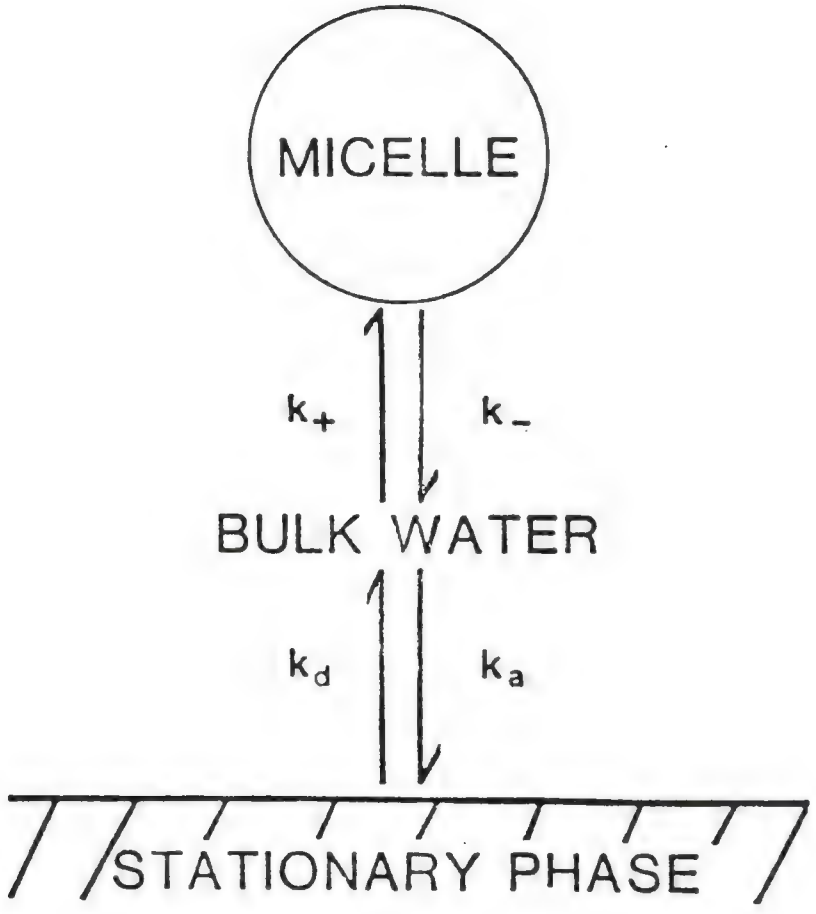

Figure 7. The two principal solute equilibria in a micellar chromatographic system, k_{+1} and k_-, are, respectively, the entrance and exit rate constants (s^{-1}) of the solute to and from the micelle; k_a and k_d are, respectively, the adsorption and desorption rate constants (s^{-1}) of the solute to and from the chromatographic stationary phase (adapted from Yarmchuk et al., 1984).

compounds, MLC has the potential to be applied to a large percentage of reversed phase separations.

The capacity factor, k, in MLC is defined (as for any chromatographic system) as the total amount of solute in phase X divided by the total amount of solute in phase Y. In chromatographic applications, the stationary phase is defined as phase X. The total amount of solute in a phase is defined as the concentration of solute in that phase times the volume of that phase. Arunyanart and Cline Love (1984) were the first to show that, by considering the two principal equilibria in MLC, the capacity factor could be given by

$$k = \frac{\phi[\text{solute in the stationary phase}]}{[\text{solute complexed with the micelle}] + [\text{solute in the bulk mobile phase}]}, \qquad \text{(eq. 1.4)}$$

where ϕ is the chromatographic phase ratio and is given by the ratio of the volume of the stationary phase to the volume of the mobile phase; [solute . . .] indicates the concentration of solute in the indicated phase. This expression serves as the basis for the pseudophase retention model which allows for the determination of valuable physicochemical information about the structure of micelles and the factors controlling efficiency in MLC. Further investigation of the applicability, validity and information yielded by the pseudophase retention model will be presented in Chapter V.

In secondary chemical equilibria separations, the strength and selectivity of the mobile phase are at least partially controlled by the concentration of the component affecting the secondary equilibrium. As previously mentioned and shown in Figure 1, the

amount of monomeric surfactant present above the critical micelle concentration in a micellar solution is approximately constant and equivalent to the CMC. Therefore, MLC provides the experimenter with the ability to change the strength of the mobile phase without changing the bulk solvent composition. It is this property of constant bulk mobile phase composition which results in many of the unique capabilities of micellar mobile phases.

Gradient elution chromatography is the most popular method for solving the general elution problem in HPLC. By increasing the strength of the mobile phase over the course of the separation, the highly retained compounds can be eluted more quickly and better detection limits resulting from sharper peaks can be achieved (Snyder, 1980; Quarry et al., 1986). The major disadvantage of the gradient elution technique is that during the course of the gradient, the stationary phase solvation structure undergoes significant modification. Therefore, the nature of the stationary phase at the completion of the gradient is different from the initial conditions. In order to perform a subsequent analysis, it is necessary to reequilibrate the chromatographic column with many column volumes of the initial mobile phase. As a result, the advantages gained in separation time due to the gradient program are often negated in terms of the total analysis time due to the time spent in the reequilibrium step. Quarry et al. (1984) have also shown that modification of the stationary phase composition leads to solvent demixing (preferential uptake of a mobile phase component) and variation in column dead time, further complicating the theoretical model of gradient elution.

The strength of the mobile phase in MLC is dependent upon the concentration of surfactant in solution. An increase in mobile phase surfactant concentration results in the formation of additional micellar aggregates but the amount of free monomeric surfactant in solution is approximately constant and equal to the CMC (Figure 1). The direct result of this is that a micellar concentration gradient may be used to speed the elution of strongly retained compounds without altering the structure of the stationary phase. Landy and Dorsey (1984) and Dorsey et al. (1984) have shown the constancy of the stationary phase structure from both the standpoint of consistent retention times for an early eluting compound and adsorption isotherms of SDS onto reversed phase materials. Berthod et al. (1986) also measured the adsorption isotherms of various cationic and ionic surfactants on five chromatographic stationary phases and reported a constant stationary phase composition with changing surfactant concentration above the CMC. It is clear that micellar mobile phases have the potential to greatly reduce analysis time and solvent consumption in gradient MLC techniques.

Micellar mobile phases also offer unique advantages for detection when compared to hydro-organic mobile phases. A majority of common surfactants possess fully saturated hydrocarbon tails, making them optically transparent at typical HPLC wavelengths of detection. Micelles have the capability to yield enhanced detectability stemming from their ability to organize solutes on a molecular level. This property has led to detection schemes employing micellar solutions to

enhance analytical fluorometry (Hinze et al., 1984) and micelle-stabilized room temperature phosphorescence (Cline Love et al., 1980, 1981; Skrilec et al., 1980). Khaledi and Dorsey (1985) have demonstrated improved gradient compatibility with amperometric electrochemical detection using micellar eluents.

The preceding discussion indicates that micellar liquid chromatography can provide unique chromatographic capabilities and that micellar mobile phases do offer solutions to problems which cannot be resolved by conventional means. Two major obstacles to the widespread acceptance of MLC are that the chromatographic efficiency and solvent strength achievable with aqueous micellar mobile phases are much less than those available with traditional hydro-organic mobile phases. In Chapter V, we will present experimental results examining the addition of low concentrations of normal alcohols to micellar mobile phases and subsequent effects upon efficiency and solvent strength in micellar liquid chromatography.

CHAPTER II
FLOW INJECTION ANALYSIS DETERMINATION OF CRITICAL MICELLE CONCENTRATIONS OF IONIC AND NONIONIC SURFACTANTS

Background

It has been sixty years since the initial observation (Ekwall, 1927) linking changes in surfactant concentration with changes in physicochemical properties of a solution. The concept of the critical micelle concentration (CMC) has arisen to describe the concentration range in which surfactant monomers assemble to form micelles. The CMC varies with the intensive parameters of the solution in which the micelle is formed. With ionic surfactants, it is observed that variations of temperature, pressure (to a lesser extent) and amount of electrolyte or nonelectrolyte added to a solution all influence the observed CMC. These variations in CMC values in response to changes in solution properties have proven useful both for the study of the driving forces of micellization and for allowing inferences about micelle shape and structure to be made. Therefore, when using surfactants, the experimenter finds it necessary to determine the CMC characteristic of the system which has been defined.

The value of the CMC is experimentally obtained by monitoring the change of a physicochemical property of the solution with changing surfactant concentration. Extrapolation of the responses obtained at high concentrations (above the CMC) and at low concentrations (below

the CMC) yields an intersection whose concentration is equivalent to the CMC. The intersection concentration obtained depends both upon the physicochemical property chosen to determine the CMC and the graphical method selected to represent the data. Numerous physicochemical properties have been monitored to determine the CMC. Measurements of surface tension, electrical conductance and spectral properties are among the most popular techniques employed. Mukerjee and Mysels (1971) address the reasons for methodical differences among CMC determinations.

A search of the literature for the past five years reveals that researchers have undertaken numerous projects in an attempt to develop novel methods for the determination of the CMC of surfactants in solution. The great majority of proposed determination methods rely upon spectrophotometric measurements of a probe molecule which has been introduced into a surfactant solution. Pyrene has been utilized as a fluorescence probe molecule (Kapoor et al., 1982; Ohyashiki and Mohri, 1983; Goddard et al., 1985) and numerous examples of dye incorporation to aid in the spectrophotometric determination of the CMC are found (Rosenthal and Koussaie, 1983; Kawashima et al., 1985; Panda and Behera, 1985). Interactions between aggregates of dye molecules and surfactant monomers can result in the formation of mixed micelles (Kali et al., 1980) at surfactant concentrations which are markedly below the true CMC (Robinson et al., 1973). The determination of mixed micelles includes the effect of the dye-surfactant interaction and does not yield an accurate determination of the CMC. The subject of dye-surfactant interactions has been recently

reviewed (Diaz Garcia and Sanz-Medel, 1986). Additionally, the CMC has been determined employing methods based upon kinetic dialysis (Lake, 1982), emulsion polymerization (Al-Shabib and Dunn, 1981), bubble pressure (Kretschemer et al., 1982), foaming power properties (Bazhenov et al., 1983) and calculations from electrical capacitance measurements (Deinega et al., 1983). The method proposed by Taylor and Nieman (1984) based upon conductance detection with exponential dilution flow circumvents the problem of repetitive measurement but the requirement for an in-house constructed, computer-controlled bipolar pulse conductance apparatus has served to limit the practical application of the technique. Other proposed CMC determination methods which will never receive widespread application due to their instrumentation-limited nature are those based on photon correlation spectroscopy (Roe and Barry, 1983) and an ultrasonic interferometric technique (Kabachnyi et al., 1982). It is concluded, therefore, that none of the above work effectively addresses the paramount problems with existing methods for CMC determination. The need to acquire many data points as a prerequisite for accurate extrapolation to the CMC requires both extensive solution preparation and repetitive measurements which exhaust both the material resources and the time of the experimenter.

Theoretical Study of Critical Micelle Concentration Determination by Flow Injection Analysis

The incorporation of a gradient chamber (Pardue and Fields, 1981a, 1981b; Pardue and Jager, 1986) as the reaction volume in FIA

produces an exponential concentration gradient as described by the tank-in-series model (Levenspiel, 1972). Here we summarize a theoretical model (Berthod et al., 1988) to explain the experimental results of this chapter and to allow optimization of experimental parameters. The present work includes (1) the set of equations representing the surfactant concentration evolution during an FIA run, (2) the conductimetric detection equations, (3) the equations representing the light absorption change observed with a micelle-solubilized dye and (4) theoretical curves illustrating the equations proposed which allow discussion of the feasibility of the method.

Surfactant Solutions in Flow Injection Analysis

The FIA manifold consisted of a pump which propelled the carrier stream at a constant flow rate, F, through a chromatographic injection valve and an exponential dilution chamber (volume V). A detector continuously monitored the output of the dilution chamber.

Injection. By using the injection valve, a volume, v_i, of micellar solution with a surfactant concentration, c_i, was injected into the flow stream with a step-concentration shape. After a delay time, t_o, corresponding to the sweeping time of the inevitable dead volume, the micellar solution reached the dilution chamber. During a time $t_i = v_i/F$, the surfactant concentration in the dilution chamber increased according to

$$dC = (c_i - C)Fdt/V \qquad \text{(eq. 2.1)}$$

in which C is the surfactant concentration, at time t, in the dilution

chamber (volume V). At $t = t_o$, $C = 0$, the integrated form of equation 2.1 is

$$C = c_i[1 - \exp(-(F/V) \times (t - t_o))]. \qquad \text{(eq. 2.2)}$$

The maximum concentration, C_{max}, was reached at time $t_o + t_i$; then

$$C_{max} = c_i[1 - \exp(-v_i/V)]. \qquad \text{(eq. 2.3)}$$

In all experiments $v_i \ll V$; then equation 2.3 can be approximated by

$$C_{max} = c_i v_i/V \qquad \text{(eq. 2.4)}$$

(Ruzicka and Hansen, 1981). For example, with a dilution chamber volume of 1 mL and an injected volume of 30 µL, equation 2.4 gives the concentration C_{max} with an error lower than 1.5%.

For this method of CMC determination, the C_{max} concentration must be higher than the CMC, which means the injected surfactant concentration must be higher than CMC × V/v_i. With an actual value of 35, for the ratio V/v_i, the injected surfactant concentration must be at least 50 times the CMC.

Dilution. After the injection step, dilution occurred. During a time dt, a volume, $dv = Fdt$, of pure carrier (without surfactant molecules) enters the chamber. The same volume, with a concentration, C, of surfactant molecules, exits the chamber. The mass-conservation equation is

$$VC(t + dt) = VC(t) - C(t)dv. \qquad \text{(eq. 2.5)}$$

By using a differential form, equation 2.5 is

$$VdC = -CFdt. \qquad \text{(eq. 2.6)}$$

With the boundary condition $C = C_{max}$ at $t = t_i + t_o$, the integrated form of equation 2.6 is

$$C = C_{max}\exp[-(F/V) \times (t - (t_i + t_o))]. \qquad \text{(eq. 2.7)}$$

If the concentration C is higher than the CMC, the micelle concentration, C_m, is C - CMC:

$$C_m = (c_i v_i/V)\exp[-(F/V) \times (t - (t_i + t_o))] - CMC. \qquad \text{(eq. 2.8)}$$

When $C_m = 0$, the CMC is reached, and the time t is t_{CMC}. Equation 2.8 gives

$$t_{CMC} = (V/F)\ln[(c_i v_i)/(CMC \times V)] + t_i + t_o. \qquad \text{(eq. 2.9)}$$

After the time t_{CMC} no more micelles are present in the dilution chamber. The monomeric surfactant concentration obeys equation 2.7 rewritten as

$$C = CMC \exp[(-F/V) \times (t - t_{CMC})]. \qquad \text{(eq. 2.10)}$$

This set of equations shows that it will be possible to determine the CMC of a surfactant, in only one run, if the micelle concentration can be monitored by the sensor.

The micelle concentration can be monitored by conductance measurements or by spectrophotometric measurements using a micelle-soluble dye.

Conductance Measurements

The conductivity, K, of an electrolytic solution depends on the electrolyte concentration and on the molar conductance Λ of the ions (Monk, 1961). The conductivity of a micellar solution is given by

$$K = \Lambda_s CMC + \Lambda_m \times (C - CMC) \qquad \text{(eq. 2.11)}$$

in which the subscripts s and m refer to surfactant monomers and micelles, respectively. The molar conductances are not constant; they obey the Onsager-Kohlrausch law,

$$\Lambda = \Lambda_o - BC^{1/2} \qquad \text{(eq. 2.12)}$$

in which Λ_o is the molar conductance at infinite dilution (C = 0) and B is a constant (Smedley, 1980). For example, at 25°C, the molar conductance of sodium dodecyl sulfate (SDS) was given to be 66.8 S cm^2 $mole^{-1}$ at CMC (8.2×10^{-3} mole $liter^{-1}$) and 72.5 S cm^2 $mole^{-1}$ at infinite dilution (Kay and Lee, 1986). The molar conductance of SDS in micellar form lies between 25 and 41 S cm^2 $mole^{-1}$ according to the method used (Kay and Lee, 1986). As a first approximation, we will assume that Λ_s and Λ_m are constant. So, by using equations 2.7, 2.8 and 2.11, the conductivity of solutions above the CMC is

$$K = \Lambda_m(c_i v_i/V) \times \exp[(-F/V) \times (t - (t_i + t_o))] + (\Lambda_s - \Lambda_m) \times CMC \qquad \text{(eq. 2.13)}$$

and, with equations 2.10 and 2.11, the conductivity of solutions below

the CMC is

$$K = \Lambda_s CMC \exp[(-F/V) \times (t - t_{CMC})]. \qquad \text{(eq. 2.14)}$$

The conductimetric detector will produce two exponential decays according to equations 2.13 and 2.14.

Spectrophotometric Measurements

The use of a dye, whose absorbance is modified by the presence of micelles, to determine surfactant CMCs, has been known for many years (Corrin and Harkins, 1947) and is still currently used (Rosenthal and Koussaie, 1983; Berthod and Georges, 1985). When a hydrophobic dye is dissolved in the hydrophobic core of a micelle, its absorption spectrum is often modified (bathochromic effect). By recording the absorbance of the dye in the mobile phase at a well-chosen wavelength, it will be possible to determine the CMC of a surfactant.

Care must be taken when choosing the dye because it has been pointed out that dyes could modify the CMC of ionic surfactants (Berthod and Georges, 1985). Premicellar aggregates can form with ionic dyes and surfactant molecules that greatly lower the observed CMC (Sato et al., 1983). This problem is minimized with nonionic surfactants, but still exists (Nemoto and Funahashi, 1981a, 1981b).

There are two possible ways to obtain the CMC of a surfactant: (i) the dye is dissolved in the mobile phase and a concentrated solution of the studied surfactant is injected in the colored mobile phase, or (ii) the mobile phase is pure water and a concentrated solution of the surfactant, in which the dye has been solubilized, is

injected, the dye being used as a micelle tracer. Both cases are studied theoretically.

Monitoring of spectral changes. The affinity of a dye for the micellar phase can be quantified by using a partition coefficient, P, that is the ratio of the dye concentration in the micellar phase, D_m, in moles per volume of micellar phase, over the dye concentration in the aqueous phase, D_a, in moles per volume of aqueous phase

$$P = D_m/D_a. \qquad \text{(eq. 2.15)}$$

Introducing $\overline{V}$, the molar volume of the surfactant in micellar form, one finds that the product $C_m\overline{V}$ is the volume fraction of the micellar phase and $1 - C_m\overline{V}$ is the volume fraction of the aqueous phase. The dye concentration, D, in the mobile phase is

$$D = D_a(1 - C_m\overline{V}) + (D_m C_m\overline{V}). \qquad \text{(eq. 2.16)}$$

From equations 2.15 and 2.16, we derived

$$D_a = D/(1 - C_m\overline{V} + PC_m\overline{V}) \qquad \text{(eq. 2.17)}$$

and

$$D_m = DP/(1 - C_m\overline{V} + PC_m\overline{V}). \qquad \text{(eq. 2.18)}$$

When micelles are present in the dilution chamber, the measured absorbance, A, is, using equations 2.16-2.18,

$$A = [D \times (A_m PC_m\overline{V} + A_a(1 - C_m\overline{V}))]/$$

$$(1 - C_m\overline{V} + PC_m\overline{V}). \qquad \text{(eq. 2.19)}$$

The symbols A_m and A_a represent the absorptivity of the dye solubilized in micelles or in aqueous phase, respectively.

After t_{CMC}, no micelles are present in the dilution chamber, and the absorbance, A, is

$$A = DA_a. \qquad \text{(eq. 2.20)}$$

To ensure that the dye concentration is constant during the FIA analysis, it is necessary to inject a concentrated surfactant solution containing the dye at the same concentration, D, as that in the mobile phase. That is not very convenient. If the injected solution does not contain the dye, it is easy to derive the equations of the time-dependent dye concentration, D(t). During the injection time ($t_o < t < t_o + t_i$), the dye concentration decreases according to

$$D(t) = D \exp[(-F/V) \times (t - t_o)]. \qquad \text{(eq. 2.21)}$$

The minimum of the dye concentration is reached at time $t_o + t_i$. As already expressed, the ratio v_i/V is small, and the approximation used in equations 2.3 and 2.4 is valid. With a dilution chamber of 1 mL and an injected volume of 30 µL, the minimum of the dye concentration is 97% of the initial dye concentration. After time $t_i + t_o$, the dye concentration increases according to

$$D(t) = (D(t_o + t_i) - D) \times \exp[(-F/V) \times (t - (t_o - t_i))]. \qquad \text{(eq. 2.22)}$$

Although these dye concentration variations are negligible, equations 2.21 and 2.22 were used in the computer program generating the theoretical spectrophotometric data.

Illustration of the Theoretical Models

Conductimetric detection. Figure 8 shows the curves obtained by using equations 2.2, 2.7, 2.10, 2.13 and 2.14 and the numerical values listed in Table III, which correspond to SDS surfactant. The effect of a time constant of 1, 2, 4 and 8 s is illustrated by Figure 9. A break, corresponding to t_{CMC}, is observed on the conductance curve, which allows calculation of the CMC value if the injected volume and concentration are known (equations 2.9 and 2.23). The time constant introduces an error to the t_{CMC} determination: the longer the time constant, the higher the error in the t_{CMC} determination.

We have experimentally verified the effect of variation in the time constant on the CMC value determined using equation 2.24 by varying the flow rate from 0.46-13 mL/min. Figure 10 shows that the error in the CMC determined for CTAB (CMC = 0.92-0.98 mM, see Table VII) increases as the flow rate in the system is increased (higher time constant). Results of this study also indicate that the CMC value calculated is approximately constant from 0.42-2.0 mL/min, verifying that the flow rates used for the CMC determinations in this work (1.00±0.05 mL/min) are valid.

Spectrophotometric measurements. Figure 8 shows the curves obtained by using equations 2.19 and 2.20 with the numerical values listed in Table III. Figures 11 and 12 show the theoretical curves obtained with different time constants. In both cases, the dye was in the mobile phase or the dye was previously solubilized in the injected micellar solution; the CMC determination will not be possible with a

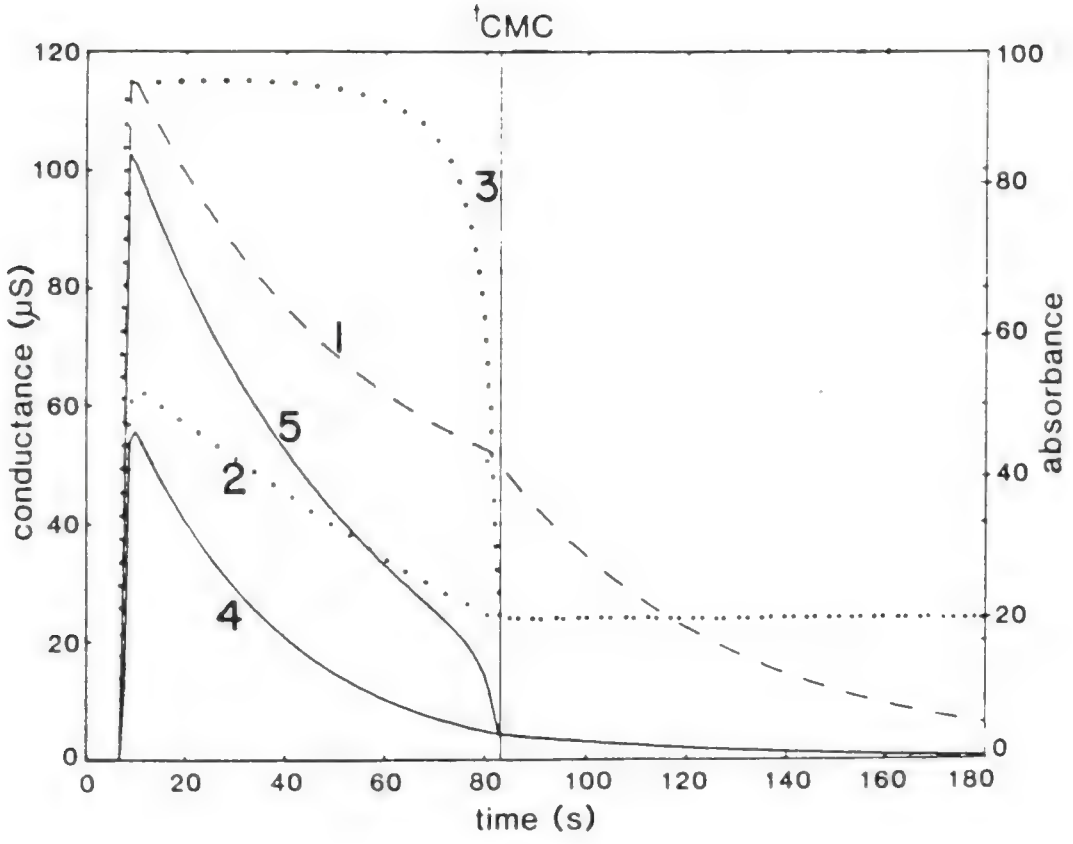

Figure 8. Theoretical curves obtained for SDS: (1) conductimetric detection (equations 2.13 and 2.14); (2 and 3) spectroscopic measurements with a dye in the carrier stream, P = 100 and 10,000, respectively (equations 2.19 and 2.20); (4 and 5) spectroscopic measurements with the dye dissolved in the injected micellar solution, P = 100 and 10,000, respectively (equations 2.7, 2.19 and 2.20). Numerical values are listed in Table III.

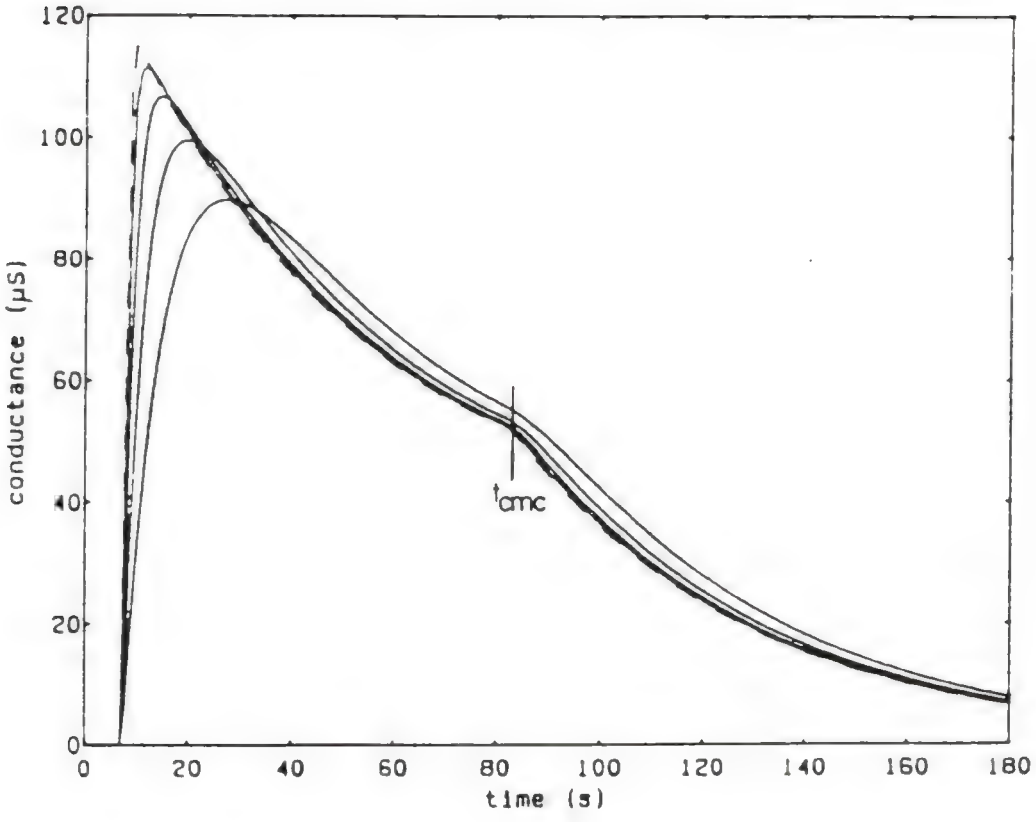

Figure 9. Theoretical conductimetric curves obtained with different time constants. Time constants: dashed line = 0 s; full lines = 1, 2, 4 and 8 s.

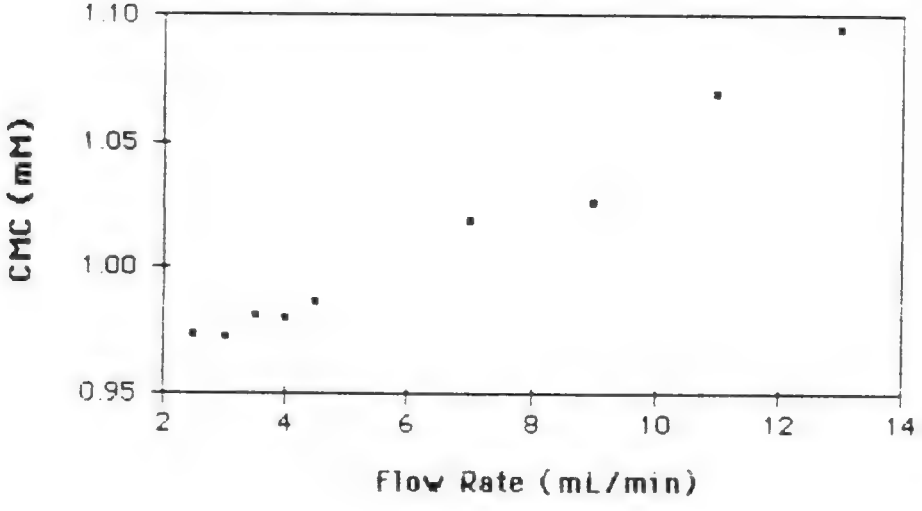

Figure 10. Variation of the determined CMC of CTAB (using equation 2.24) with flow rate.

Table III. Numerical value of the parameters used to draw the curves of Figures 8, 9, 11 and 12.

Parameter	Symbol	Value	Unit
Dye absorptivity in water	A_a	2×10^6	Absorb. unit mole^{-1} liter
Dye absorptivity in micelles	A_m	10^7	Absorb. unit mole^{-1} liter
Injected concentration	c_i	1	moles liter^{-1}
CMC of SDS	CMC	8.2×10^{-3}	moles liter^{-1}
Dye concentration in the carrier stream	D	10^{-5}	moles liter^{-1}
Dye concentration in the injected solution	D_i	2.5×10^{-4}	moles liter^{-1}
Flow rate	F	0.98 16.27	mL min^{-1} µL s^{-1}
Dye partition coefficient	P	100 and 10,000	Dimensionless
Dead time	t_o	7.4	s
Injection time	t_i	1.8	s
CMC time	t_{CMC}	81.3	s
Dilution chamber volume	V	765	µL
Injected volume	v_i	30	µL
SDS molar volume	$\bar{V}$	0.246	liters mole^{-1}
Dead volume	--	120	µL
Monomer molar conductivity	Λ_s	6.38×10^{-2}	S mole^{-1} liter cm^{-1}
Micellar molar conductivity	Λ_m	2.01×10^{-2}	S mole^{-1} liter cm^{-1}

Note: These parameters correspond to our setup and to SDS surfactant.

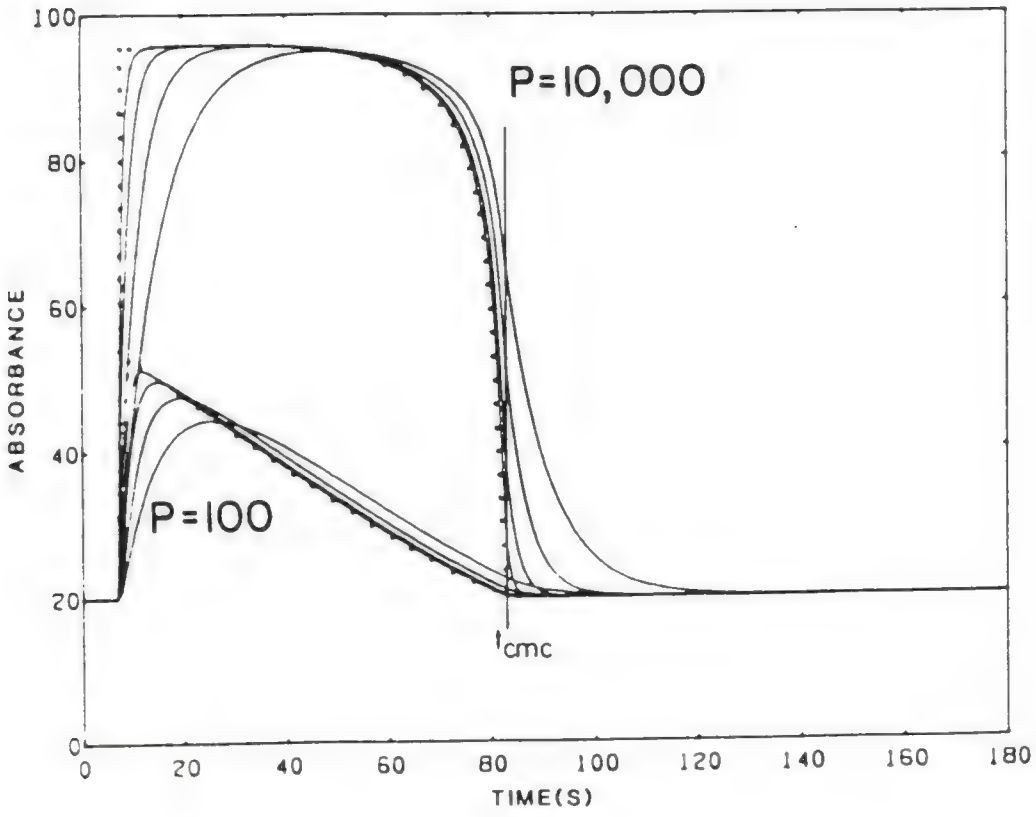

Figure 11. Theoretical absorbance curves with the dye solubilized in the carrier stream with partition coefficients equal to 100 and 10,000. Time constants: dotted line = 0 s; full lines = 1, 2, 4 and 8 s.

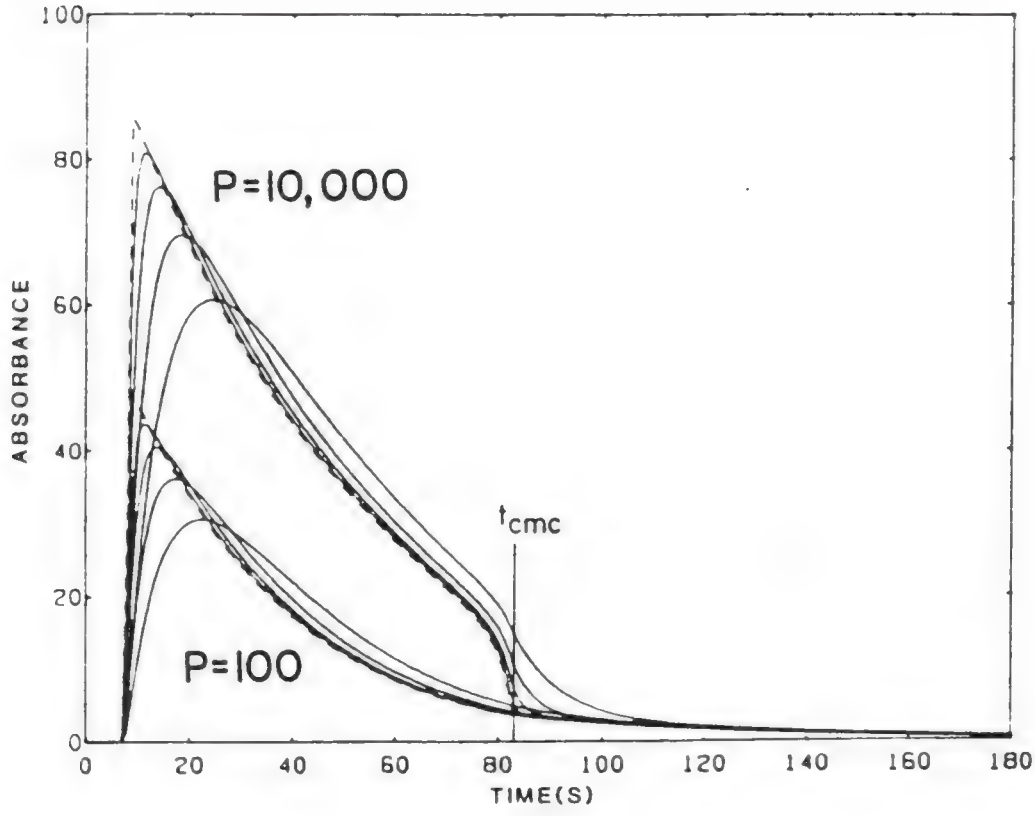

Figure 12. Theoretical absorbance curves with the dye solubilized in the injected surfactant solution. Time constants: dashed line = 0 s; full lines = 1, 2, 4 and 8 s.

partition coefficient equal to or lower than 100. With partition coefficient values of 10,000 or higher, the CMC determination seems possible by determining t_{CMC} at the inflection point of the experimental curves (Figures 11 and 12) and using equation 2.23, as long as the time constant is lower than approximately 4 s. For partition coefficient values lying between 100 and 10,000, the CMC determination should be possible if the spectrum of the dye is greatly modified by the micelle solubilization (Figures 15 and 16). To give one an idea of typical values in SDS micellar solution, the partition coefficients of methyl red, bromphenol blue and neutral red are 8,000, 5,000 and 28,000, respectively (Berthod and Georges, 1985).

Experimental Section

The following work then experimentally verifies the findings of the preceding theoretical treatment of CMC determinations by FIA and associated detection. It has been shown previously (Baxter-Hammond et al., 1980) that a conductance vs. concentration curve for exponentially diluted surfactants displays a change in slope at the CMC. Knowledge of the time at which this change in slope occurs yields the CMC through equation 2.23 given below. The validity of the presented method for ionic surfactants is verified by a determination of CMC values for the following surfactants: hexadecyl-trimethylammonium bromide (CTAB), hexadecyltrimethylammonium chloride (CTAC) and sodium dodecyl sulfate (SDS). Figure 13 shows the molecular formulas of the ionic surfactants investigated in the present work.

IONIC SURFACTANTS

Anionic

SDS : $C_{12}H_{25}OSO_3^-\ Na^+$

Cationic

TTAB : $C_{14}H_{29}N^+Br^-(CH_3)_3$

CTAB : $C_{16}H_{33}N^+Br^-(CH_3)_3$

CTAC : $C_{16}H_{33}N^+Cl^-(CH_3)_3$

Figure 13. Ionic surfactants (with molecular formulas) under investigation.

The absorbance spectrum of many dyes exhibits a shift in the presence of micelles, and for many years this has been exploited to determine the CMC of surfactant solutions (Corrin and Harkins, 1947). Coomassie Brilliant Blue G 250 (CBBG) has had several applications as a micelle-tracer for the determination of CMCs (Rosenthal and Koussaie, 1983; Samsonoff et al., 1985). The use of CBBG, however, requires the preparation of an acidic dye solution (Bradford, 1976), introducing compounds into solution which may potentially modify the CMC. Coomassie Brilliant Blue R 250 (CBBR) is the dye selected for the present work (Figure 14). This dye requires no pretreatment and is dissolved directly in the aqueous carrier stream at a concentration of 1.3×10^{-5} M. Additionally, in nonionic micellar solutions, the wavelength of maximum absorbance of the dye is red-shifted by ca. 50 nm, regardless of surfactant. Figures 15 and 16 show the bathochromic shift of CBBR when present in the micellar environment of Brij 35 and Triton X-100, respectively. The application of the present technique to nonionic surfactants is introduced with the determination of CMC values for Brij 35, Brij 56, Brij 99 and Triton X-100 (Figure 17).

Apparatus

A block diagram of the FIA manifold employed for the present work is shown in Figure 18. An Isco (Lincoln, NE) Tris model peristaltic pump propelled the aqueous carrier stream. Samples were introduced by a Rheodyne (Cotati, CA) model 7125 sample injection valve. All connecting tubing was teflon (1/16" od, 0.5 mm id) supplied by the Anspec Co., Inc. (Ann Arbor, MI). The gradient chamber was machined

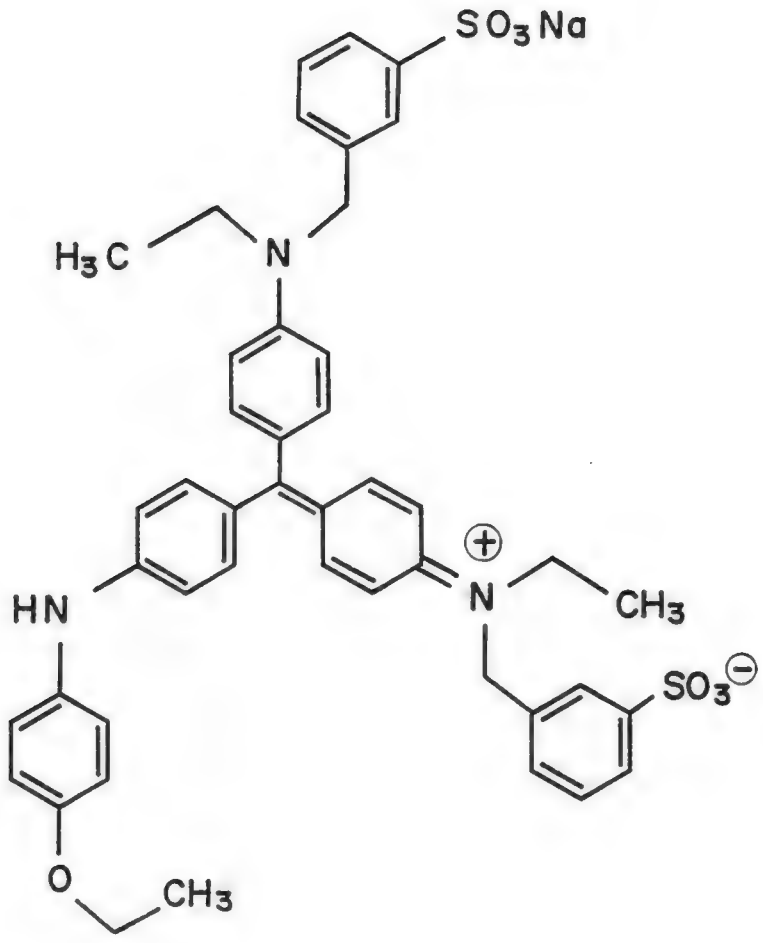

Coomassie Brilliant Blue R 250

MW = 826.0 g/mol

[6104-59-2]

Figure 14. Structural formula of Coomassie Brilliant Blue R 250 (CBBR).

Figure 15. Visible spectra of 4.34×10^{-5} M CBBR in (A) aqueous and (B) 2.5×10^{-3} M Brij 35 solution.

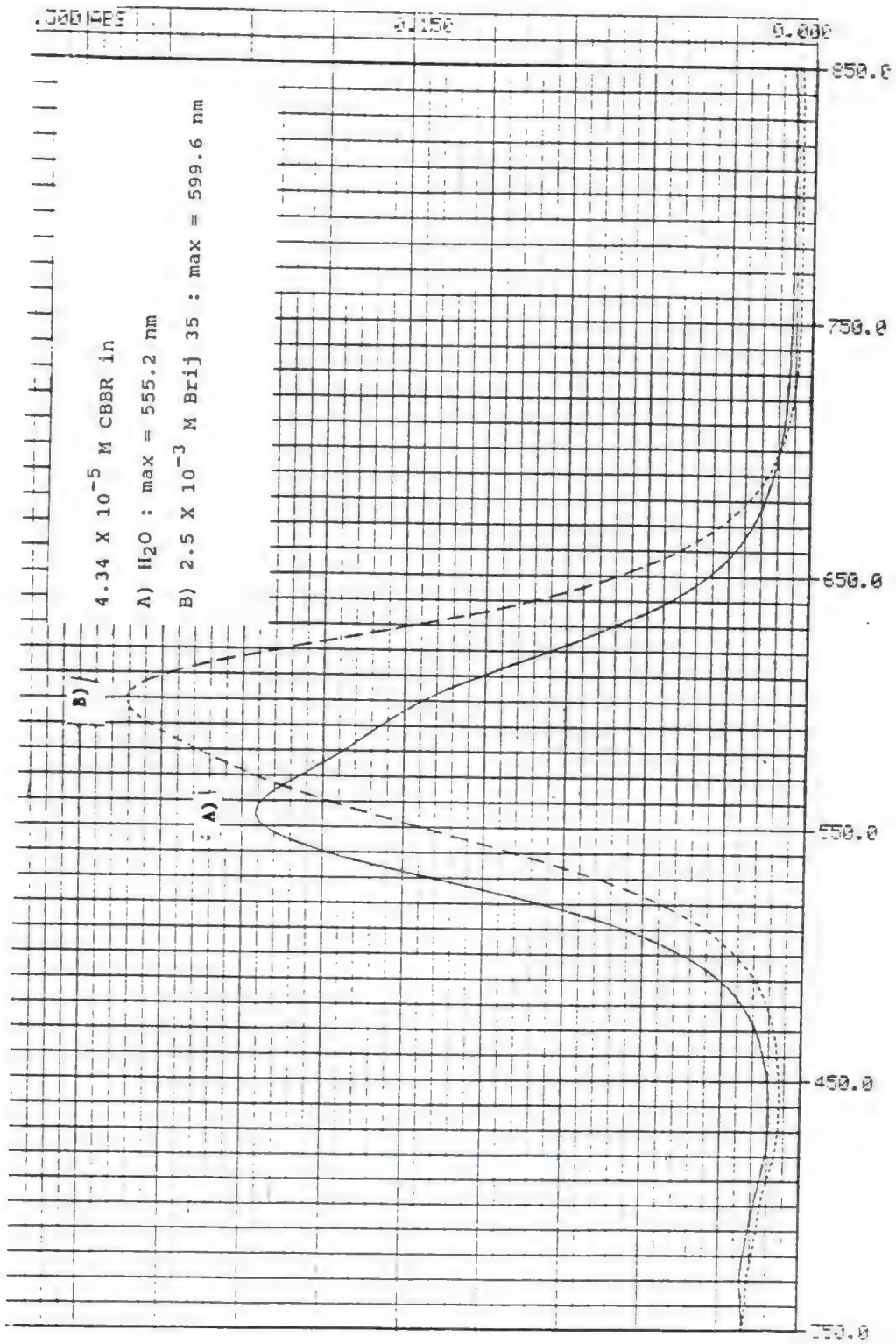
4.34 X 10⁻⁵ M CBBR in
A) H2O : max = 555.2 nm
B) 2.5 X 10⁻³ M Brij 35 : max = 599.6 nm
A)
B)
850.0
750.0
650.0
550.0
450.0

Figure 16. Visible spectra of 4.57×10^{-5} M CBBR in (A) aqueous and (B) 4.2×10^{-3} M Triton X-100 solution.

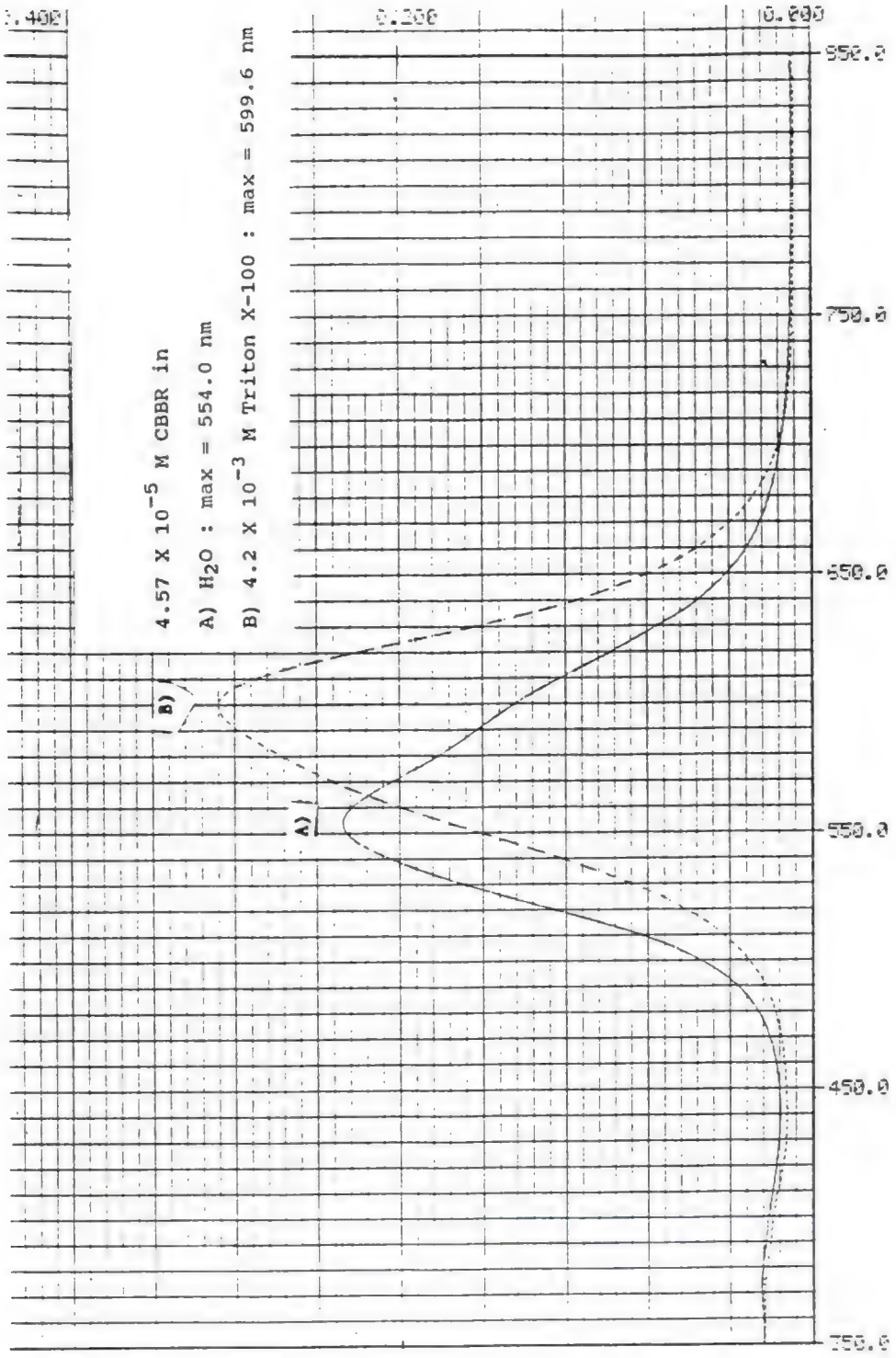
4.57 X 10⁻⁵ M CBBR in
A) H2O : max = 554.0 nm
B) 4.2 X 10⁻³ M Triton X-100 : max = 599.6 nm
B)
A)
550.0
650.0
750.0
450.0

NONIONIC SURFACTANTS

Triton X-100: C_8H_{17} 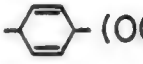 $(OCH_2CH_2)_{9.5}OH$

Brij 35 : $C_{12}H_{25}(OCH_2CH_2)_{23}OH$

Brij 56 : $C_{16}H_{33}(OCH_2CH_2)_{10}OH$

Brij 99 : $C_{18}H_{37}(OCH_2CH_2)_{20}OH$

Figure 17. Nonionic surfactants (with molecular formulas) under investigation.

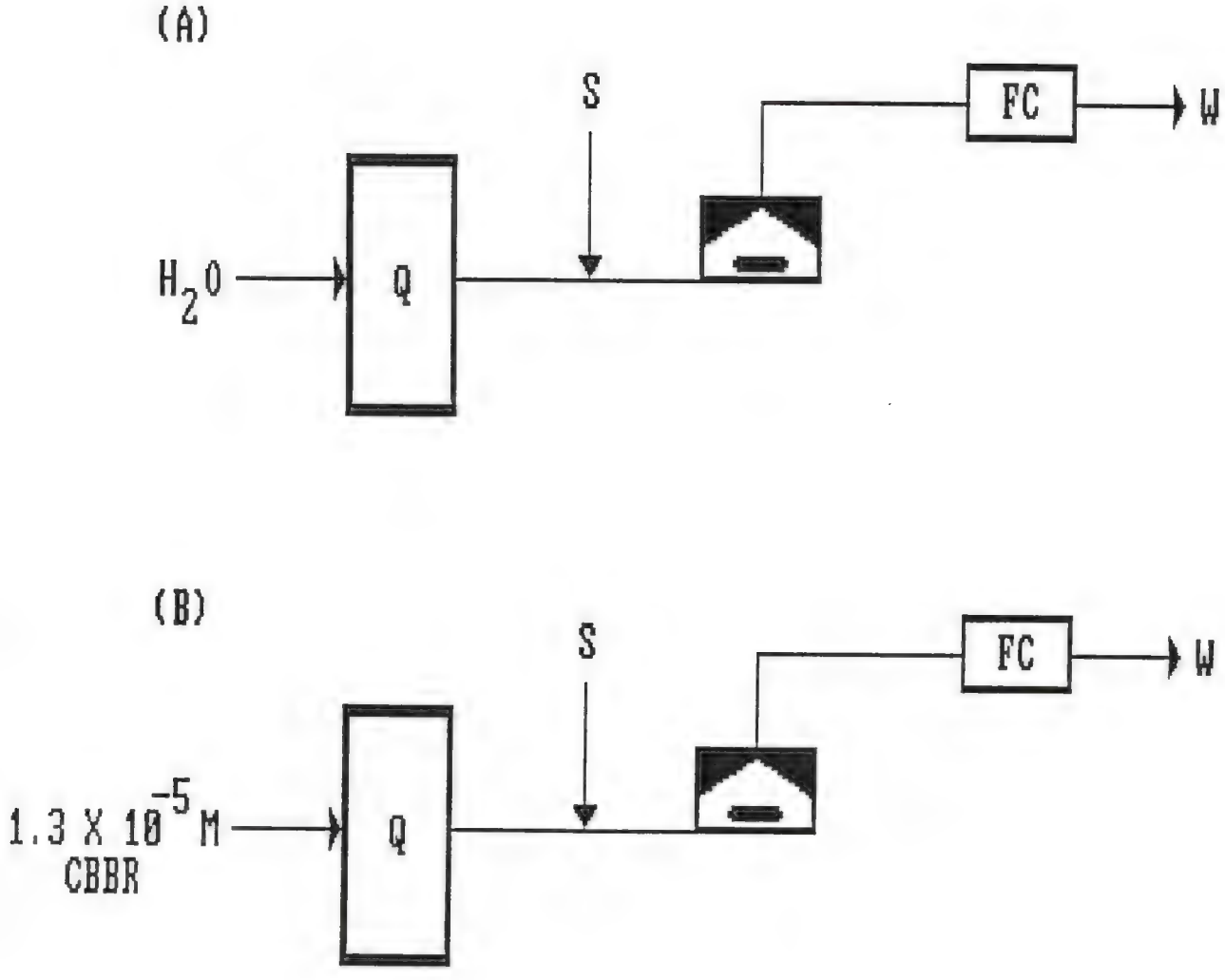

Figure 18. (A) FIA manifold for the determination of the CMC of ionic surfactants and (B) the analogous FIA manifold for the determination of the CMC of nonionic surfactants with CBBR dissolved in the carrier stream. Symbols: Q = flow rate of aqueous carrier stream (mL/min), S = sample injection, FC = flow-through detector cell, and W = waste.

from stainless steel, consisting of two parts (Figure 19). The lower portion is circular (0.478 in. id) and contains a 2 mm × 7 mm teflon covered magnetic stirring bar (Anspec). The upper part has a dome-shaped inner cavity designed to avoid entrapment of air. The upper and lower portions are held together by six equally spaced screws. A teflon O-ring is placed between the upper and lower parts and the screws are tightened, creating a leak-free seal. A hole drilled at the base of the lower chamber accommodates the teflon tubing which carries the incoming solution. To avoid leakage from this connection, a larger hole may be drilled and threaded to accommodate a 1/16" male nut into the assembly. A hole drilled in the center of the upper part provides the outlet for the solution and the teflon tubing may be push-fitted at this connection. The chamber was placed on a Precision Scientific (Chicago, IL) Mag-Mix model magnetic stirrer and mixing was found to be equally effective in the range of 60-240 rpm. The ionic surfactants were directly detected by an LDC/Milton Roy (Riviera Beach, FL) conductoMonitor III conductivity detector. In the determination of the nonionic surfactants, the absorbance of the dissolved dye in the carrier stream was monitored at 599.6 nm by a Kratos (Ramsey, NJ) Spectroflow 757 absorbance detector. The resulting output signals were recorded on a Fisher Recordall Series 5000 recorder. All least squares calculations were performed by Interactive Microware, Inc. (State College, PA) Curve Fitter program run on an Apple II Plus microcomputer.

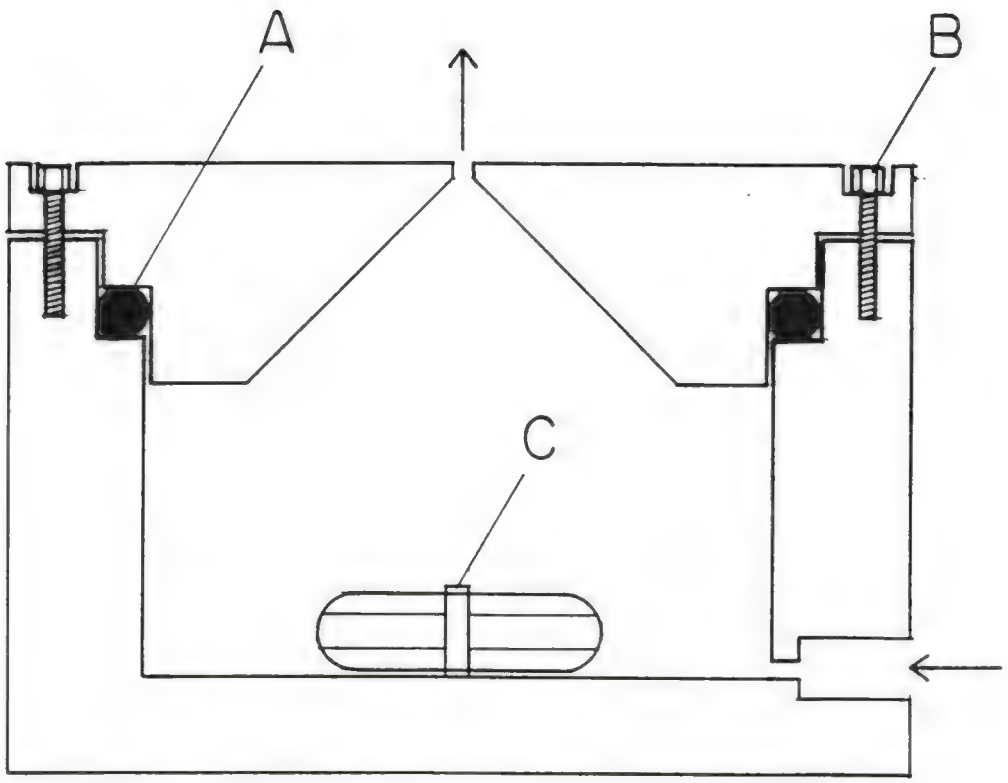

Figure 19. Gradient chamber with arrows indicating the carrier stream direction of flow: (A) teflon O-ring, (B) connecting screw, and (C) magnetic stirring bar.

Chemicals

Brij 35 (polyoxyethylene 10 cetyl ether, m.w. 680), Brij 99 (polyoxyethylene 20 oleyl ether, m.w. 1150), Coomassie Brilliant Blue R 250 (C.I. 42660, m.w. 826) were from Sigma Chemical (St. Louis, MO); purum grade CTAB (cetyl trimethylammonium bromide, m.w. 364.5) and SDS (sodium dodecyl sulfate, m.w. 288.3) were from Fluka Chemical (Hauppauge, NY); Triton X-100 (polyoxyethylene 11 p-octyl benzyl ether, m.w. 690) and Eriochrome Black T (C.I. 14645, Mordant black 11) were from Fisher Scientific (Fairlawn, NJ); Brij 25 (polyoxyethylene 23 dodecyl ether, m.w. 1200) was from Aldrich Chemical (Milwaukee, WI); reagent grade CTAC (cetyl trimethylammonium chloride, m.w. 320) was from Eastman Kodak (Rochester, NY); methyl red sodium salt (C.I. 13020, m.w. 301) was from Matheson, Coleman and Bell (Norwood, OH); ethylene glycol and sodium chloride were from Mallinkrodt (St. Louis, MO); TTAB (tetradecyltrimethylammonium bromide, m.w. 336.4) was from Chemical Dynamics Corporation (South Plainfield, NJ). All were used as received. Water used for the preparation of solutions and the carrier streams was deionized.

Procedure

Initially, a concentrated surfactant solution (approx. 100X the CMC) of known concentration must be prepared. A known volume of this standard solution is then injected via a fully loaded sample loop (see "Practical Considerations") such that the post-dispersion peak height is a minimum of 2 times the CMC of the surfactant. This initial injection is performed to determine the response height equivalent to the CMC. Visual inspection of the resulting response curve recorded

at 1 cm/min yields the response height equivalent to the CMC. With ionic surfactants, this response is recognized by noting an abrupt change in curvature on the descending edge of the response curve which occurs at the intersection of the micellar and monomeric exponential response gradients as shown in Figure 20. When employing a dye as a micelle-tracer, the response height equivalent to the CMC is defined by the inflection point of the response curve as shown in Figures 11 and 21.

Having determined the response height equivalent to the CMC, a second injection is performed with the detector response being monitored at a chart speed of 10-20 cm/min in an effort to provide greater time resolution. The value obtained (at a chart speed of 1 cm/min) for the response height equivalent to the CMC is then transposed to the response curve obtained at 10-20 cm/min in order to accurately determine the postinjection time at which the concentration of surfactant is equivalent to the CMC.

Knowledge of the time at which the concentration of the injected surfactant solution is equal to the CMC allows the experimenter to determine the CMC through

$$CMC = (c_i v_i)/V \exp[-(F/V)(t_{CMC} - t_o - t_i)] \qquad \text{(eq. 2.23)}$$

where c_i is the molar concentration of the injected solution (mol/L),

v_i is the volume (μL) of the injected solution,

V is the volume (μL) of the gradient chamber,

F is the flow rate (μL/s),

Figure 20. Detector response to the injection of an ionic surfactant (CTAB) recorded at a chart speed of (A) 1 cm/min and (B) 10 cm/min. The abrupt change in curvature in (A) allows for determination of the response height equivalent to the CMC (R_{cmc}) by visual inspection. The error intervals included represent t_{cmc} plus and minus 3 s.

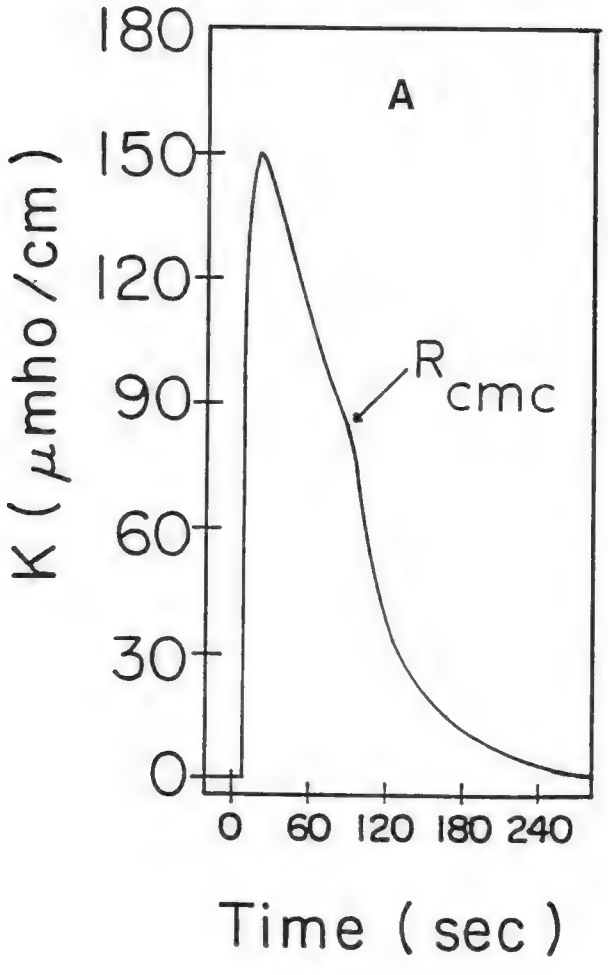
180
150
120
90
60
30
0
A
K (μmho/cm)
R_{cmc}
0
60
120
180
240
Time (sec)

Figure 20--continued.

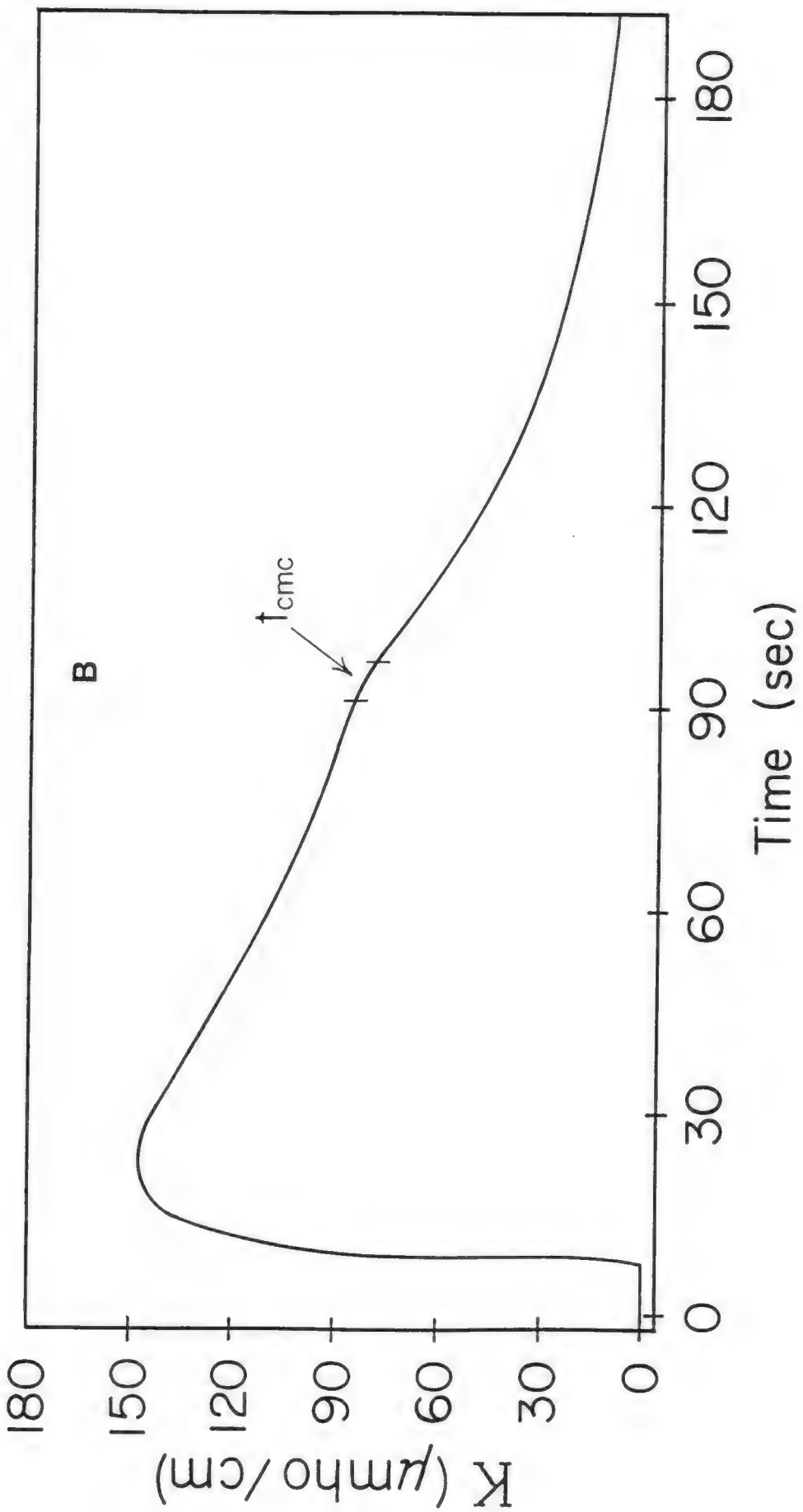
B
t_{cmc}
K (μmho/cm)
Time (sec)
0
30
60
90
120
150
180

Figure 21. Detector response to the injection of a nonionic surfactant (Triton X-100) into an aqueous carrier stream containing Coomassie Brilliant Blue R 250 (1.3×10^{-5}). The inflection point on the descending portion of the curve allows determination of the response height equivalent to the CMC (R_{cmc}) by visual inspection. The error intervals included represent t_{cmc}^{cmc} plus and minus 5 s.

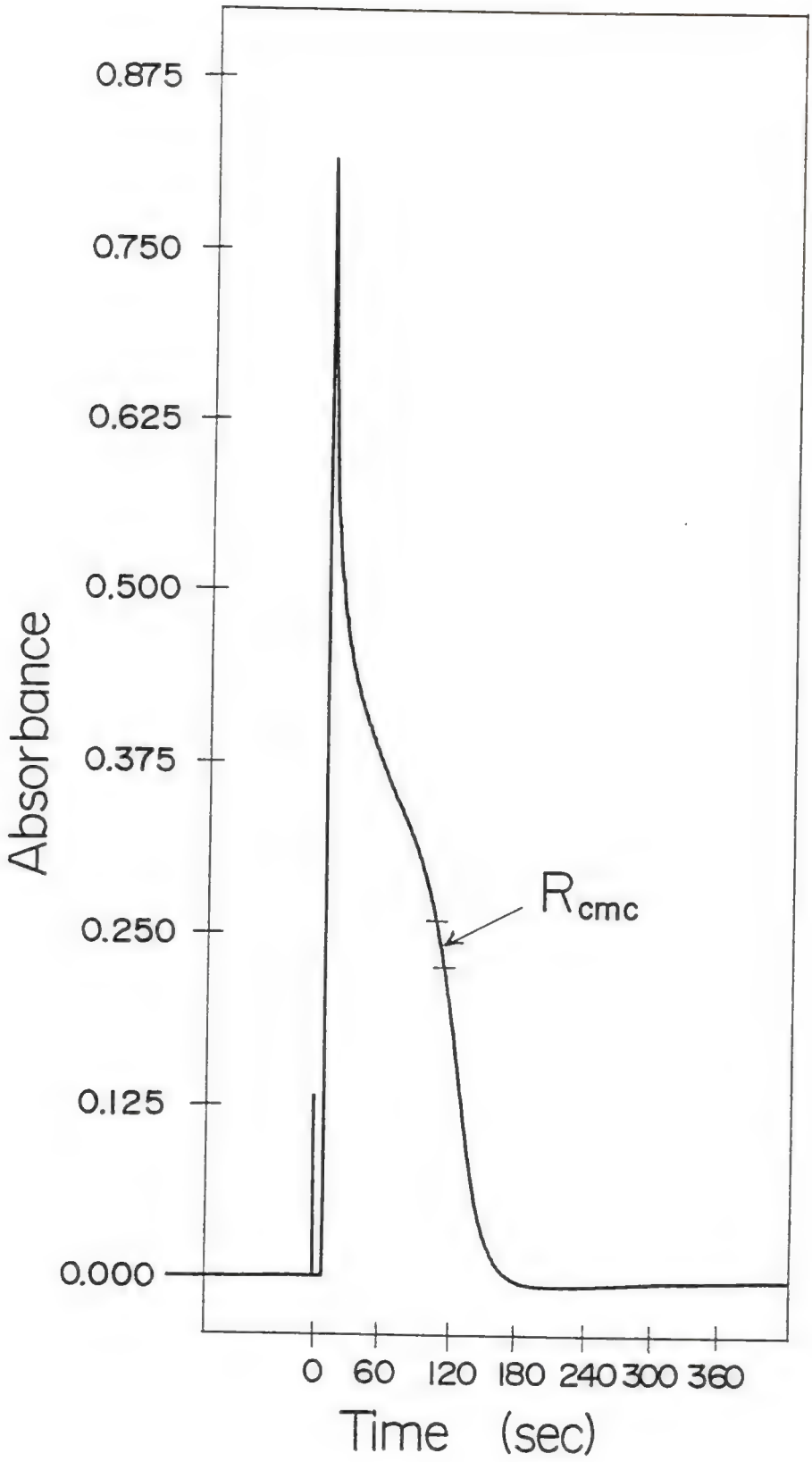
0.875
0.750
0.625
0.500
0.375
0.250
0.125
0.000
Absorbance
R_{cmc}
0
60
120
180
240
300
360
Time (sec)

t_{CMC} is the time (s) on the response gradient which corresponds to the concentration at the CMC,

t_o is the experimentally determined time between injection and the initial appearance of the peak, and

t_i is the theoretical time of the sample injection process (Berthod et al., 1988).

This time, t_i, during which the surfactant concentration increases in the gradient chamber as a result of the sample injection process is equal to v_i/F. Once the experimenter has defined the constant parameters of the system (C, c_i and v_i), it is only necessary to perform two injections and to measure the flow rate (using a buret located at the outlet of the manifold) to determine the CMC of surfactant solutions. The total time necessary for the determination of CMCs of either ionic or nonionic surfactant solutions is less than 30 minutes and requires a minimal amount of both solution preparation and surfactant, greatly conserving the material and personal resources of the experimenter.

Results and Discussion

Considerations for Practical Operation

When attempting to design, characterize and effectively operate an FIA system for the determination of CMCs of surfactant solutions there are certain guidelines which should be adhered to in order to ensure the accuracy and precision of the determination.

Exponential character. The exponential character of the system was verified by the injection and subsequent absorbance detection of a

20 µL sample of 2.61×10^{-3} M Eriochrome Black T solution. A plot (Figure 22) of log Absorbance vs. time (s) yielded a straight line (average $r^2 = 0.998$ for 4 trials). A 50 µL sample volume (maximum syringe capacity) of 11.72 mM NaCl solution was then injected to investigate the effects of increased sample volume on the exponential response gradient. An exponential least squares treatment of the plot of response vs. time again yielded a straight line ($r^2 = 0.999$), verifying the exponential character of the concentration gradient produced by the mixing chamber for the range of sample volumes employed.

Solutions of high surfactant concentration (e.g. >100X the CMC) possess a viscosity which greatly exceeds that of solutions with concentrations of the same order of magnitude as the CMC. Thus, the effect of variations in the viscosity on the exponential character of the gradient chamber was examined. The desired viscosities were provided by varying the weight percentage of ethylene glycol from 0 to 48% in aqueous solutions of NaCl. This varied the relative viscosity (CRC Handbook of Chemistry and Physics, 1980a) of the solution from 1.00 to 3.54 (versus water at 20°C), adequately spanning the range of viscosities encountered when employing this method (Figure 23). A Q-test examining the exponential least squares slopes of a plot of log conductance vs. time showed no statistical difference in the slopes from 0-48% ethylene glycol, verifying that the viscosity of the injected solute has no effect on the exponential concentration gradient (Table IV). For comparison purposes, the average efflux time

Figure 22. Verification of the exponential character of the FIA manifold by injection of 2.61×10^{-3} M Eriochrome Black T with 437 nm detection.

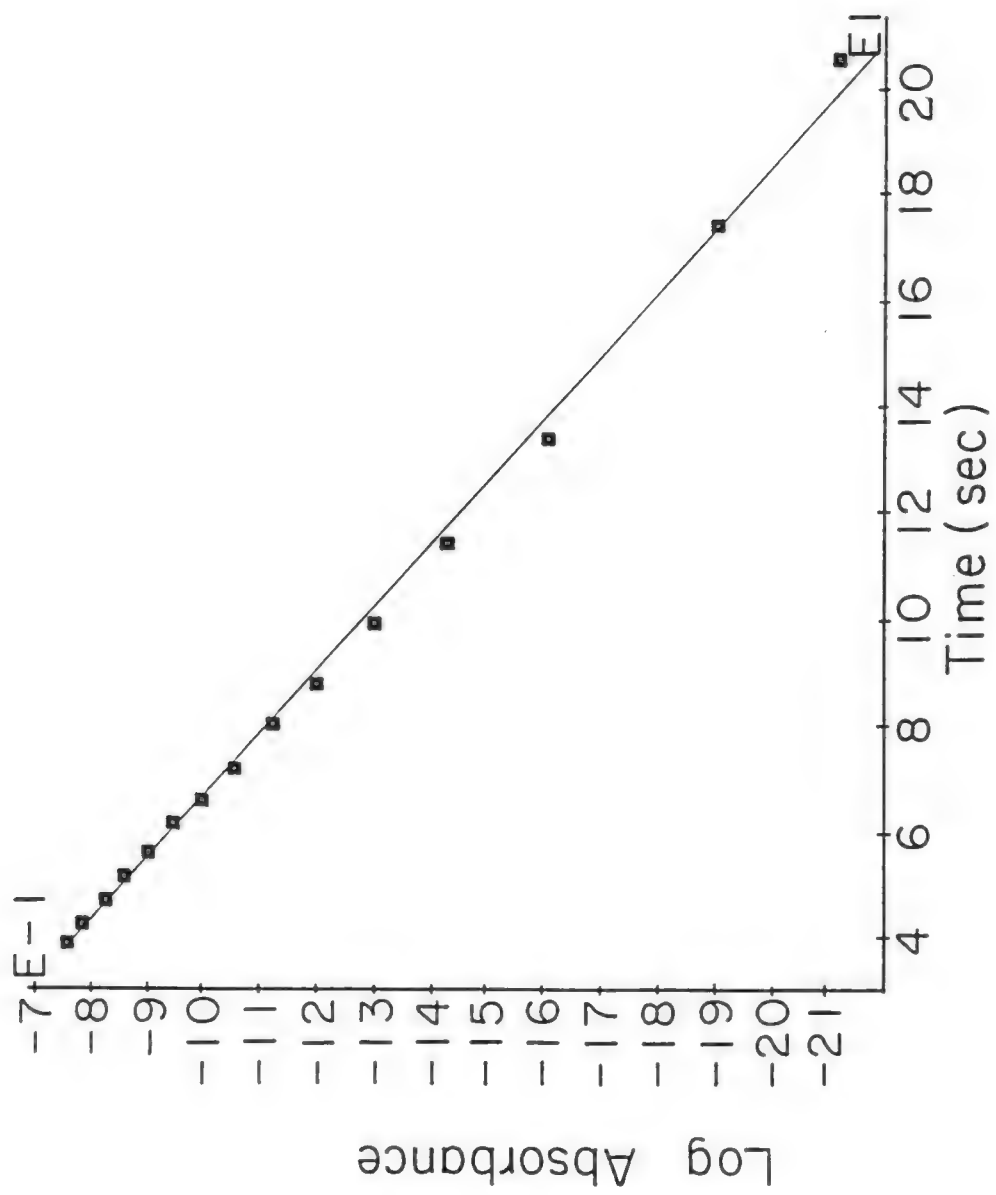
E-1
EI
Log Absorbance
-7
-8
-9
-10
-11
-12
-13
-14
-15
-16
-17
-18
-19
-20
-21
4
6
8
10
12
14
16
18
20
Time (sec)

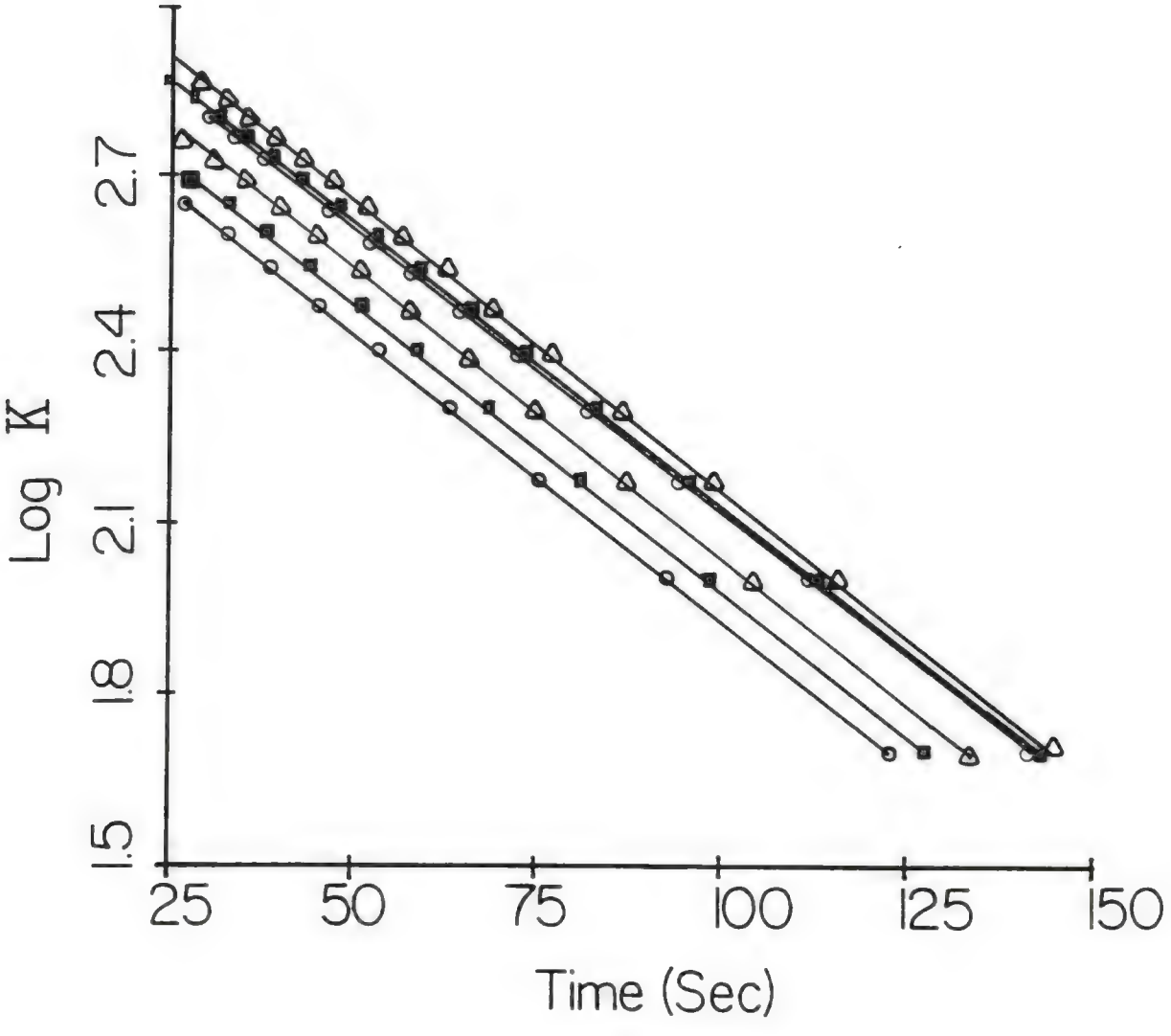

Figure 23. Effects of increasing solution viscosity upon the exponential character of the FIA manifold. The relative viscosity of the injected solution increases (see Table VI), from left to right, from 1.00 to 3.54 times that of water at 20°C.

Table IV. Variation of relative viscosity (vs. 20°C) and slopes of log K vs. time as the weight percentage of ethylene glycol is varied from 0-48% in the injected solution.

% Ethylene Glycol	[NaCl] (M)	η/η 20°C	Slope ($\times 10^{-3}$)
0	0.469	1.00	-10.14
10	0.426	1.27	-9.97
20	0.383	1.66	-10.03
28	0.347	2.04	-10.15
40	0.293	2.83	-10.09
48	0.256	3.54	-10.00

Data adapted from CRC Handbook of Chemistry and Physics (1980a).

in a #75 Ostwald capillary viscometer (Atkins, 1982) at 25±0.1°C for an aqueous, 40% ethylene glycol and 300 mM CTAB solution are given in Table V. These results indicate that the 40% ethylene glycol solution has approximately the same viscosity as the 300 mM (300X the CMC) CTAB solution.

Effective mixing volume. In order to use equation 2.23, the effective mixing volume of the FIA manifold must be experimentally determined. The presence of varying amounts of preflow cell tubing in different detectors ensures that the mixing volume of the system will vary with the flow-through detector employed. Therefore, the effective mixing volume of the system must be determined for each different type of detector used. The time during which any initial concentration of a purely exponential concentration profile decreases by one half of its initial value ($t_{1/2}$) is defined as

$$t_{1/2} = 0.693\ V/F. \qquad \text{(eq. 2.24)}$$

The effective mixing volume of the system can be experimentally determined by examining the variation of $t_{1/2}$ with the flow rate. A plot of $t_{1/2}$ vs. 0.693/F yields a straight line with a slope equal to the effective mixing volume of the system.

For conductance detection, a constant volume (10 µL) of a 0.47 M NaCl solution was repetitively injected into the manifold as the flow rate was varied from 0.49-1.66 mL/min. The plot of $t_{1/2}$ vs. 0.693/F yielded a straight line ($r^2 = 0.999$) of the form $y = 0.765X + 3.28 \times 10^{-3}$, resulting in an effective mixing volume equal to 765 µL (Figure 24).

Table V. Determination of the efflux time for various solutions in a #75 Ostwald capillary viscometer.

Solution[a]	Efflux Time (s)	Average Efflux Time (s)
H_2O	105.9 105.6 105.7	105.7
40% Ethylene Glycol	257.6 258.0 258.5	258.0
300 mM CTAB	253.3 255.0 254.2	254.2

[a] Temperature 25±0.1°C.

Figure 24. A plot of $t_{1/2}$ vs. 0.693/Q for the determination of the effective mixing volume of the conductance FIA manifold: $t_{1/2}$ (min) is the time required for any concentration of an exponential concentration profile to decrease to one half of its initial value, Q is the flow rate (mL/min).

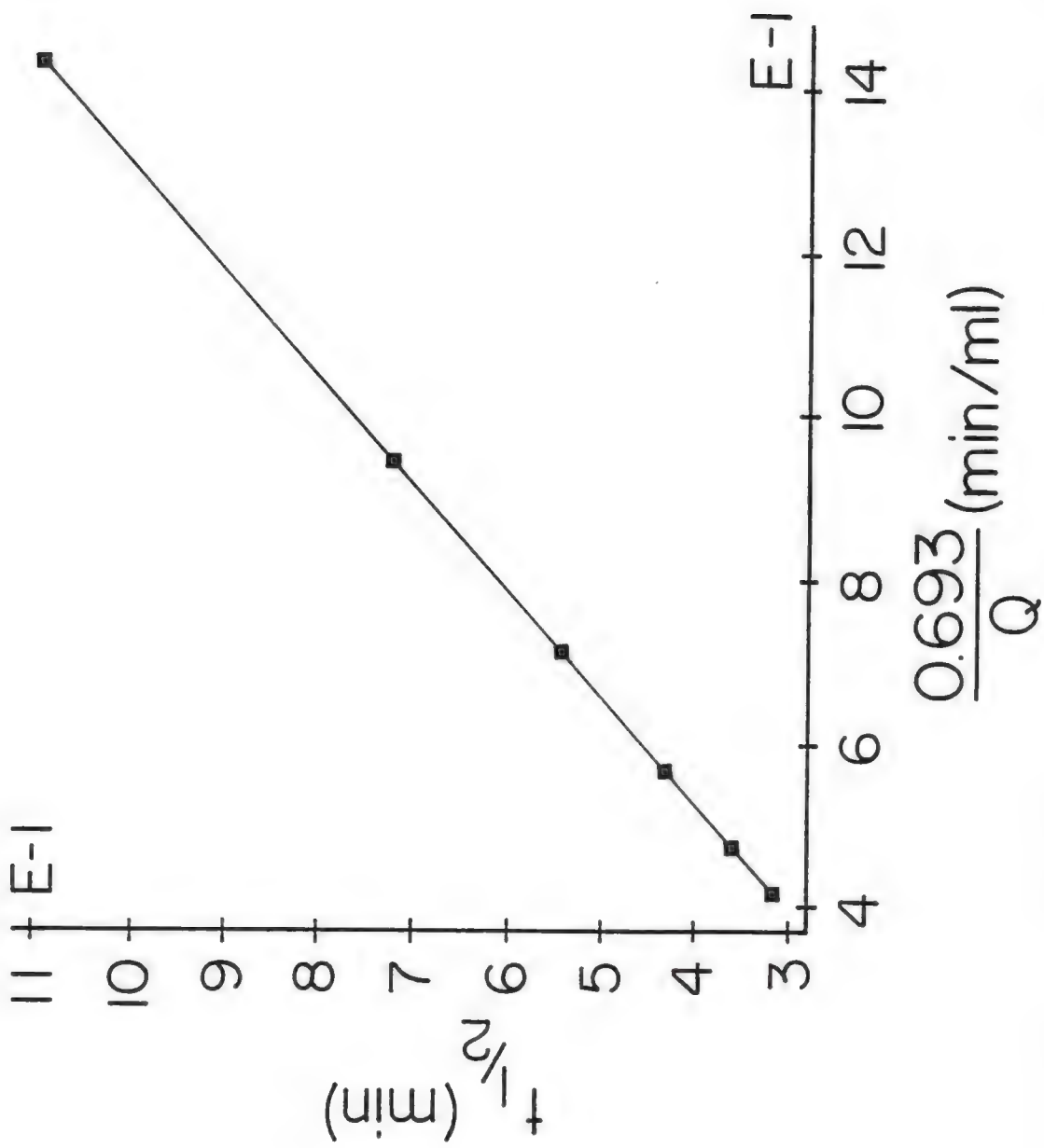
E-1
11
10
9
8
7
6
5
4
3
$t_{1/2}$ (min)
E-1
4
6
8
10
12
14
$\frac{0.693}{Q}$ (min/ml)

When using absorbance detection, an accurate value of V is best obtained by monitoring the absorbance of a compound which has a spectral region (wavelength of maximum absorbance or absorbance plateau) which does not shift upon dilution by the carrier stream. This ensures that changes in response are due only to concentration changes and not spectral shifts (i.e. a 50% decrease in the response curve truly corresponds to a 50% decrease in concentration). The effective mixing volume for absorbance detection was determined by the injection of 10 µL of a 2.62×10^{-3} M aqueous solution of Eriochrome Black T and subsequent 437 nm detection. This compound exhibits an absorbance plateau from 433-441 nm (Figure 25) and an accompanying linear calibration curve over the concentration range of $2.38\text{-}95.2 \times 10^{-6}$ M. The plot of $t_{1/2}$ vs. 0.693/F for flow rates ranging from 0.52-1.91 mL/min yielded an effective mixing volume of 814 µL.

Sample injection process. An HPLC sample injection valve is a convenient way to introduce samples into an FIA manifold. In chromatographic separations, it is a common practice (Bakalyar and Spruce, 1983) to use partially filled sample loops for sample introduction. After injection, the sample is concentrated at the head of the column, with no loss in sensitivity or reproducibility due to the injection process.

In FIA, however, dispersion of the injected sample (and accompanying loss of sensitivity) occurs as a result of its interaction with the surrounding carrier stream. This interaction between the sample and the carrier stream can also occur in a

Figure 25. The UV-visible spectra of 1.25×10^{-3} M Eriochrome Black T after aqueous dilution by factors of 10, 50 and 100.

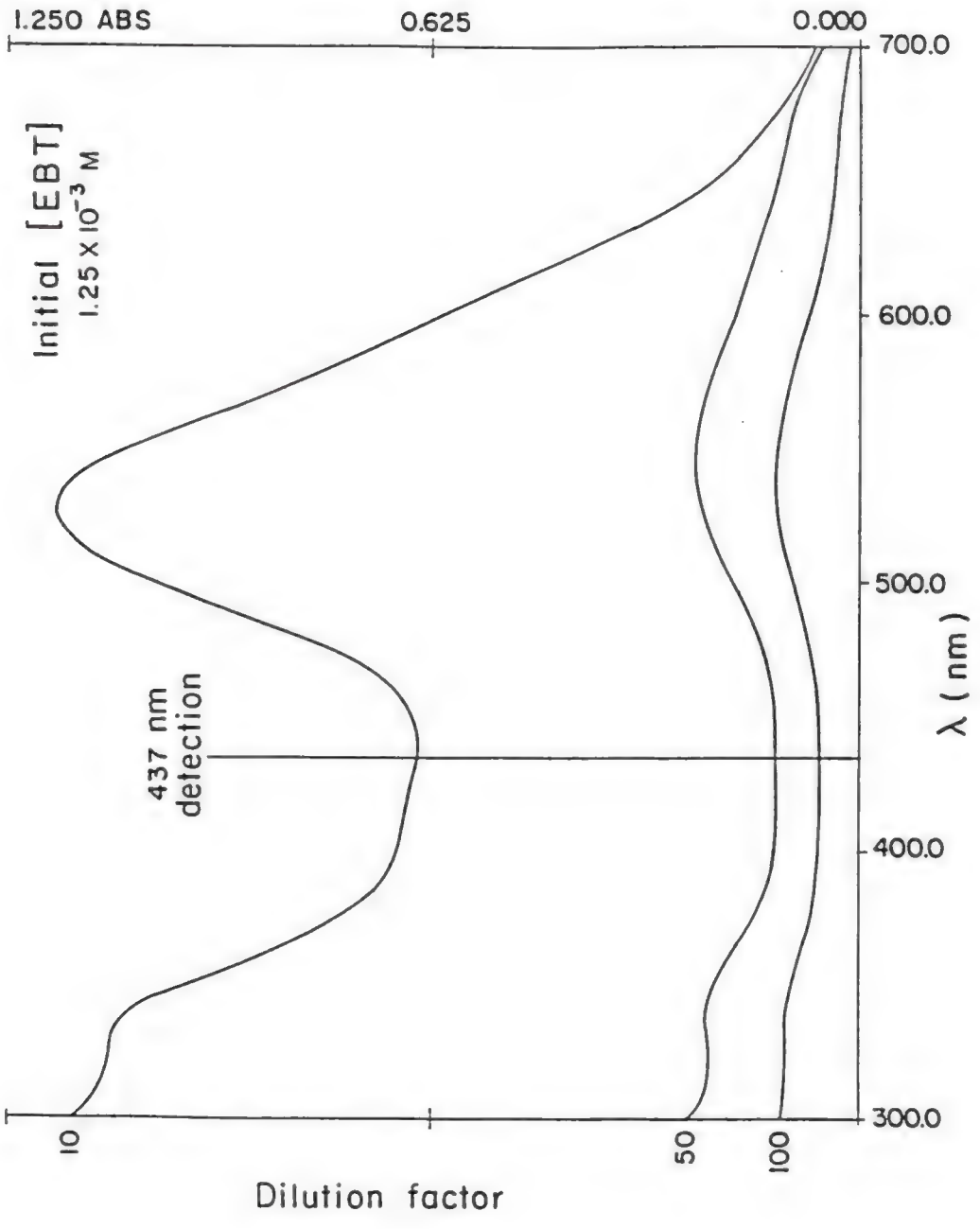
1.250 ABS
0.625
0.000
700.0
600.0
500.0
400.0
300.0
λ (nm)
Initial [EBT]
1.25 X 10⁻³ M
437 nm
detection
10
50
100
Dilution factor

partially filled sample loop before the injection is made. Therefore, it is necessary to use a completely filled sample loop to ensure the greatest sensitivity and a reproducible introduction of both a constant amount and concentration of sample at the point of injection.

In order to quantify this phenomenon, a comparison of a 10 µL injection via a fully loaded 10 µL loop (20 µL load) and a partially loaded 100 µL loop (10 µL load) was undertaken. For this investigation of the sample injection process, the sample loop and pregradient chamber tubing were connected directly to the absorbance detector flow cell. The injected compound, 2.39×10^{-5} M aqueous methyl red, was detected at 430 nm. As shown in Table VI, the loss of sensitivity ranges from approximately 21-26% in the partially filled loop when compared to the fully loaded 10 µL loop. In all trials, the time from completion of sample load to sample injection never exceeded 5 s. In the partially filled loop, an increase in the length of time between sample loading and injection results in an increase in dispersion, further decreasing sensitivity. The results of Table VI also indicate that the average relative standard deviation of the sample injection process is less for the completely filled loop (1.3%) compared to the partially filled loop (2.0%). Therefore, to ensure the greatest possible reproducibility of the technique, a completely filled sample loop is again recommended.

Practical use of equation 2.23. The theoretical treatment we derived earlier (Berthod et al., 1988) assumes that the surfactant solution is injected with a plug profile whose duration, t_1, is

Table VI. Investigation of the sample injection process.

Average Flow Rate (mL min^{-1})	Maximum absorbance[a] ($\times 10^2$) 100-µL Loop (10-µL load)	RSD(%)	10-µL Loop (20-µL load)	RSD(%)	Ratio of Responses (100 µL:10 µL)
0.25	3.68	2.6	4.76	1.3	77.3
0.52	3.85	2.4	5.05	1.3	76.2
0.97	4.48	1.7	5.73	1.5	78.2
1.45	4.37	1.3	5.70	1.8	76.7
1.93	4.05	2.1	5.44	0.8	74.4

[a] Injected compound, methyl red (2.39×10^{-5} M); detection at 430 nm. The number of observations was ≥ 12 in all cases.

v_i/F. As shown in Table VII, this is never the case; the injection has an exponentially modified Gaussian profile as shown by Figure 26. Then, the injection time, t_i, is greatly underestimated when calculated as v_i/F. For example, when 10 µL were injected with a 20 µL/s flow rate (1.2 mL/min), the theoretical value of t_i is 0.5 s (Figure 26). The actual value may lie between 5 and 15 s, that is between 10 and 30 times higher than the theoretical value. To use our theoretical treatment (Berthod et al., 1988), it is possible to describe the injection as a plug of lower concentration, c_i', and higher volume, v_i', such that the product $c_i'v_i''$ is equal to c_iv_i, as shown by Figure 26. This replaces the theoretical value, t_i, of the injection time by an empirical one, t_i'. It is not possible to mathematically quantify this effect because the band broadening, occurring during the injection process, depends on the connecting volume, on the flow rate and on the viscosity and concentration of the injected solution. To minimize the error on the CMC determination, the connecting tubing volume must be as low as possible, and the injected surfactant concentration must be as high as possible. Indeed, the higher the surfactant concentration, the longer the time, t_{CMC}, and the smaller the relative influence of t_i on the CMC value (equation 2.23). It must be noted that there is an upper limit to t_{CMC}; the observed break must occur in the middle of the range used. If the break occurs too close to the baseline (i.e. t_{CMC} is too long), it will be unnoticed.

Empirically, we found that the maximum value of the recorded signal (conductance or absorbance) could be used to obtain an

Table VII. A comparison of the theoretical and empirical sample injection processes, v_i = 10 µL.

Flow Rate (µL)	Time t_i (s)		Time t_i' (s)[a]
	Theoretical	Experimental	
1.67	6.0	145	97
3.33	3.0	76	51
6.67	1.5	35	23
13.33	0.75	14	9
26.67	0.37	6	4

[a] $t_i' = 2\ t_i/3$ (experimental).

Figure 26. The sample injection process: (A) a theoretical sample plug injection, (B) the actual injection profile corresponding to (A), and (C) the plug with the t_i' value actually used in equation 2.23.

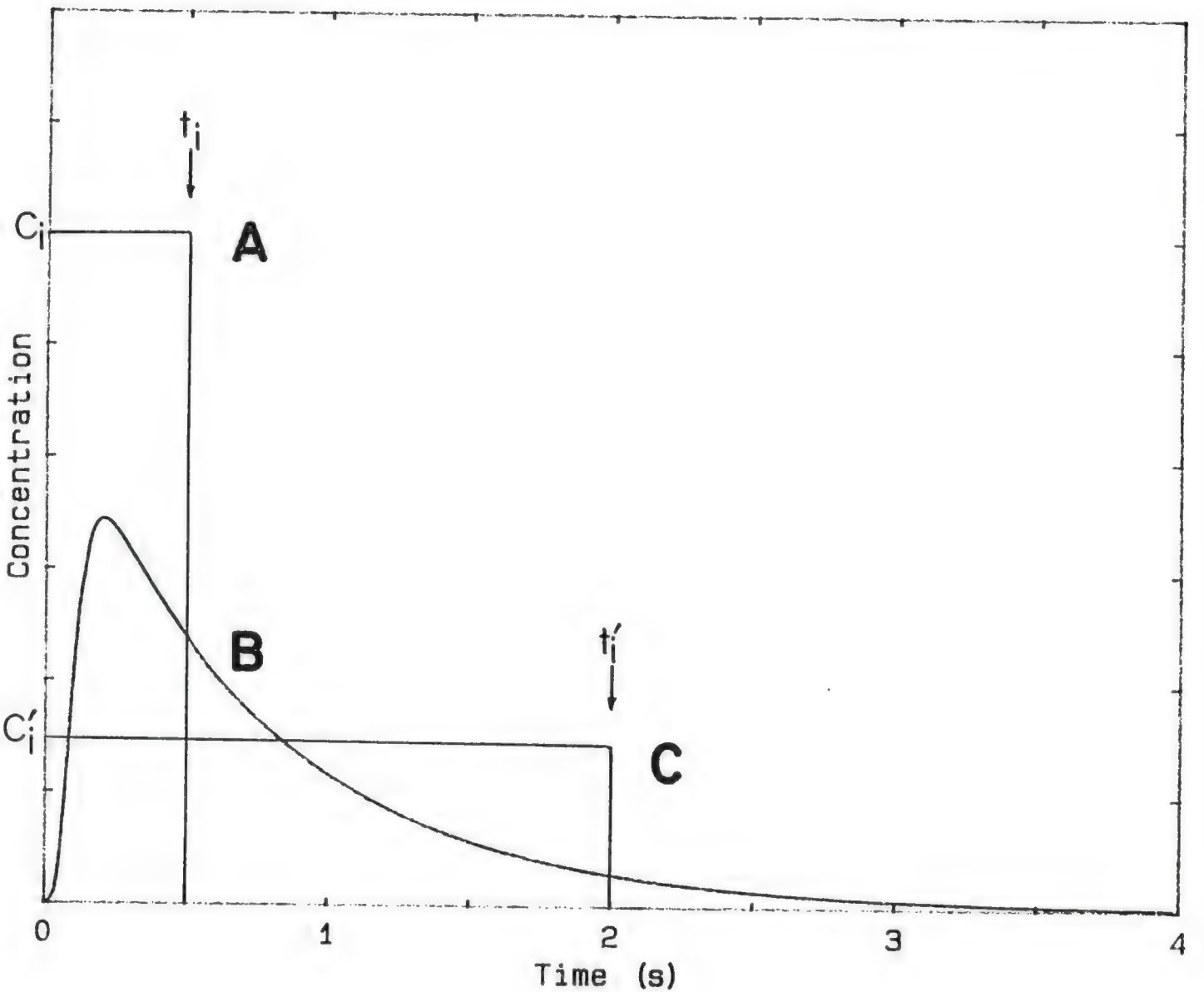
t_i
C_i
A
Concentration
B
t'_i
C'_i
C
0
1
2
3
4
Time (s)

estimated value, t_i', to be used instead of t_i in equation 2.23. The value of t_i corresponds to 2/3 of the time needed to reach the maximum recorded value, as shown in Figures 27 and 28.

The validity of the results acquired using equation 2.23 was additionally proven by calibrating the system with a standard surfactant solution and subsequent determination of the CMC. A standard surfactant solution (with a concentration approximately one and one half times the CMC) was introduced directly into the detector and a steady-state response was obtained. With this standard concentration as a reference point, the CMC was determined using

$$CMC = C_s \exp[F(t_s - t_{CMC})/V], \qquad \text{(eq. 2.24)}$$

where C_s is the concentration of the standard and t_s is the time on the response curve (10-20 cm/min) corresponding to the standard concentration. The CMCs determined using equation 2.24 and three trials were CTAB, 0.96±0.01 mM; CTAC, 1.4±0.05 mM; SDS, 8.3±0.01 mM; and TTAB, 4.2±0.20 mM. All of these values lie within the range of literature values and the error boundaries for the CMCs determined and tabulated in Table VIII, a strong indication that the empirically derived t_i' value is valid for our system.

CMC determinations. The CMCs determined for the investigated surfactants are listed in Table VIII. For the ionic surfactants (t_{CMC} varies from 60-76 s for those studied), the error intervals represent t_{CMC} plus and minus 3 s while the corresponding intervals

Figure 27. Computer-generated curves modelling conductance detection in an FIA system. The value t_i' is the value of the experimental time of injection used in equation 2.23 for the calculation of the CMC.

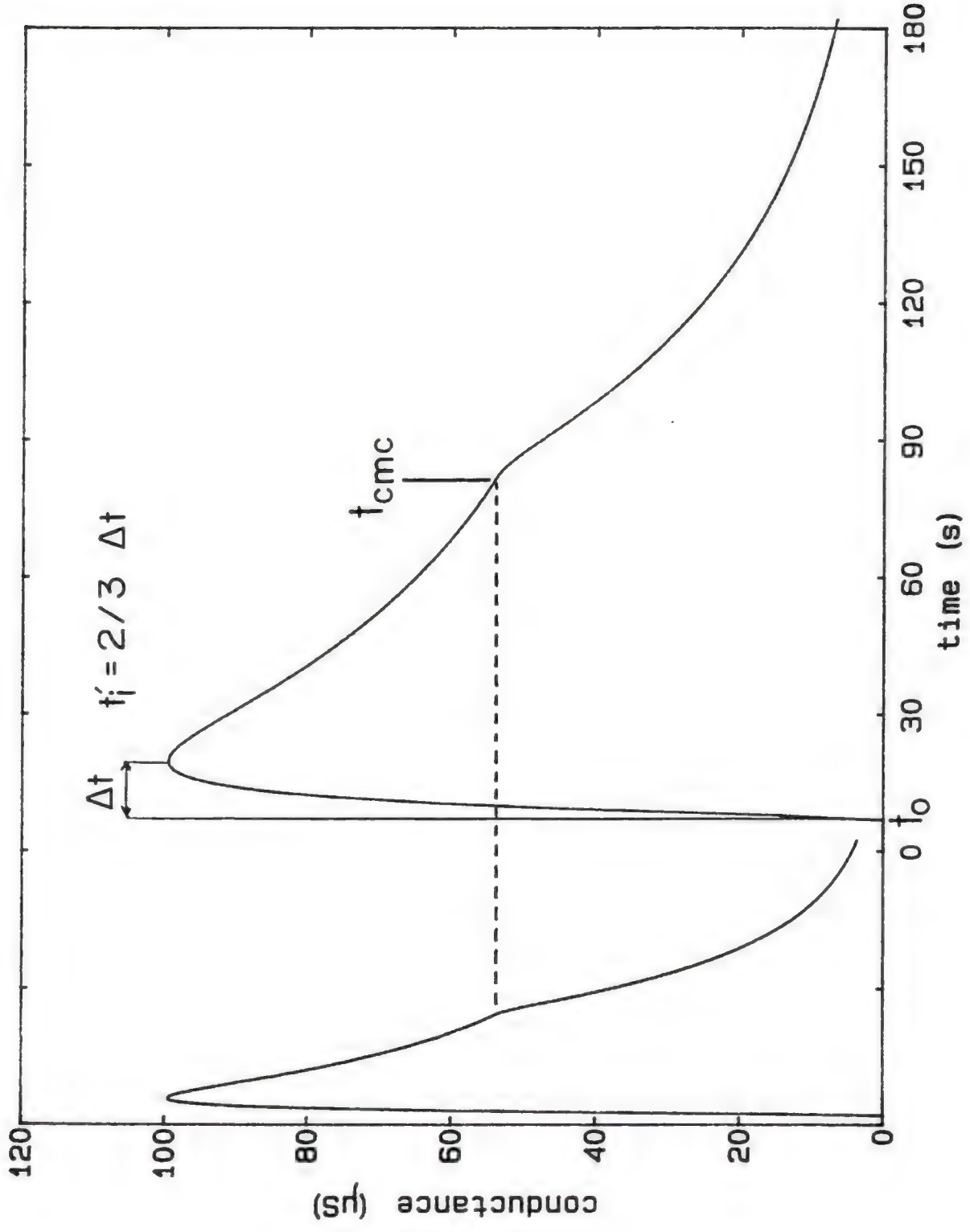
conductance (μS)
120
100
80
60
40
20
0
0 t_0 30 60 90 120 150 180
time (s)
t_{cmc}
$t_i' = 2/3\ \Delta t$
Δt

Figure 28. Computer-generated curves modelling the use of a dye as a micelle-tracer in an FIA system: (A) the dye is solubilized in the carrier stream and (B) the dye is solubilized within the injected surfactant solution (see text and Figure 26 for discussion of t_i').

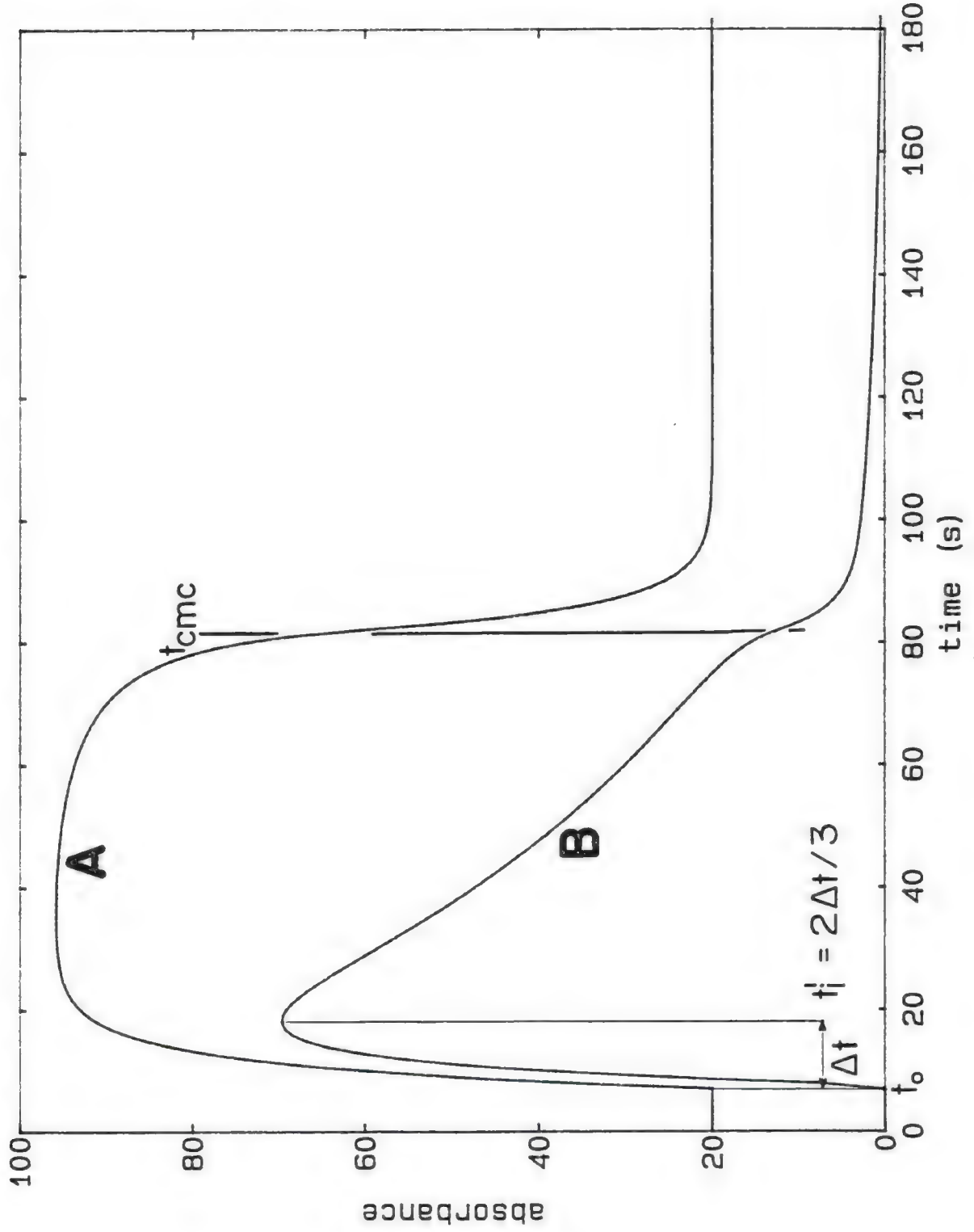
absorbance
time (s)
A
B
t_{cmc}
t_o
Δt
$t_i' = 2\Delta t/3$
0
20
40
60
80
100
120
140
160
180

Table VIII. Values of CMC for various surfactants.

Surfactant	Critical Micelle Concentration (mM) This Study	Literature Range	Number of Reports	References
Ionic				
CTAB	0.99 ±0.06	0.92 -0.98	4	Mukerjee and Mysels (1971), Kali (1980), Ohyashiki and Mohri (1983)
CTAC	1.47 ±0.10	1.3 -1.5[a]	2	Mukerjee and Mysels (1971)
SDS	8.10 ±0.60	8.1 -8.5	18	Mukerjee and Mysels (1971), Kali (1980)
Nonionic				
Brij-35	0.150±0.016	0.048-0.17	12	Mukerjee and Mysels (1971), Taylor and Nieman (1984)
Brij-56	0.099±0.001	NA	-	-
Brij-99	0.068±0.008	0.04	1	Roe and Barry (1983)
Triton X-100	0.310±0.033	0.16 -0.33	3	Mukerjee and Mysels (1971), Diaz Garcia and Sanz-Medel (1986)

[a] The value of 1.3 mM was obtained at 30°C but is included because of the paucity of conductance data available for CTAC at 25°C.

for the nonionic surfactants (99 < t_{CMC} < 186 s) are plus and minus 5 s. These error intervals are included to account for inherent inaccuracies in the visual inspection of the response curves and possible error in the value of t_i.

Certain dyes have been shown to modify the CMC of nonionic surfactants (typically to a much lesser degree than ionic surfactants) using the spectral shift method (Nemoto and Funahashi, 1981). However, Samsonoff et al. (1985) have shown that variation of the Coomassie concentration (CBBG) from 0.1-0.05 mg/mL yielded consistent CMC values. Therefore, it can be inferred from the concentration of CBBR used here (0.011 mg/mL or 1.3×10^{-5} mol/L) and the agreement with literature values that the CMCs determined in the present work are not being modified by the presence of a dye.

This proposed method has been shown to be both a simple and accurate method for the determination of the critical micelle concentrations of both ionic and nonionic surfactants. The CMC value calculated from equation 2.23 is approximately constant from 0.42-2.0 mL/min, verifying that the flow rates used (1.05±0.05 mL/min) in this work are valid. The practical application of this technique eliminates many of the problems encountered in current CMC determination methods. Several hundred milligrams of surfactant provides sufficient analyte to perform many determinations, ensuring conservation of material resources. The technique ensures minimization of solution preparation, boasts experimental and instrumental simplicity as well as speed. The total time required, from sample injection to manual calculation, for determination of the

CMC is approximately 30 minutes. The potential application of this technique to other types of traditional HPLC detectors should provide the surface and colloid chemist with an expanded range of experimentally simple techniques to accurately determine the CMCs of surfactant solutions.

CHAPTER III
COMPARISON OF AQUEOUS, MICELLAR AND MICROEMULSION CARRIERS IN FLOW INJECTION ANALYSIS: THE BASE HYDROLYSIS OF ACETYLSALICYLIC ACID

Introduction

The use of organized media is well established as a means of promoting the rates of chemical reactions in solution (Fendler and Fendler, 1975; Mittal, 1977a, 1977b; Hinze, 1979). The majority of the work in this field has focused upon the use of micellar surfactant solutions to achieve rate enhancements. In aqueous solutions, the greatest enhancements occur when one reactant has significant hydrophobic character (allowing partitioning to the micelle) and the other is a charged species which is electrostatically attracted to the oppositely charged surfactant headgroups. Judiciously chosen surfactant aggregates allow both the proximity and the microconcentration of reacting species to be increased, resulting in the desired effect.

The term microemulsion (Hoar and Schulman, 1943) has long been applied to a thermodynamically stable, single optically isotropic system (Danielsson and Lindman, 1981) of water, oil (cosurfactant) and amphiphile. Although commercial production and applications of microemulsions have existed for decades, a clear understanding of the true nature of these solutions has not been reached. Microemulsions are currently viewed as either solutions of swollen micelles

(Shinoda and Friberg, 1975) or as 10-200 nm diameter droplets of amphiphile and cosurfactant surrounded by an interfacial film (Prince, 1975). More recently, these organized surfactant systems also have been shown to exhibit rate of reaction promotion in solution (Mittal and Lindman, 1984) and have received analytical application as carrier streams in flow injection analysis (Memon and Worsfold, 1986a, 1986b). This work demonstrated the compatibility of microemulsions with FIA combined with spectrofluorimetric detection and suggested the extension of the microemulsive carrier stream in FIA in conjunction with other detection systems.

The present work concerns the use of ultraviolet detection to examine the microemulsion enhanced hydrolysis of acetylsalicylic acid and its potential application in FIA. While all previous work employing microemulsions in FIA has been concerned only with detection enhancement, here direct comparisons are made between aqueous and microemulsion carriers concerning rates of reaction, peak dispersion and analytical figures of merit.

Experimental

Apparatus

Reaction rate constants were determined by monitoring the appearance of product (salicylic acid) with time using a Hewlett Packard (Palo Alto, CA) model 8450A diode array spectrophotometer and resulting spectra were recorded on a Hewlett Packard model 7470A plotter.

The flow injection analysis manifold employed consisted of an Altex (San Ramon, CA) Model 100A solvent metering system which delivered the carrier streams at the desired flow rates. Sample volumes of 20 µL were introduced by a Rheodyne (Cotati, CA) model 7125 sample injection valve. All tubing used was teflon (1/16" od, 0.5 mm id) from the Anspec Co. (Ann Arbor, MI) and included a 200-cm long reaction coil with a coiling diameter of approximately 14 mm. All reactions were carried out at room temperature (25±1°C). The absorbance of the products in the carrier stream was determined by a Kratos (Ramsey, NJ) Spectroflow 757 absorbance detector.

Chemicals

Acetylsalicylic acid was obtained from Sigma Chemical (St. Louis, MO) and prior to use it was recrystallized from chloroform. Reagent grade (Class 1C) butyl alcohol (Fisher Scientific, Fairlawn, NJ), purum grade cetyltrimethylammonium bromide (Sigma) and reagent grade sodium hydroxide (Fisher Scientific) were used as received. All water used in the preparation of solutions and carrier streams was deionized.

Results and Discussion

Organized media have received numerous applications as carrier streams in FIA. The use of micellar enhanced chemiluminescence has been employed for the determination of Copper (II) (Yamada and Suzuki, 1984) by flow injection analysis. More recently, bilayer vesicle-catalyzed chemiluminescence for the determination of cyanide (Ishii et al., 1986) as well as the use of liposomes containing a marker

compound for signal enhancement in an immunochemical-based FIA system (Locascio-Brown et al., 1988) have been reported. The organized surfactant assembly enhances chemiluminescence efficiency and/or energy transfer efficiency in these applications, resulting in an increased signal (Nomura et al., 1984).

Micellar carrier streams have been used in FIA to promote fluorescence enhancement in the detection of pyridoxal (Hernandez Torres et al., 1987), Terbium (III) (Aihara and Tomitsugu, 1986a) and Europium (III) (Aihara and Tomitsgu, 1986b) in solution. Additional work has employed microemulsions as carrier streams in FIA for the enhancement of fluorescence signals in the determination of primary amines (Memon and Worsfold, 1986a, 1986b). In both micellar and microemulsion solutions, fluorescence sensitivity is increased by decreasing quenching effects, increasing microviscosity of the solvent and minimizing interference effects by shielding (Hinze et al., 1984).

An examination of the current applications of organized media as carrier streams in FIA indicates that little attention has been given to a direct examination of the physical and chemical interactions between the solute and the reaction media. Memon and Worsfold (1986a, 1986b) examined the "efficiency" of microemulsion carrier streams in flow injection analysis by a comparison of calibration curves obtained in a microemulsion and in a totally nonaqueous system (hexane). This solvent is not capable of enhancing the fluorescence signal and as such simply serves as a blank for comparison. In order to accurately evaluate the possibility of the widespread application of microemulsion carrier streams in FIA to a range of detection systems,

examination of dispersion characteristics as well as rate enhancements obtained in static and flowing systems is necessary.

Initially, a comparison was made in a static system between the base catalyzed hydrolysis of acetylsalicylic acid in aqueous solution and in organized media. The reaction for the hydrolysis of acetylsalicylic acid under basic conditions is depicted in Figure 29. The sodium hydroxide concentration in all work was 1×10^{-2} M. Acetylsalicylic acid is expected to partition to the organized media as a result of hydrophobic interactions. Additionally, electrostatic interactions between the cationic surfactant headgroups and the oppositely charged hydroxyl ions in solution indicate that the reaction is an excellent candidate for organized media catalysis.

Kinetics: Static vs. Flowing System

The kinetics of this reaction were studied in aqueous, micellar and microemulsive solutions by examining the change in product absorbance versus time as the reaction proceeded. Under the chosen reaction conditions the large excess of NaOH in solution ensures that the reaction follows pseudo first-order kinetics. The progress of the reaction versus time and wavelength in a static system was monitored for aqueous, micellar and microemulsive media and the results are shown in Figures 30, 31 and 32, respectively. The wavelength interval from 250-350 nm was examined and the absorbance maximum for the salicylic acid product was determined to be 298 nm (wavelength of detection) in both aqueous and organized media. In agreement with previously published results (Rodenas and Vera, 1985), the addition of

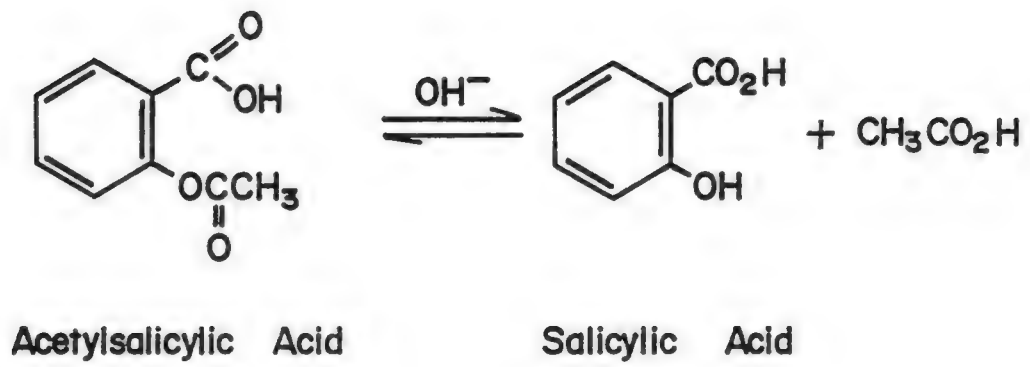

Figure 29. The base hydrolysis of acetylsalicylic acid.

Figure 30. Absorbance versus wavelength (nm) in aqueous media following the progress of the acetylsalicylic acid hydrolysis. Acetylsalicylic acid 9.72×10^{-5} M, NaOH 1×10^{-2} M, 1 cm cell, at room temperature. Spectra were run at 1 minute intervals.

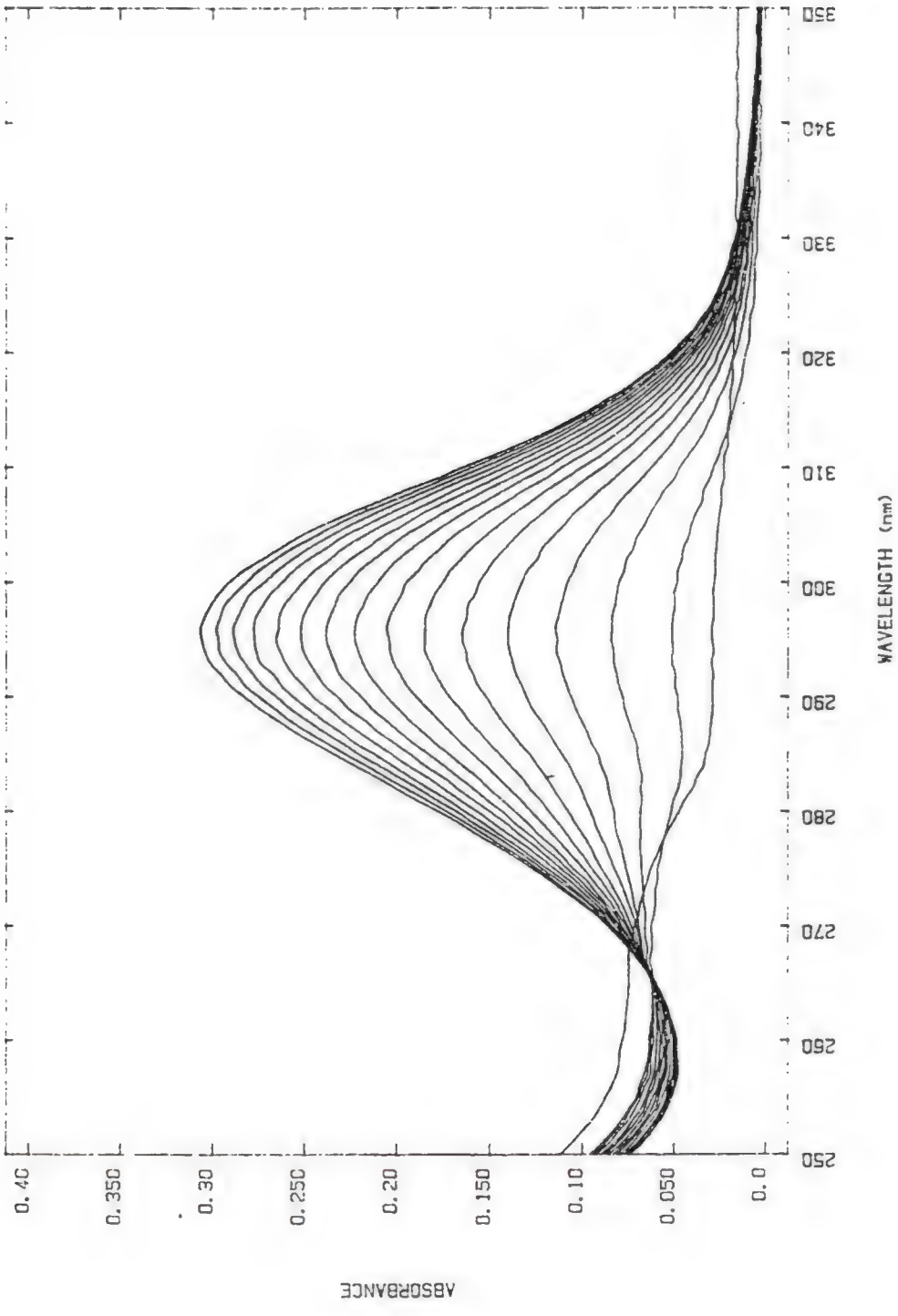
0.40
0.350
0.30
0.250
0.20
0.150
0.10
0.050
0.0
ABSORBANCE
250
260
270
280
290
300
310
320
330
340
350
WAVELENGTH (nm)

Figure 31. Absorbance versus wavelength (nm) in a 3.38×10^{-3} M CTAB micellar system following the progress of the acetylsalicylic acid hydrolysis. Acetylsalicylic acid 9.72×10^{-5} M, NaOH 1×10^{-2} M, 1 cm cell, at room temperature. Spectra were run at 1 minute intervals.

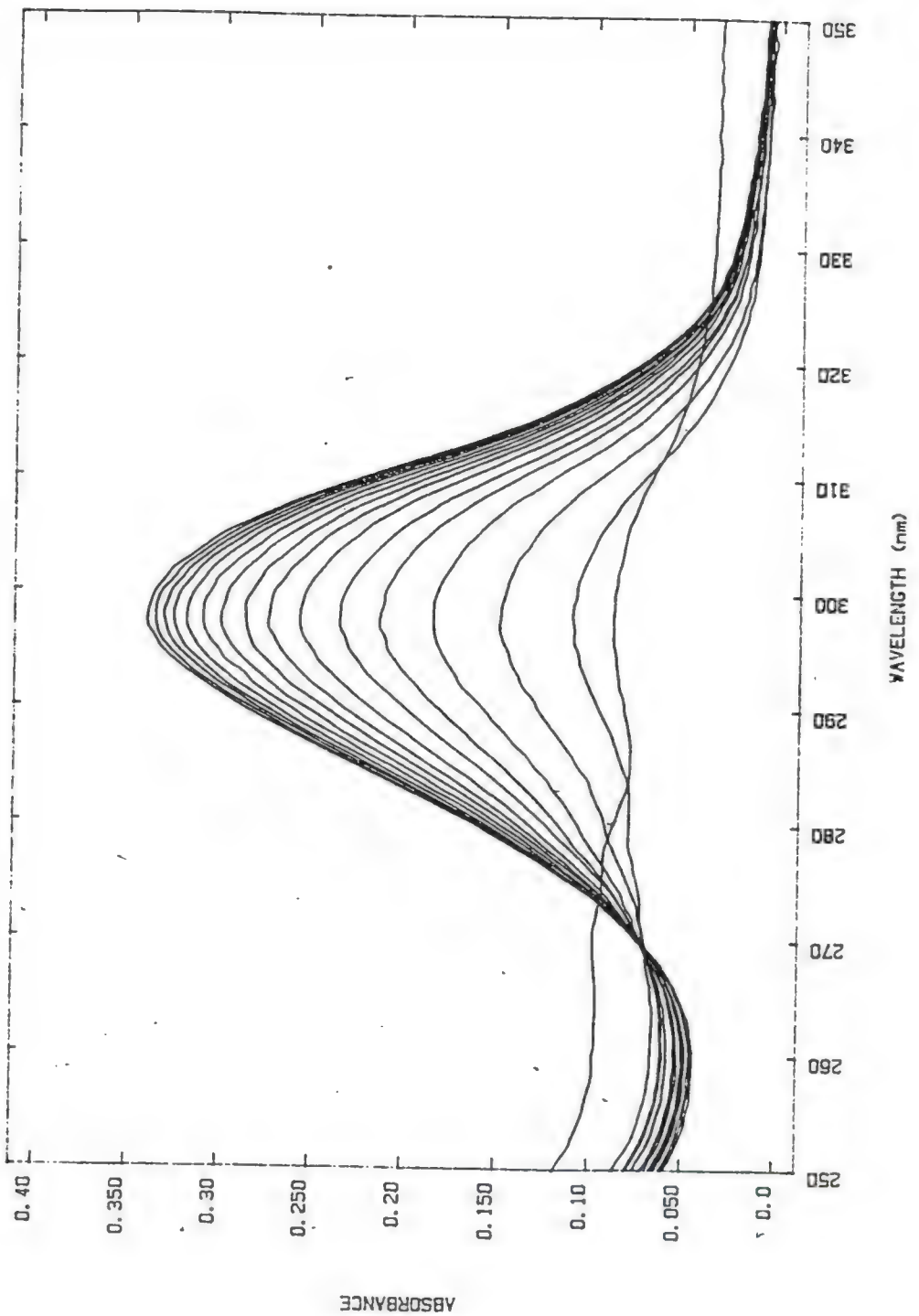
ABSORBANCE
0.40
0.350
0.30
0.250
0.20
0.150
0.10
0.050
0.0
WAVELENGTH (nm)
250
260
270
280
290
300
310
320
330
340
350

Figure 32. Absorbance versus wavelength (nm) in 99.28% (by weight) water:0.36% CTAB (9.88×10^{-3} M):0.36% butanol microemulsion system following the progress of the acetylsalicylic acid hydrolysis. Acetylsalicylic acid 9.72×10^{-5} M, NaOH 1×10^{-2} M, 1 cm cell, at room temperature. Spectra were run at 1 minute intervals.

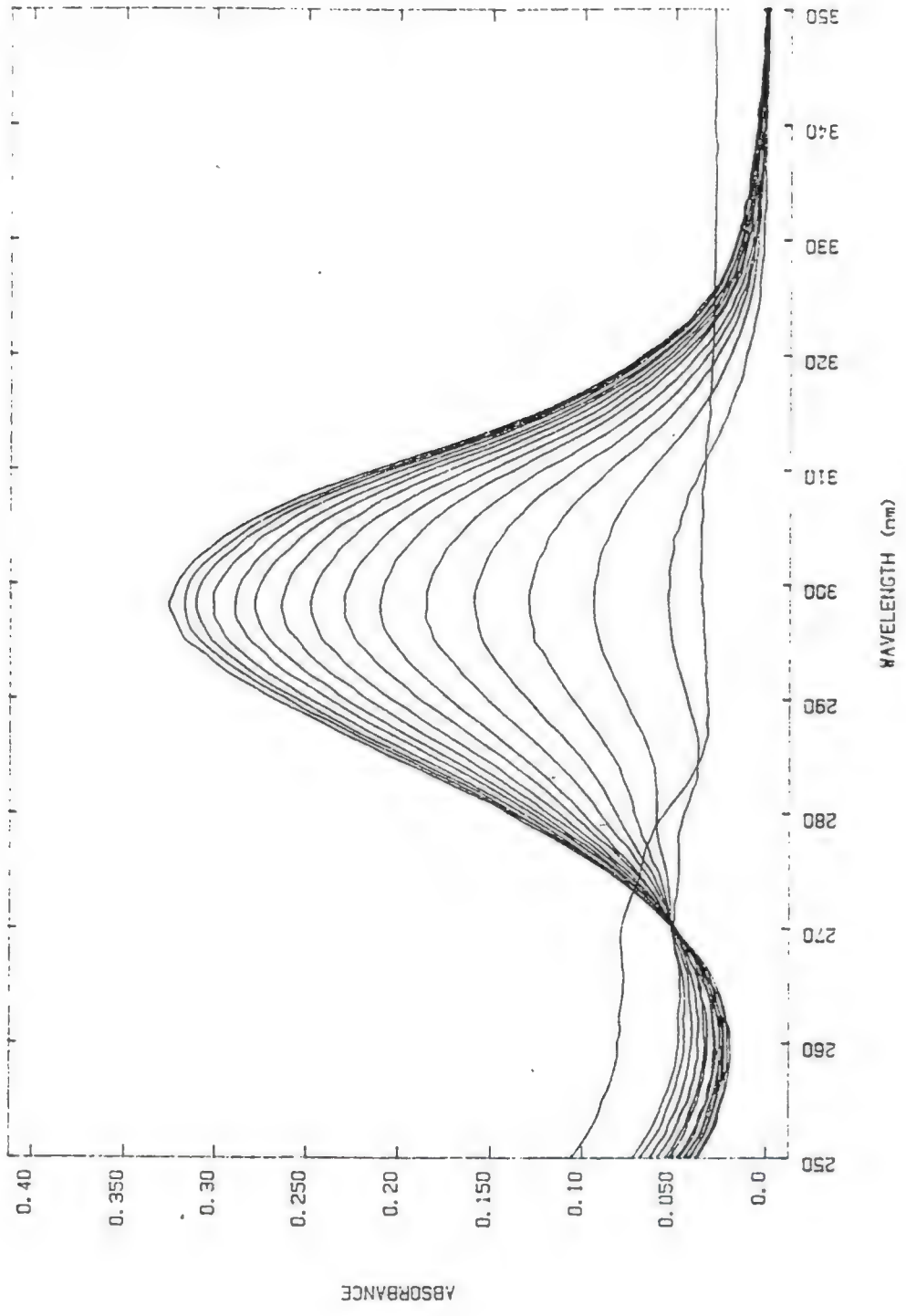
ABSORBANCE
0.40
0.350
0.30
0.250
0.20
0.150
0.10
0.050
0.0
WAVELENGTH (nm)
250
260
270
280
290
300
310
320
330
340
350

the cationic surfactant promotes the reaction. Additionally, the addition of butanol to the surfactant solution and subsequent microemulsion formation results in a further increase in the reaction rate.

Kinetic studies were performed to determine the rate constants of the reaction in aqueous, 3.38×10^{-3} M CTAB and microemulsive media (98.8% (by weight) water:0.6% CTAB:0.6% butanol). The curves showing the change in absorbance versus time in these three media at a maximum wavelength of 298 nm are shown in Figures 33-35. The rate constants for this pseudo first-order reaction were calculated using

$$\log(A_\infty - A_t) = (-kt/2.303) + \log(A_\infty - A_o), \qquad \text{(eq. 3.1)}$$

where A_∞, A_o, and A_t are the absorbances at infinite, initial and time t, respectively; t is in minutes and the rate constant, k, is in min^{-1} (Moore and Pearsen, 1981). The rate constants are then calculated from the slope (multiplying by -2.303) of the plots of $\log(A_\infty - A_t)$ vs. time. The results of this study are shown in Figures 36-38 and in Table IX.

When compared to the aqueous NaOH reaction media, these results show a rate enhancement in the micellar/NaOH system of 16% and are in agreement with literature values (Rodenas and Vera, 1985). For the microemulsion system, the rate enhancement exceeds that of both the micellar (21%) and aqueous NaOH media (41%). Therefore, the microemulsion system, providing maximum rate enhancement, was the carrier stream of choice for the flow injection manifold.

Figure 33. Change in maximum absorbance (298 nm) versus time (s) in aqueous media for the detection of salicylic acid. Acetylsalicylic acid 9.72×10^{-5} M, NaOH 1×10^{-2} M, 1 cm cell, at room temperature.

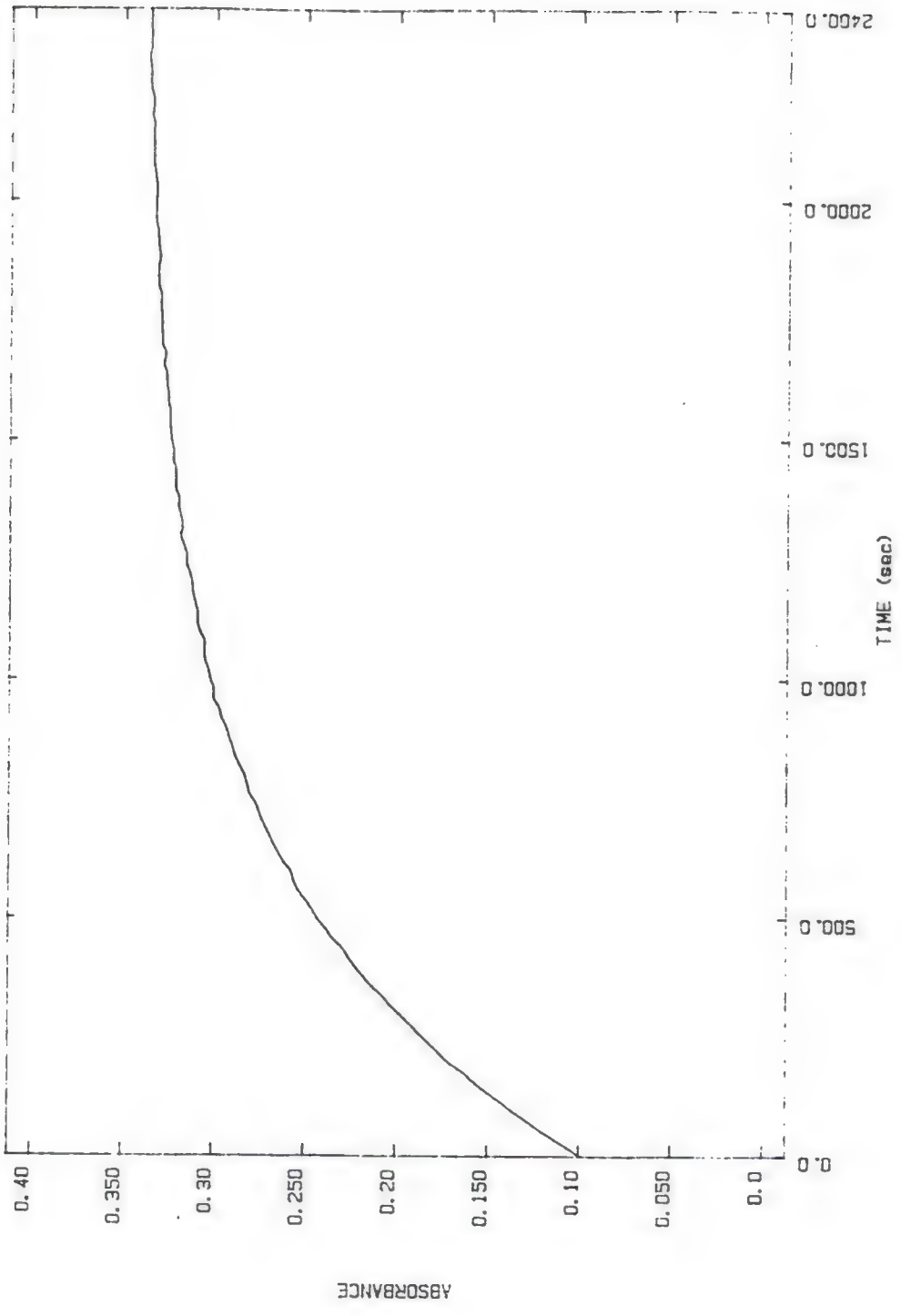
0.40
0.350
0.30
0.250
0.20
0.150
0.10
0.050
0.0
ABSORBANCE
0.0
500.0
1000.0
1500.0
2000.0
2400.0
TIME (sec)

Figure 34. Change in maximum absorbance (298 nm) versus time (s) in a 3.38×10^{-3} M CTAB micellar system for the detection of salicylic acid. Acetylsalicylic acid 9.72×10^{-5} M, NaOH 1×10^{-2} M, 1 cm cell, at room temperature.

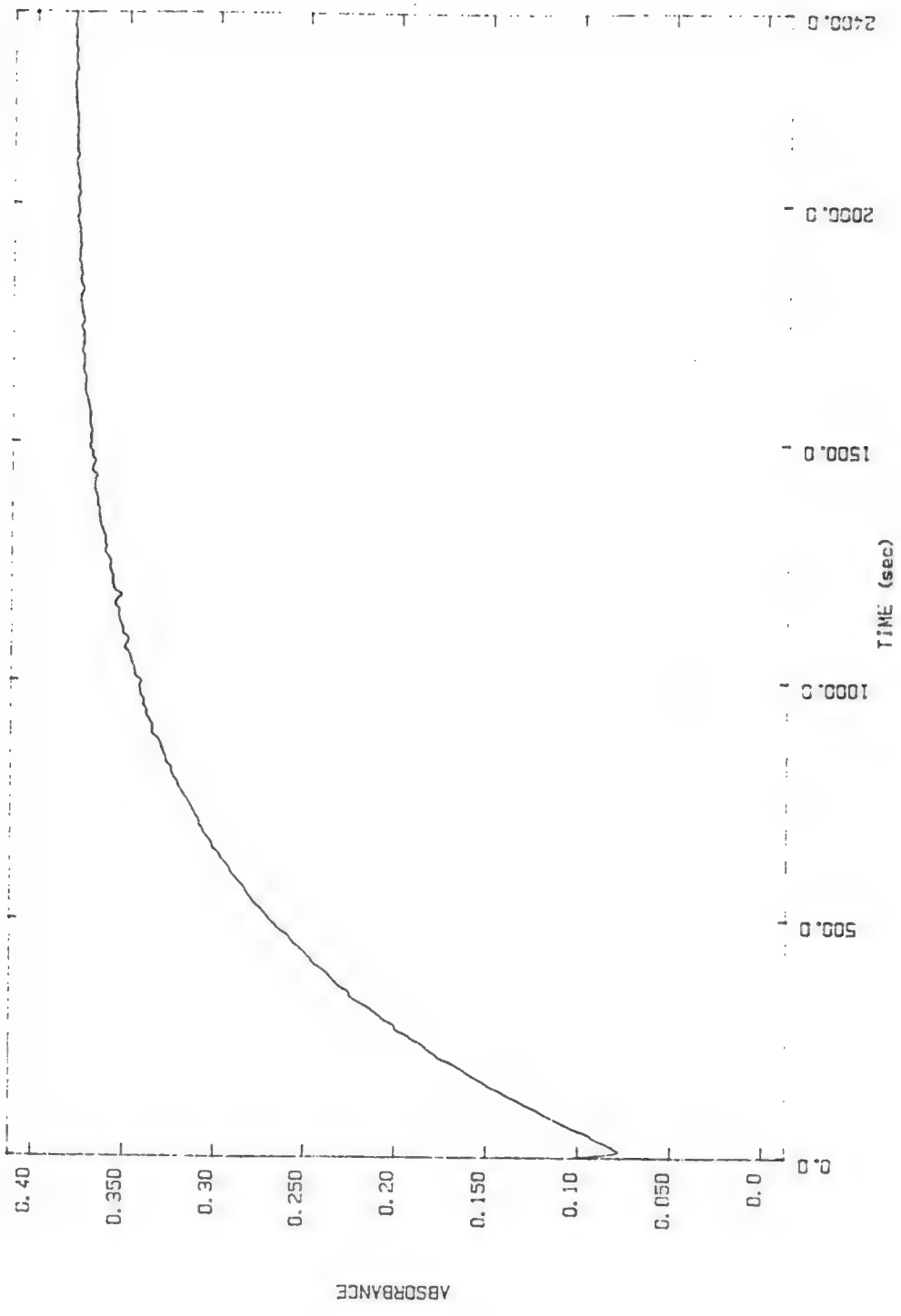
0.40
0.350
0.30
0.250
0.20
0.150
0.10
0.050
0.0
ABSORBANCE
0.0
500.0
1000.0
1500.0
2000.0
2400.0
TIME (sec)

Figure 35. Change in maximum absorbance (298 nm) versus time (s) in a 99.28% (by weight) water:0.36% CTAB (9.88×10^{-3} M):0.36% butanol microemulsion system for the detection of salicylic acid. Acetylsalicylic acid 9.72×10^{-5} M, NaOH 1×10^{-2} M, 1 cm cell, at room temperature.

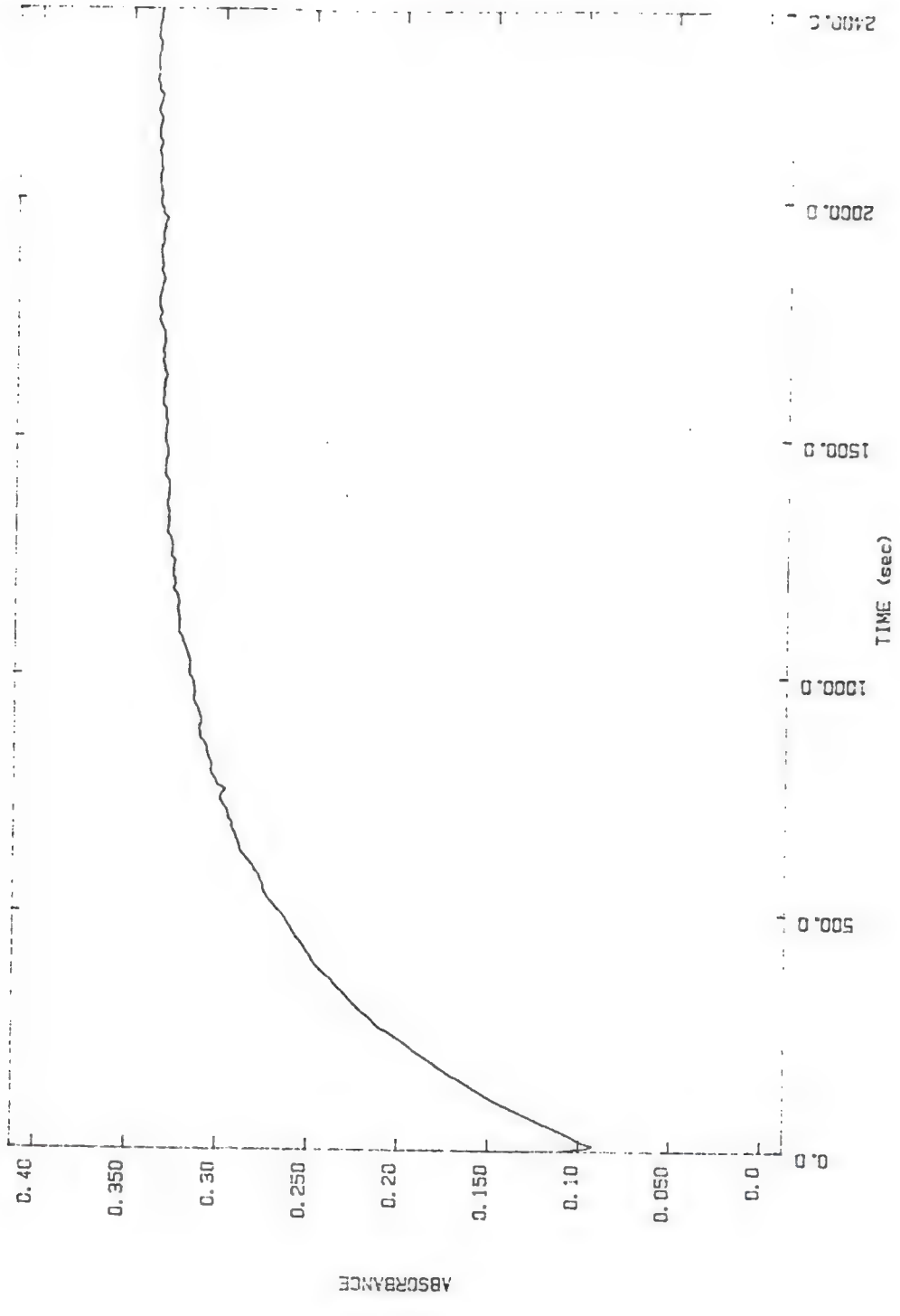
ABSORBANCE
0.40
0.350
0.30
0.250
0.20
0.150
0.10
0.050
0.0
0.0
500.0
1000.0
1500.0
2000.0
2400.0
TIME (sec)

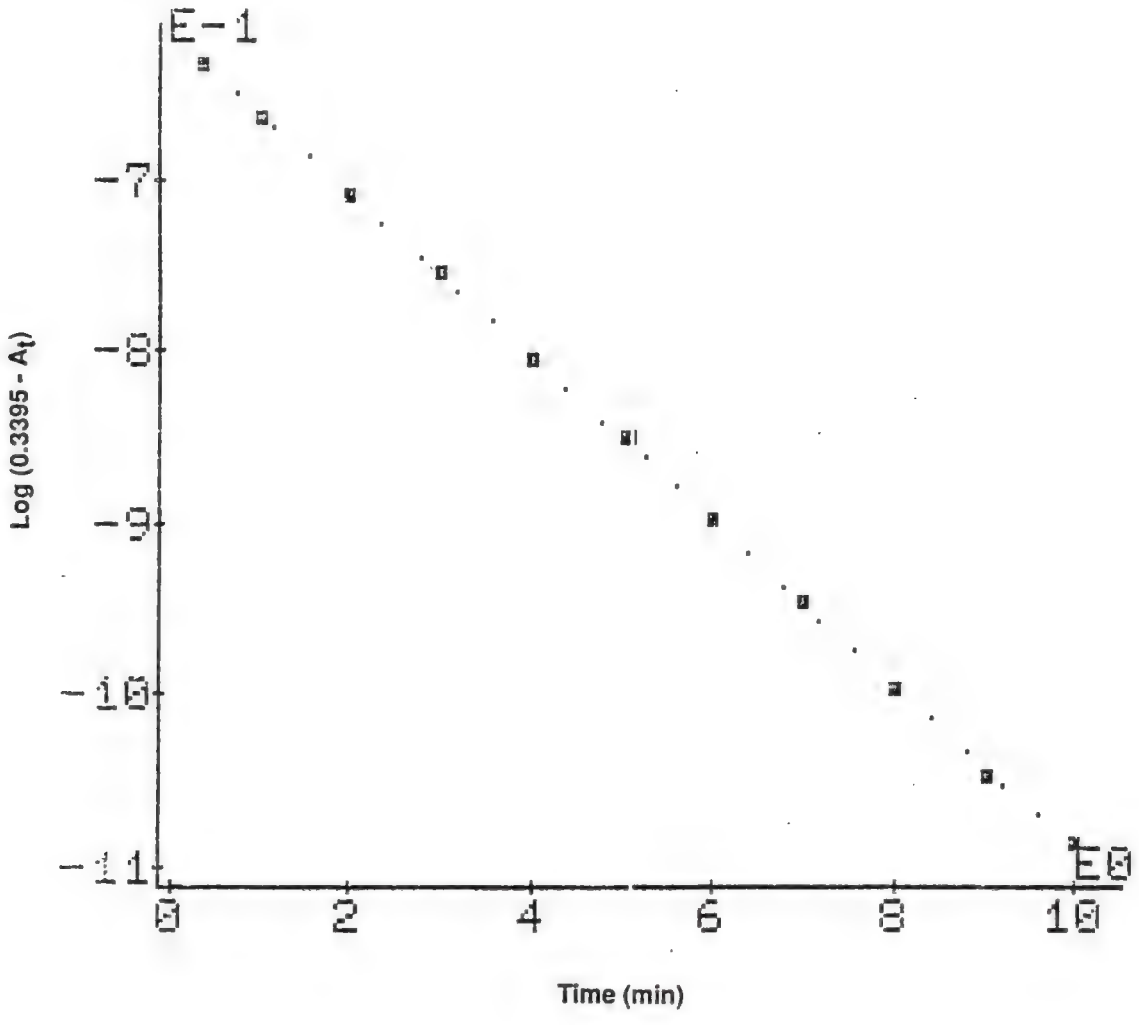

Figure 36. Log ($A_\infty - A_t$) versus time (min) for the detection of salicylic acid in an aqueous system. Acetylsalicylic acid 9.27×10^{-5} M, NaOH 1×10^{-2} M, 1 cm cell, at room temperature, absorbance measured at 298 nm.

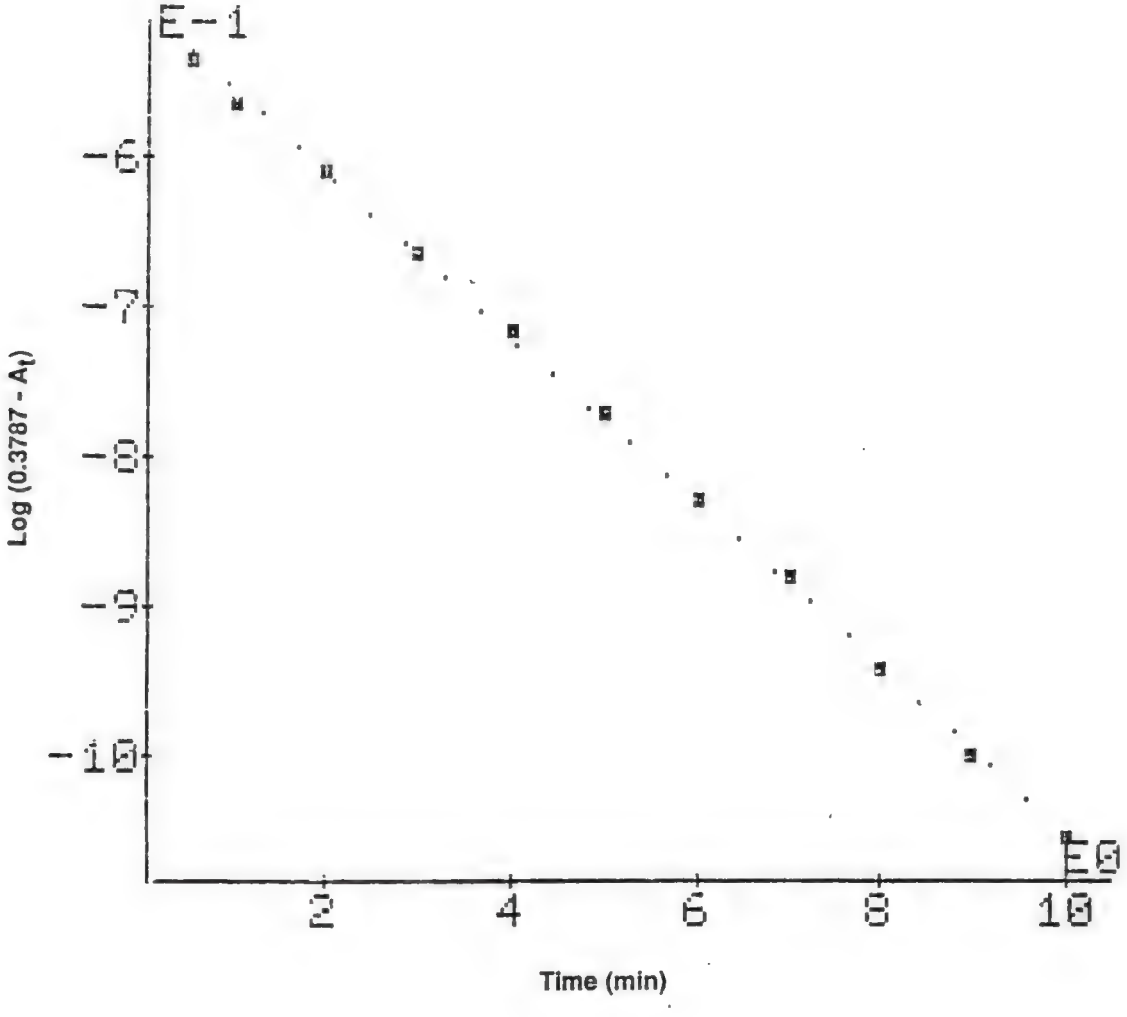

Figure 37. Log (A_∞ - A_t) versus time (min) for the detection of salicylic acid in a 3.38×10^{-3} M CTAB micellar system. Acetylsalicylic acid 9.72×10^{-5} M, NaOH 1×10^{-2} M, 1 cm cell, at room temperature, absorbance measured at 298 nm.

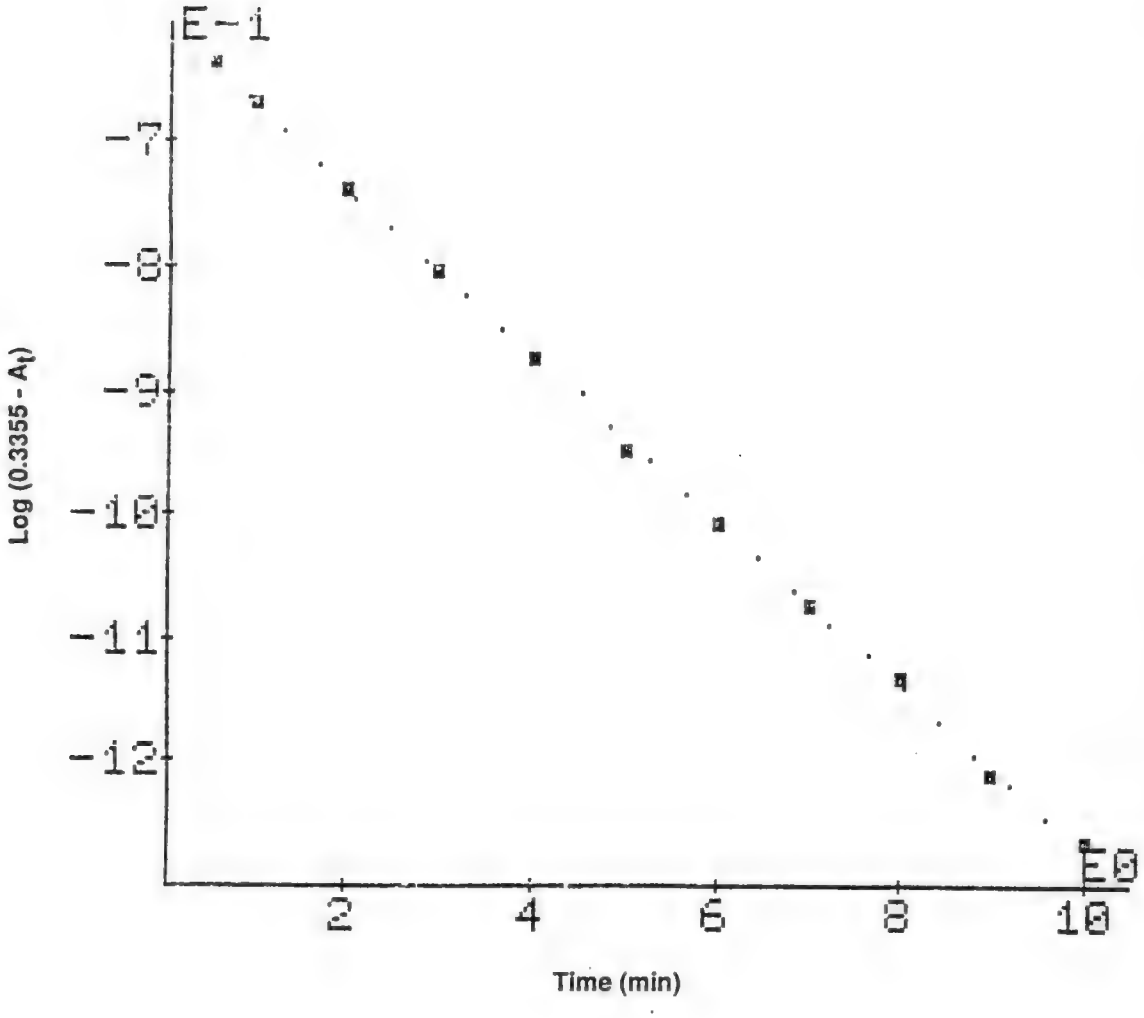

Figure 38. Log ($A_\infty - A_t$) versus time (min) for the detection of salicylic acid in a 99.28% (by weight) water:0.36% CTAB (9.88×10^{-3} M):0.36% butanol microemulsion system. Acetylsalicylic acid 9.72×10^{-5} M, NaOH 1×10^{-2} M, 1 cm cell, at room temperature, absorbance measured at 298 nm.

Table IX. Reaction rate of acetylsalicylic acid (ASA) hydrolysis in various media.

Conc. ASA (10^{-5} M)	Solvent[a]	Abs. at Infinite Time	Rate Constant (min^{-1})
9.72	H_2O	0.340	0.109
9.72	CTAB[b]	0.379	0.127
9.72	Microemulsion[c]	0.335	0.153

[a] All systems 1×10^{-2} M NaOH.

[b] 3.38×10^{-3}M.

[c] Microemulsion composition (wt %):98.8 H_2O:0.6 CTAB:0.6 Butanol. All following references to microemulsion are of this composition.

The rate constants determined for these systems are sufficiently slow to ensure that pseudo first-order kinetics are obeyed (the reaction does not reach completion) throughout the entire flow injection manifold (see Figure 39). The design of the flow manifold should allow for the formation of the product to reach detectable levels within the time from sample injection to detection (residence time). The amount of product formed increases with residence time in the reaction coil but in opposition to this increased product formation is increased dispersion (dilution) and decreased sample throughput which results from increased residence time. Therefore, when determining the operating conditions of an FIA system, it is also necessary to determine which flow rates will yield maximum sample throughput with detectable signals with the optimum system dispersion. The effect of flow rate variation and accompanying dispersion upon the amount of detectable product was examined and a flow rate of 1.0 mL/min was determined to provide maximum peak response (298 nm), minimum interference from reactant (acetylsalicylic acid, 276 nm) and optimum sample throughput.

The performance of the aqueous and microemulsion carrier streams in FIA was then examined by introduction of the acetylsalicylic acid sample into both the microemulsion and aqueous carrier streams. The analytical figures of merit for the base catalyzed hydrolysis of acetylsalicylic acid are summarized in Table X.

As previously mentioned, the experimental parameters (flow rate, reactant concentrations, etc.) of the FIA system have been adjusted to ensure that at the point of detection, the reaction had not reached

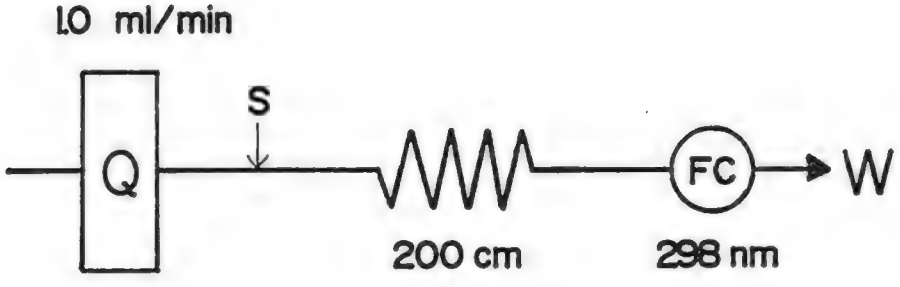

Figure 39. The flow injection manifold employed for the acetylsalicylic acid determination.

Table X. Figures of merit for the base catalyzed hydrolysis of acetylsalicylic acid: wavelength of detection, 298 nm; volume of injection, 20 µL; flow rate, 1.0 mL/min; temperature, 25°C.

	Aqueous[a]	Microemulsion[a]
Sensitivity[b]	3.77×10^{-4}	3.43×10^{-4}
Coefficient of Correlation	0.9993	0.9998
Limit of Detection (ng)[c]	3.5	3.8
Relative Standard Deviation (%)[d]	0.8	1.5
Linear Dynamic Range (ng)	$3.5\text{-}1.77 \times 10^{3}$	$3.8\text{-}1.77 \times 10^{3}$

[a] All solutions 1×10^{-2} M NaOH.

[b] The slope of the calibration curve. Absorbance units/ppm.

[c] Amount of material resulting in a signal three times the standard deviation of baseline noise.

[d] Twelve determinations at four concentrations from 8.86 to 88.6 ppm. The relative standard deviations are pooled estimates (Anderson, 1987).

completion. Equivalent flow rates result in equivalent reaction times for both systems, allowing for an absolute comparison of the progress of the reaction to be made. The response curves for the base-catalyzed reaction of acetylsalicylic acid in aqueous and micro-emulsion systems are shown in Figure 40. The ratio of the slopes of the calibration curves is then equivalent to the ratio of the rates of the two systems. The ratio of the analytical sensitivities (slopes of the calibration curves) of the microemulsion and aqueous systems is 0.9, indicating that the rate enhancement observed in a static system (ratio of sensitivities = 1.4) is not evidenced in the microemulsion/FIA system. The reason for this apparent loss of rate enhancement in the flowing system can be explained by an examination of both physical and chemical contributions to dispersion in flow injection analysis.

As discussed in Chapter I, the dispersion coefficient, D, is the most commonly employed parameter for examining the amount of dilution occurring in a flow injection system. As proposed by Ruzicka and Hansen (1981), it is defined as

$$D = C^{o}/C^{max}, \qquad \text{(eq. 3.2)}$$

where C^{o} is the concentration of the injected sample and C^{max} is the concentration of the sample after the dispersion process. Practically, under conditions which obey the Beer-Lambert law, the definition of D is modified to enable the experimenter to obtain D by

Figure 40. Response signals for the base-catalyzed hydrolysis of acetylsalicylic acid in an aqueous (A) and microemulsion (B) carrier stream (98.8% (by weight) water:0.6% CTAB:0.6% butanol), NaOH 1×10^{-2} M.

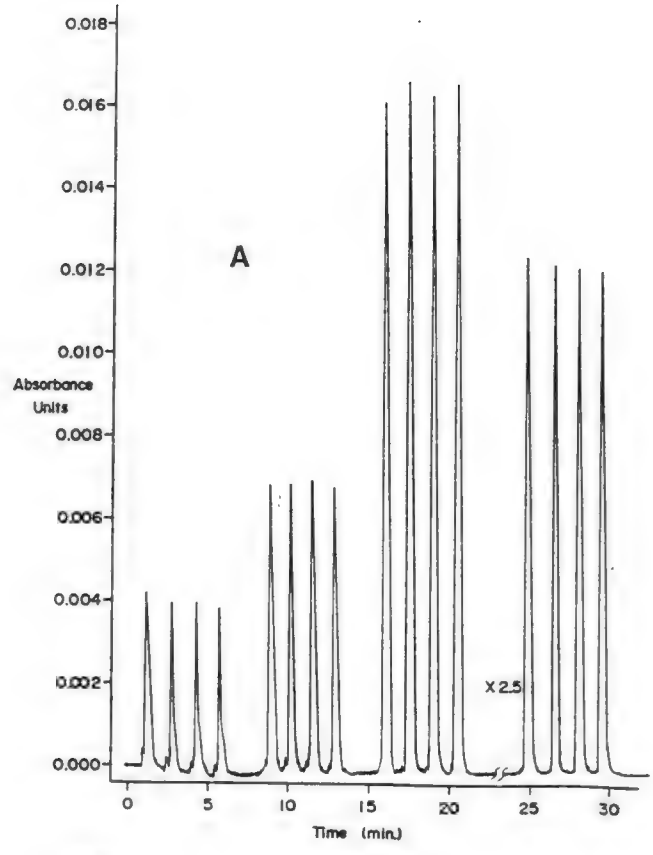
A
0.018
0.016
0.014
0.012
0.010
Absorbance Units
0.008
0.006
0.004
0.002
0.000
X2.5
0
5
10
15
20
25
30
Time (min.)

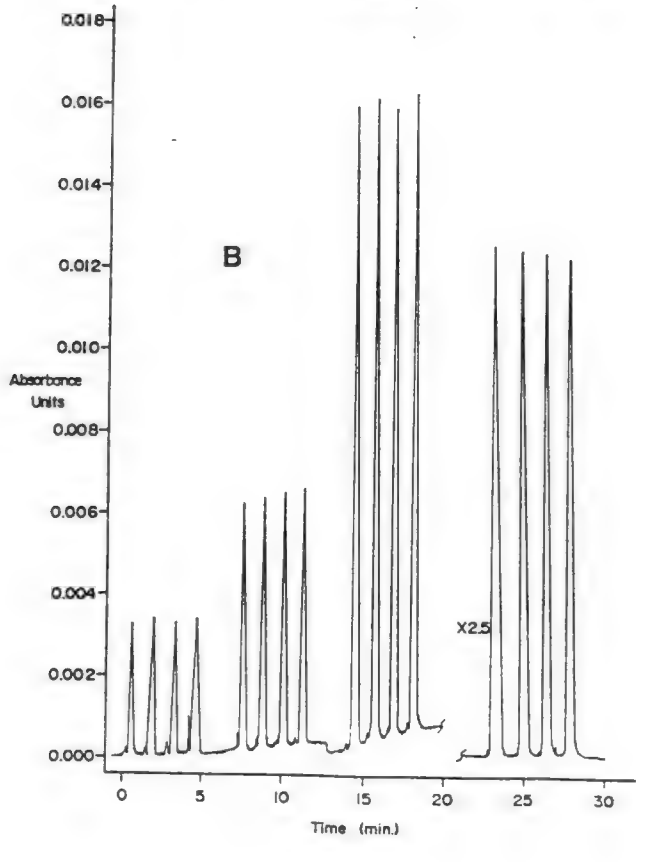
B
0.018
0.016
0.014
0.012
0.010
Absorbance Units
0.008
0.006
0.004
0.002
0.000
X2.5
0
5
10
15
20
25
30
Time (min.)

taking the ratio of peak heights:

$$D = H^{o}/H^{max}, \qquad \text{(eq. 3.3)}$$

where H^{o} is the difference between the baseline and the steady-state response when the sample is introduced directly into the detector and H^{max} is the maximum detector response following the injection and subsequent dispersion of the sample in the FIA system.

The dispersion coefficient for the system was determined using equation 3.3 and the results are given in Table XI. These results are in agreement with earlier findings (Hernandez Torres et al., 1987) which indicate that the dispersion coefficient increases with both an increase in carrier stream viscosity and as the difference in viscosity between the injected sample and the carrier stream increases. Both the increased difference in viscosity between the injected sample and the carrier stream and the absolute viscosity increase ensure a decrease in mass transfer in the radial direction in the reaction coil. This decrease in mixing which occurs across the stream leads to an increase in dilution of the sample plug in the longitudinal direction (Painton and Mottola, 1981). Therefore, due to increased physical dispersion, greater dilution of product concentration will occur in a microemulsive FIA system when compared to an analogous aqueous (nonsurfactant containing) system.

The actual dispersive behavior of the sample plug was determined by an examination of the b/a value (an effective measure of peak tailing) at 10% peak height (Foley and Dorsey, 1983) obtained for the product (salicylic acid) in both microemulsion and aqueous carrier

Table XI. Dispersion values in aqueous and microemulsive systems.

Conc. ASA (10^{-4} M)	Sample Solvent	Carrier Stream	D[a]
5.45	H_2O	H_2O	12.52
5.34	Microemulsion	Microemulsion	14.36
5.45	H_2O	Micromeulsion	16.68

[a] $n \geq 4$ in all cases.

streams. The results of this study are shown in Table XII. An examination of these results yields further information about the physical dispersion process occurring in the sample plug. It is observed that the relative tailing (b/a ratio) which occurs in the microemulsion system is more than 3.5 times that observed in the aqueous system. At the same time it should also be noted that the a value of the microemulsion system is considerably smaller than that of the corresponding aqueous system, a direct indication that the concentration gradient in the leading edge of the sample plug is greater in the case of the microemulsion. This can be attributed to the increased viscosity of the microemulsion and interactions with the inner wall of the tubing in the microemulsion system. The leading portion of the sample plug is compacted due to increased drag effects while the remainder of the sample plug is subject to tailing as a result of adhesion to the tubing walls. For comparison, the resulting sample profiles for two media with physical dispersion only are depicted in Figure 41.

An attempt was then made to examine the contribution of reaction kinetics to the dispersion of the FIA peaks in aqueous and microemulsion systems. Peak shapes obtained in FIA have been described by a modified Gaussian function (Reijn et al., 1981a; Vanderslice et al., 1986). Foley has recently introduced a new method which allows for the accurate manual calculation of peak area as a means of testing the fit of unknown peaks to the exponentially modified Gaussian (EMG) model (Foley, 1987). The consistency of

Table XII. Examination of peak broadening under reactive and nonreactive conditions: wavelength of detection, 298 nm; volume of injection, 20 µL; injected sample, 4.92×10^{-4} M.

	b/a[a]	a (µL)	b (µL)	% Area Variation[b]
No Reaction				
Aqueous	1.24	199	248	2.8
Microemulsion	4.53	91	412	-
Reaction				
Aqueous[c]	1.50	157	234	7.5
Microemulsion[c]	5.69	80	454	-

[a] The average values of a and b for three observations.

[b] Percentage difference in areas determined at 10%, 25%, 50% and 75% peak height (see Chapter IV).

[c] Solutions 1×10^{-2} M NaOH.

Figure 41. A comparison of acetylsalicylic acid sample profiles for plug dispersion in an aqueous (---) and microemulsion (98.8% (by weight) water:0.6% CTAB:0.6% butanol) carrier stream. No reaction occurring, 276 nm detection.

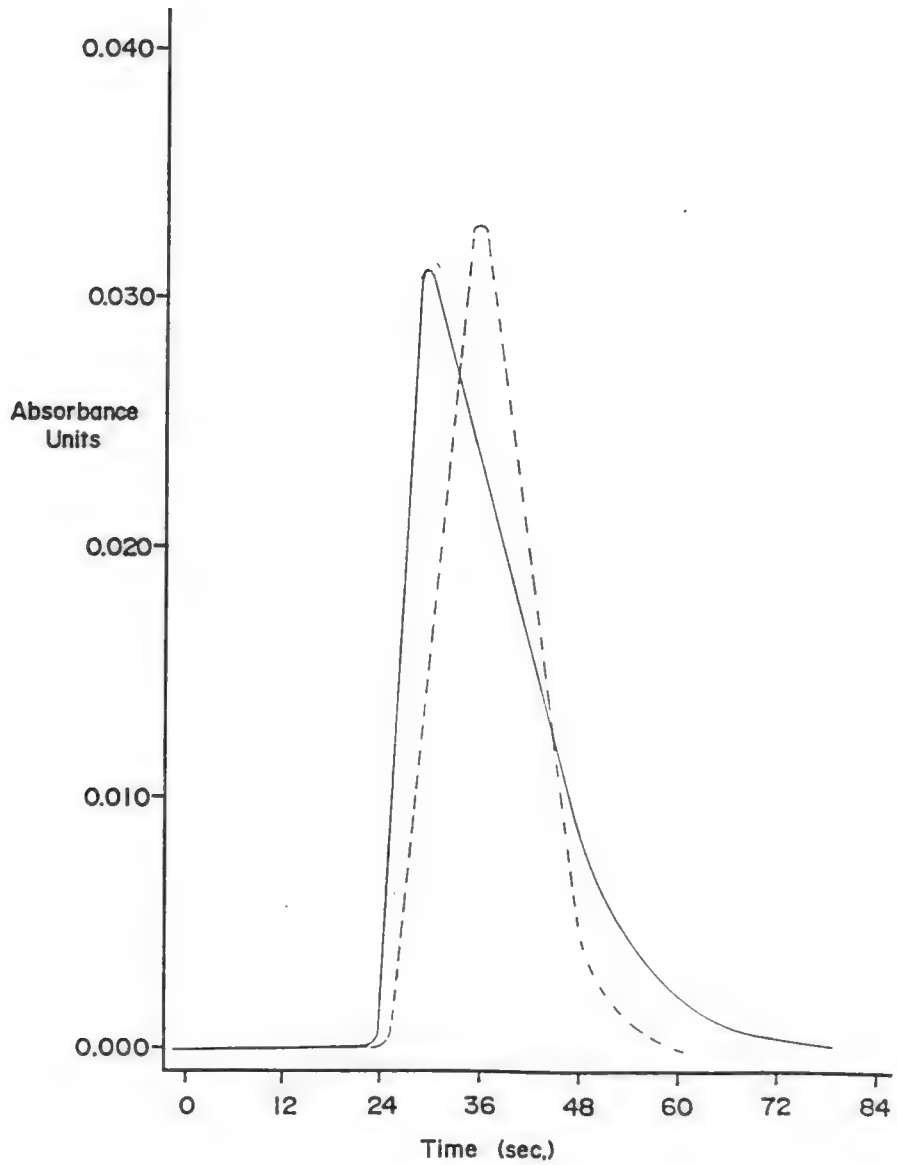
0.040
0.030
Absorbance Units
0.020
0.010
0.000
0
12
24
36
48
60
72
84
Time (sec.)

calculated areas at 10%, 25%, 50% and 75% of total peak height allows for the determination of EMG character in an asymmetric peak. Agreement of calculated areas to within 10% of the average area value will constitute an EMG peak for the present work. Table XII indicates that EMG peaks are obtained for the aqueous system but the large b/a ratio in the case of the microemulsion carrier streams excludes the peaks from theoretical consideration (the accuracy of the Foley model is for the range $1.00 \leq b/a \leq 3.60$). It is apparent that in the presence of a chemical reaction, for the reaction under investigation, the dispersion of the system and the shape of the peak itself is modified.

An extension of this work (Chapter IV) is aimed at deconvoluting the individual contributions to dispersion (physical and chemical) and arriving at an improved measure of dispersion in an FIA system. The generation of EMG peaks and application of existing theory (Foley and Dorsey, 1983; Anderson and Walters, 1984) to the manual calculation of statistical moments (M_2) may allow for the separation of the contributions from purely physical and chemical phenomena in FIA by the principle of the additivity of variances.

The results presented in this chapter indicate that to justify the use of a microemulsive carrier stream in flow injection analysis, the accompanying increase in reaction rate due to microemulsion catalysis or in detectability must be large enough to overcome inherent losses in sensitivity which are encountered when using higher microviscosity carrier streams. Additionally, the dispersion processes are clearly different in the case of aqueous and surfactant

containing carrier streams. A method for the separation of those contributions to the dispersion process which are purely physical from those resulting from chemical reactions will provide valuable fundamental information, leading to a better understanding of the differences between the two systems and an improved method for the measurement of dispersion in an FIA system.

CHAPTER IV
THE SECOND MOMENT AS A DIRECT MEASURE OF DISPERSION IN FLOW INJECTION SYSTEMS

Introduction

Flow injection analysis (FIA) is firmly established as a rapid, precise, efficient and extremely versatile analytical tool. Ruzicka and Hansen (1986), however, recently reviewed the status quo in the field of FIA and concluded that

> the theory of FIA, unfortunately, is still at a rather lamentable level compared with the sophisticated level of many of the practical developments. The concept of controlled dispersion, based on the dispersion coefficient, is a useful tool for the rational design of a flow system and for comparison and scaling of channels in FIA, yet it does not describe the response in a comprehensive fashion. (p. 20)

There have been numerous attempts to derive a general expression to describe concentration as a function of time in a flow injection system. Historically, Taylor (1953, 1954) was the first to quantitatively treat the concept of axial dispersion occurring in straight, open tubes. Taylor's solutions of the diffusion-convection equation are most accurate for regions of flow where convection (high flow rates) or diffusion (low flow rates) are the dominant contributions to dispersion. Flow rates commonly employed in FIA result in conditions which are intermediate between these two limiting regions and are described by laminar flow. Dispersion in FIA is a

consequence of both convective transport (axial direction) and diffusional transport (axial and radial directions) of sample molecules within the flow manifold. Ananthakrishnan and coworkers (Ananthakrishnan et al., 1965; Gill and Ananthakrishnan, 1967) were the first to provide numerical methods for the solution of the diffusion-convection equation for intermediate values of reduced mean residence times. Most FIA experiments do not lie within these theoretically treated regions (Vanderslice et al., 1981) and, therefore, are not accurately described by either of these models. Painton and Mottola (1983, 1984) were the first to derive and test a numerical model which included values of reduced time (τ) and Peclet numbers (Pe) that are typically found in flow injection systems.

The general aim of the theoretical work in the field has been to relate the characteristics of the signal profile to the experimental parameters of the FIA system. Common descriptors of an FIA response curve include the baseline-to-baseline time of the peak, travel time, mean residence time, theoretical plate height, peak area and peak height. Experimental parameters which directly affect the response curve (and the descriptors of the response curve) and are commonly used to describe the manifold conditions include flow rate, sample volume, tube radius, coil radius and reactor length. Additionally, the intrinsic characteristics of the carrier stream itself drastically affect the resulting response curve and must be considered in an accurate theoretical treatment for flow injection systems. It is obvious that any universally applicable theoretical treatment of FIA manifolds must include all iterations of the FIA manifold and

resulting effects upon the response curve, requiring the consideration of a myriad of experimental variables.

The dispersion coefficient, D, is the most common descriptor of dilution in an FIA system and is defined as the ratio of the concentration injected into the system to the concentration at peak maximum. Experimentally, the value of D is determined by introducing an undiluted standard sample of known concentration directly into the flow-through detector to obtain a steady-state response height, H_o. The FIA manifold is then operated with the carrier stream of choice and the standard is introduced into the continuously moving stream in the form of an injected sample. This ensures that the sample molecules will interact with the surrounding carrier stream, resulting in dilution of the sample and a subsequent peak height response, H_{max}, which is less than or equal to H_o. If the linear region of the calibration curve includes both C_o and C_{max} (the concentrations corresponding to H_o and H_{max}), $D = H_o/H_{max}$ and is equivalent to the dispersion of the flow injection manifold under investigation. The overall dispersion within an FIA system is equivalent to the sum of the dispersions originating from the injection, transport and detection processes in the system:

$$D_{total} = D_{injection} + D_{transport} + D_{detection} \qquad \text{(eq. 4.1)}$$

Many workers have examined the effect of manifold design and experimental parameters upon the response curve in an attempt to develop a more accurate measure of dispersion in a flow injection

system. Coiling of the tubing has been shown to introduce additional mechanisms of transport (Tijssen, 1980; Reijn et al., 1981; LeClerc et al., 1986) which obscure the significance of D. Additionally, as the FIA manifold becomes more complex in design, any available theory becomes increasingly inadequate in attempts to predict the behavior of the system. Vanderslice et al. (1981) first showed that the solute diffusion coefficient and tube radius directly affect dispersion. More recently, Hernandez Torres et al. (1987) and Loscascio-Brown et al. (1988) have shown that carrier stream viscosity plays a role in dispersion. Stults et al. (1987) investigated the effect of temperature on dispersion in flow injection systems with and without a chemical reaction occurring. The major advantage of basing the dispersion measurement upon peak height is that the peak maximum is easily located on the response curve. The concept of dispersion, however, is of limited utility in conveying information about the FIA system since it only accounts for dilution which affects peak height. The measurement of peak height also places an upper limit on the working range of concentrations as a result of either detector sensitivity limits or limited linearity of the analyte calibration curve.

Ruzicka et al. (1977) and Vanderslice et al. (1981) have derived expressions which allow one to derive a relationship between the geometric and hydrodynamic characteristics of a flow manifold and the resultant FIA peak shape. In practice, however, these expressions cannot be directly used, due to the effect of the longitudinal dispersion number (Levenspiel and Smith, 1957) and the accommodation

factor (Vanderslice et al., 1981) upon the FIA signal. The longitudinal dispersion number accounts for the non-Gaussian character of the observed response curves and is directly related to the variance of the response curve (Ramsing et al., 1981). The accommodation factor was introduced to compensate for the difference between the theoretical data and experimental values obtained for peak descriptors. Application of a computer program and a logarithmic multiple regression analysis allowed Valcarcel and Luque de Castro (1987) to obtain empirically fitted equations which allow for the determination of the relationship between the geometric and hydrodynamic characteristics of a defined manifold and the FIA signal. Unfortunately, these equations, derived for a given system, cannot be directly applied to any other FIA system due to different characteristics of the injector, connectors and flow cell.

Much less visible in the literature have been attempts to examine FIA peak shapes and to use these descriptors to gain a better understanding of the dispersion process in the system. Tyson (1986) derived equations for relating peak width to injected concentration for single line and merging stream manifolds containing a mixing chamber to generate concentration gradients. Poppe (1981) first reported that the total peak broadening in an FIA system was the sum of the individual contributions. Analogous to chromatographic systems (Huber, 1969; Kirkland, 1977), the total variance of the system was described by the contributions from the injection process, flow-through reactors and connectors, the flow-through volume of the detector and the time constants of the associated electronics. The

total band broadening under conditions of no reaction contains contributions from these sources (Reijn et al., 1981) and results in an equation that is completely analogous to equation 4.1:

$$\sigma^2_{peak} = \sigma^2_{injection} + \sigma^2_{transport} + \sigma^2_{detection} \qquad \text{(eq. 4.2)}$$

Assuming that the flow-through detector and the electronics of the detector are well designed, $\sigma^2_{detection}$ may be neglected and the total variance is given by

$$\sigma^2_{peak} = \sigma^2_{injection} + \sigma^2_{transport} \qquad \text{(eq. 4.3)}$$

Several workers (Reijn et al., 1981; Vanderslice et al., 1986; Hernandez Torres et al., 1987) have described the distribution curve of a flow injection peak to be a modified Gaussian function. The exponentially modified Gaussian (EMG) function is obtained by the convolution of the Gaussian function and an exponential decay function, providing an asymmetric peak profile. The exponentially modified Gaussian function describes many peaks of analytical interest and the EMG model itself has recently been reviewed (Foley and Dorsey, 1984). Ramsing et al. (1981) were the first to propose the use of variance as a measure of peak width and to explore its relationship to dispersion in FIA. Reijn et al. (1984) proposed that more fundamental information about the dispersion process in flow injection systems could be obtained by analyzing the statistical moments of the residence time distribution function. Statistical moments have not

been commonly used to describe FIA peaks due to the need for digital data acquisition and subsequent computer processing. Foley and Dorsey (1983), however, have derived expressions for the calculation of chromatographic figures of merit of Gaussian and EMG peaks which allow for manual calculation of statistical moments.

Only limited attention has been given to the effect of chemical reaction upon dispersion (Betteridge et al., 1983; Painton and Mottola, 1983, 1984; Hungerford and Christian, 1987). Painton and Mottola (1981) were the first to assess the kinetic contribution to the overall dispersion in a flow injection system. The kinetic contribution to dispersion was determined by subtracting the dispersion coefficient due to purely physical factors from the dispersion coefficient obtained in the presence of a chemical reaction. In the presence of chemical reactions, the dispersion coefficient loses much of its significance, since it conveys little information related to peak width (an indication of the throughput of the system) and there is much difficulty in determining H_o (with a reaction occurring, H_o is no longer time independent). For a flow injection system which produces Gaussian or EMG peaks under conditions without chemical reaction, the principle of additivity of variances allows the addition of the effect of a chemical reaction to equation 4.3 and the total variance of the resulting EMG peak is given by

$$\sigma^2_{peak} = \sigma^2_{injection} + \sigma^2_{transport} + \sigma^2_{chemical\ reaction} \qquad \text{(eq. 4.4)}$$

This chapter examines a new method for defining dispersion in FIA based upon the presence of EMG peaks and calculation of the resulting second central moment. Reporting dispersion in an FIA system as a variance offers several advantages over the classical dispersion coefficient: (1) peak width is immediately obtainable from the variance, (2) two FIA systems can be readily compared from their variance values, (3) the difference in peak widths may be obtained in either units of time or volume, yielding a more direct measure of sample throughput and (4) the individual contributions to the total peak variance (including the contribution of the chemical reaction to the total variance) may be easily obtained through the additivity of variances.

Experimental

An Isco (Lincoln, NE) Tris model peristaltic pump propelled the carrier streams. Sample volumes of 20 µL were introduced by a Valco Instrument Co. (Houston, TX) C6W injector. All tubing used was teflon (1/16" od, 0.5 mm id) from the Anspec Co. (Ann Arbor, MI). The flow manifold was a 100 cm tubing, with its shape being straight or coiled with a coiling diameter of approximately 14 mm. The total volume of the flow manifold (including injector and preflow cell detector tubing) was determined by measuring the time from sample injection to initial baseline disturbance at 10 flow rates (3 trials each) between 0.058 and 0.26 mL/min. The injection of an aqueous 0.10 M NaI solution yielded a manifold volume of 299±2 µL. Ionic solutes in the carrier stream were detected by an LDC/Milton Roy (Riviera Beach, FL)

conductoMonitor III conductivity detector and the resulting output signals were recorded on a Houston Instrument (Austin, TX) Fisher Randall Series 5000 recorder. All least squares calculations were performed by Interactive Microware, Inc. (State College, PA) Curve Fitter program run on an Apple II Plus microcomputer. All injections were performed at room temperature (25±1°C) without temperature control.

Chemicals

Sodium iodide (Fisher Scientific Co., Fairlawn, NJ), 2-iodo-2-methylbutane (tert-amyl iodide) (ICN Biomedicals, Inc., K + K Labs, Plainview, NY) and absolute ethyl alcohol (Florida Distillers Co., Lake Alfred, FL) were all used as received. The water used in the preparation of carrier streams was deionized.

Reaction

The reaction chosen for this study was the hydrolysis of 2-iodo-2-methylbutane in aqueous ethanol (80% by volume ethanol in water):

$$C_5H_{11}I + 2H_2O \longrightarrow C_5H_{11}OH + H_3O^+ + I^-$$

The conductivity of the sample zone is monitored in the FIA system and increases as the reaction proceeds, due to the formation of the hydronium and iodide ions. The reaction is first order in $C_5H_{11}I$ and the rate of the reaction is independent of the pH of the solution (Matthews, 1985).

Theory

Foley (1987) has recently developed empirical equations for the accurate calculation of peak area of Gaussian and exponentially

modified Gaussian peaks. Based on measurements of peak height, width and asymmetry, the equations are also useful in determining whether or not an experimental peak is Gaussian or EMG in nature. Equations 4.5-4.8 were used here to calculate the peak areas at 10%, 25%, 50% and 75%, respectively, of the total peak height.

$$A = 0.586 h_p W_{0.10} (b/a)^{-0.133} \qquad \text{(eq. 4.5)}$$

$$A = 0.573 h_p W_{0.25} \qquad \text{(eq. 4.6)}$$

$$A = 1.07 h_p W_{0.50} (b/a)^{+0.235} \qquad \text{(eq. 4.7)}$$

$$A = 1.64 h_p W_{0.75} (b/a)^{+0.717} \qquad \text{(eq. 4.8)}$$

where A is the peak area, h_p is the height of the peak, W is the width of the peak at the designated peak height fraction as indicated by the subscript and b/a is the asymmetry factor measured at the same peak height fraction as the width (Figure 42). A Gaussian or EMG peak is indicated by agreement of calculated areas at the four peak heights. The largest relative error of equations 4.5-4.8 from the true area of a Gaussian or EMG peak is given by the author as -1.2%, +1.0% over the interval $1.00 \leq (b/a)_{0.1} \leq 3.60$ (Foley, 1987).

Equations 4.5-4.8 were used to verify that the peaks exiting the flow injection system were either Gaussian or EMG in character. These equations can be used to examine unknown peaks for their fit to the Gaussian or EMG model. The goodness of fit is determined by the agreement of calculated areas at the four peak heights. For the present work, if the largest outlier from the mean area determined

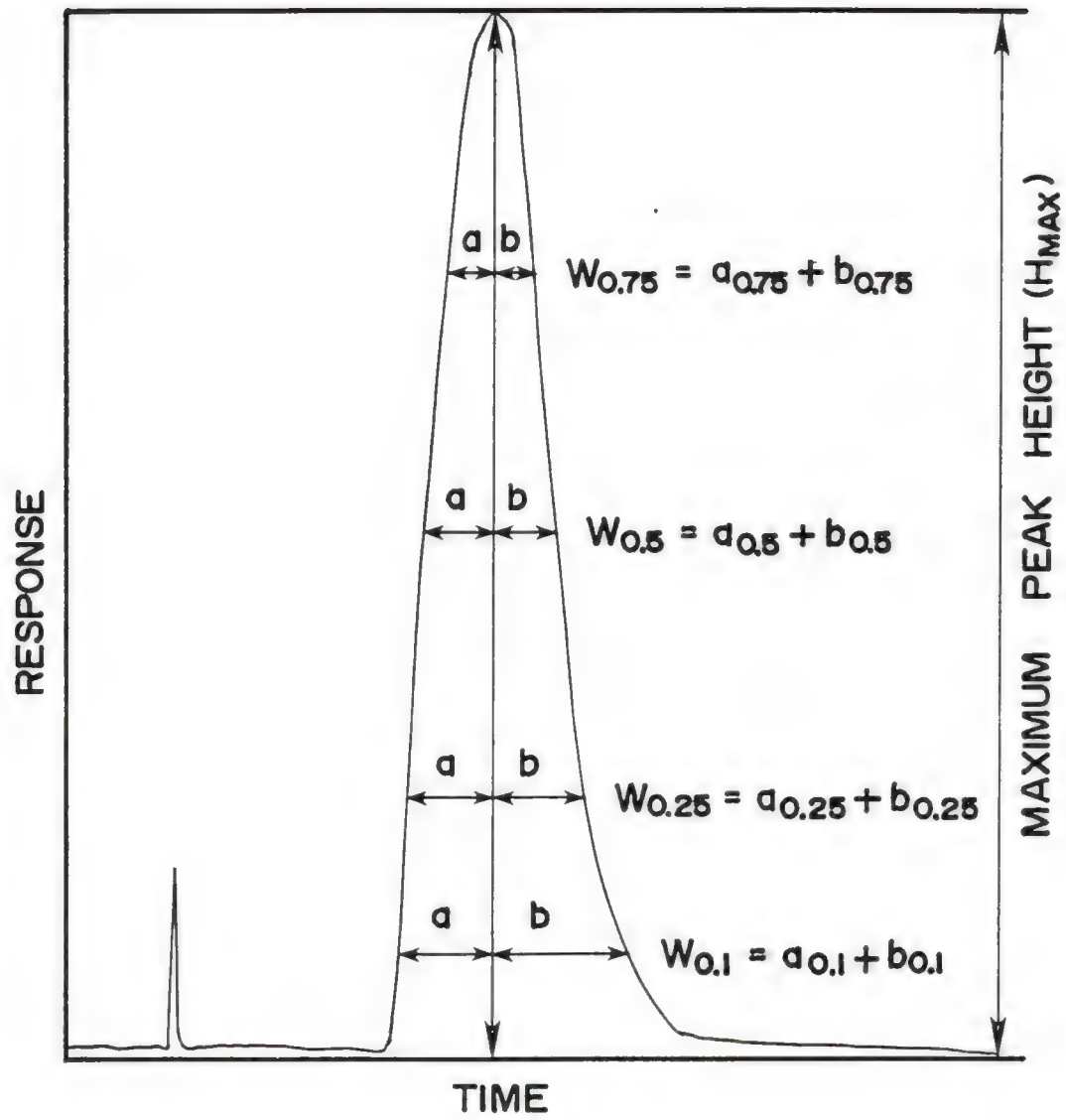

Figure 42. Measurement of peak width, W, and asymmetry factor, b/a, at 10, 25, 50, and 75% of peak height on an FIA response curve.

using equations 4.5-4.8 was within 20% of the mean area calculated at the four heights, the peak was considered to be EMG in nature (3 trials). Once the Gaussian character of the peak was verified, the following equation was used to calculate the second moment (variance) of the peak:

$$M_2 = (W_{0.1})^2/[1.764(b/a)^2 - 11.15(b/a) + 28] \qquad \text{(eq. 4.9)}$$

where M_2 is the second moment (Foley and Dorsey, 1983) and the additional variables are defined as in equations 4.5-4.8. For the asymmetry range of $1.00 \leq (b/a) \leq 2.76$, equation 4.9 results in a relative error of -1.5%, +0.5%.

For asymmetry values greater than 2.76, Anderson and Walters (1984) have modified the equations of Foley and Dorsey (1983) and extended the range of usable asymmetry values to b/a = 5.6 ($\tau/\sigma = 6.8$). Using this modification, the second moments for the asymmetry range $2.77 \leq (b/a) \leq 5.6$ were calculated using

$$M_2 = (W_{0.1})^2/[7.35 + 22.6\exp(-0.708(b/a)_{0.1})] \qquad \text{(eq. 4.10)}$$

The maximum relative error using equation 4.10 is given as -0.7%, +1.0% by the authors (Anderson and Walters, 1984).

As previously mentioned, an EMG function is a convolution of the pure Gaussian function and an exponential modifier. The variance of an exponentially modified Gaussian peak is equivalent to the second moment (M_2) and is described by

$$\sigma^2_{\text{EMG peak}} = M_2 = \sigma_G^2 + \tau^2 \qquad \text{(eq. 4.11)}$$

where σ_G^2 is the variance resulting from purely Gaussian processes and τ is the time constant of the exponential peak tailing function.

The methods of Foley and Dorsey (1983) and Anderson and Walters (1984) can again be used to calculate the variance of the peak due to processes which are purely Gaussian in nature:

$$\sigma_G = W_{0.1}/[3.27(b/a) + 1.2] \qquad \text{(eq. 4.12)}$$

for $1.09 \leq (b/a) \leq 2.76$, percent relative error limit of -1.0%, +0.5% and

$$\sigma_G = W_{0.1}/[3.38(b/a) + 0.969] \qquad \text{(eq. 4.13)}$$

for $2.77 \leq (b/a) \leq 5.6$, percent relative error limit of -1.3%, +1.6%. Having calculated the second moment and the variance of the underlying Gaussian peak, it is possible to quantitatively separate both the exponential time constant and the contribution resulting from Gaussian processes from the overal peak variance through equation 4.11.

The use of this asymmetry-based method for peak analysis is appealing because of the simplicity of measurement of the necessary variables needed to find M_2, σ_G and τ. Once the exponentially modified Gaussian character of a peak has been verified, it is necessary only to measure the values of a and b at 10% peak height to obtain M_2, σ_G and τ. The accuracy of measurement using this method can be maximized by adhering to the following suggested measurement

conditions (Foley and Dorsey, 1983): (1) a chart speed yielding $W_{0.1} \geq 4.3$ cm, (2) minimum distance for appearance of flow injection peak maximum: 10 cm and (3) a minimum peak height, $h_p \geq 10$ cm. The b/a ratio itself has the additional advantage of agreeing with the intuitive perception of peak asymmetry (Bidlingmeyer and Warren, 1984).

Results and Discussion

The dispersion coefficient of the system was determined using an aqueous NaI solution. The value of the time-independent conductance signal height (H_o) corresponding to undiluted 0.10 M NaI was determined to be 585 μS. To determine the response height equivalent to the maximum concentration of the injected sample (H_{max}), 20 μL of 0.10 M NaI was injected into a straight 100 cm tubing with an aqueous carrier stream. The straightness of the tubing was ensured by strapping it to a 98 cm length of angle iron. The variation of D (3 trials) with flow rate was examined over the range of 0.058-1.03 mL/min. Figure 43 shows that the resulting plot of dispersion vs. flow rate is fit by a logarithmic equation of the form $Y = 7.99X^{0.397}$ with a correlation coefficient of 0.999.

Another common descriptor of flow injection response curves is the area of the peak. Using equations 4.5-4.8, the average area of the response curves (3 trials) was determined for the 100 cm straight tubing manifold over the flow rate range of 0.058-1.03 mL/min. Figure 44 shows the relationship between peak area and flow rate is again

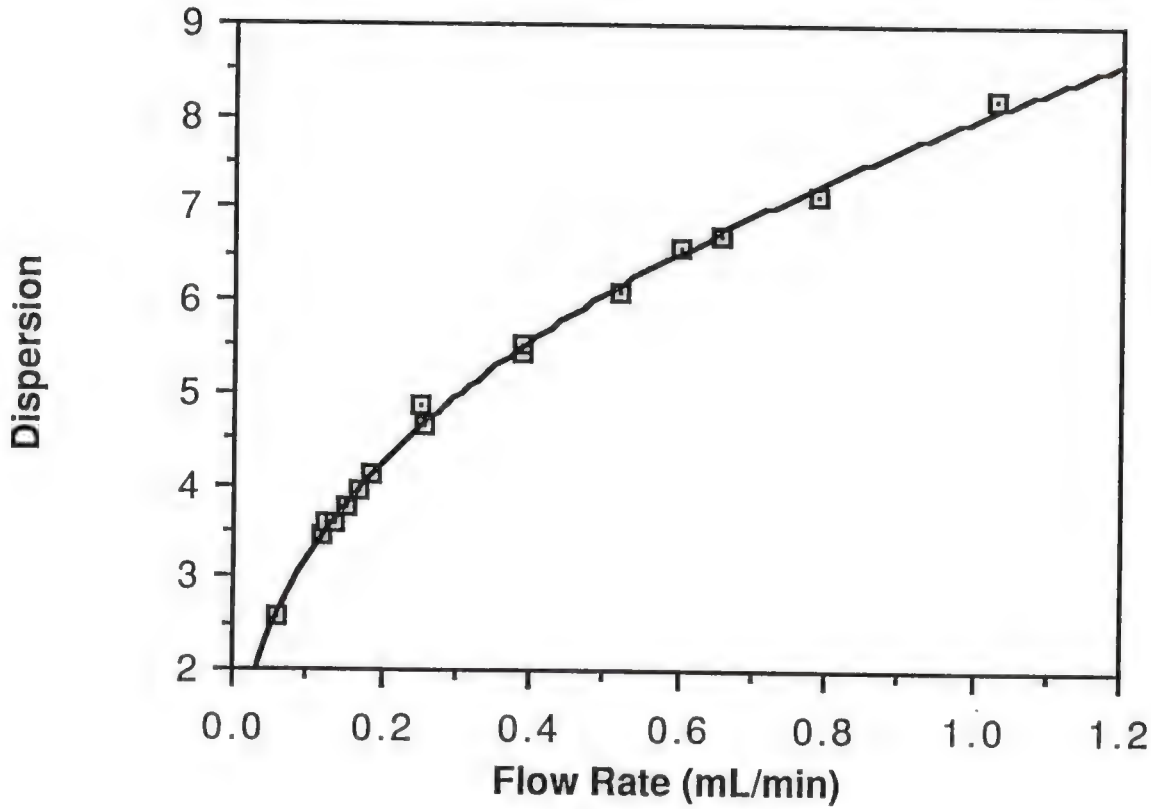

Figure 43. Plot of dispersion versus flow rate for a 20 µL sample of 0.10 M NaI injected into a 100 cm straight tubing manifold.

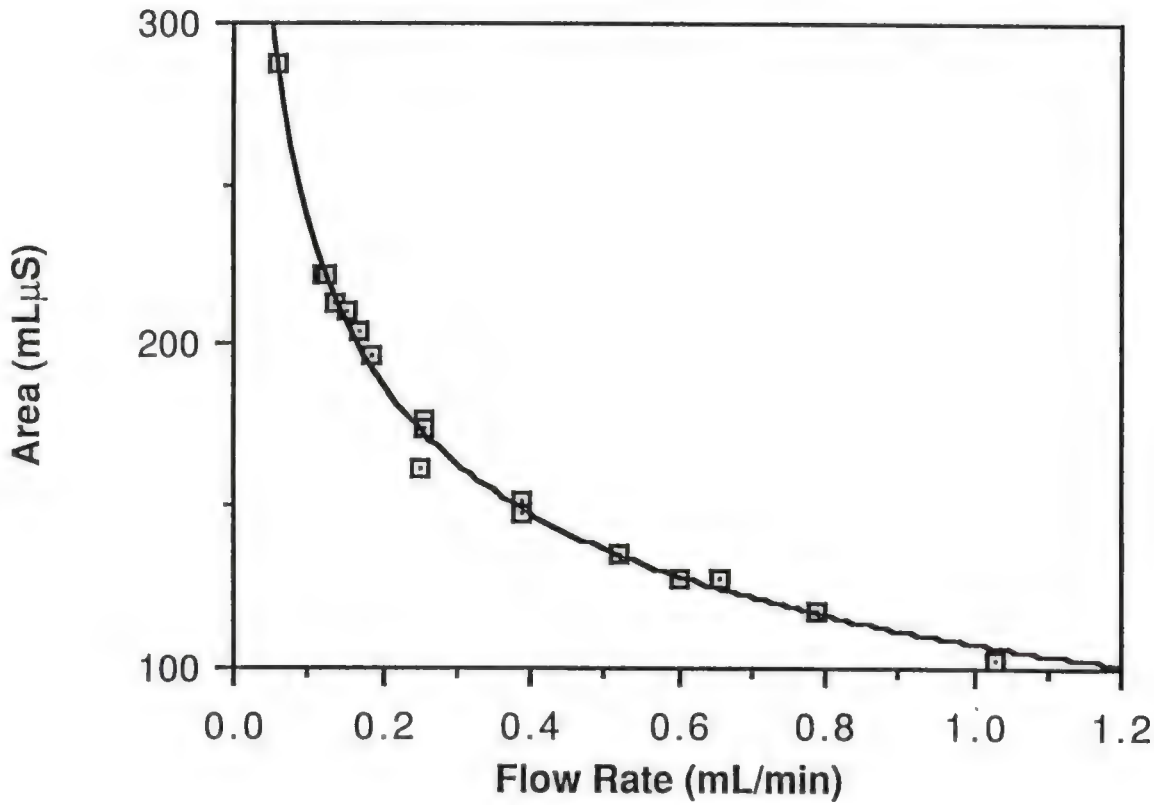

Figure 44. Plot of peak area (as determined by equations 4.5-4.8) versus flow rate for a 20 μL sample of 0.10 M NaI injected into a 100 cm straight tubing manifold.

most accurately described by a logarithmic equation, $Y = 107.6X^{-0.349}$ with a correlation coefficient of 0.999. Although peak area relays more direct information of peak size than the dispersion coefficient, it yields no information concerning the shape of the peak and no information in the time domain. For the detection system employed in this work, an additional drawback of area as an FIA peak descriptor was that as the sensitivity setting of the conductance detector was varied, the absolute area values were not consistent, severely limiting the linear range of the descriptor.

The agreement of the calculated areas at 10%, 25%, 50% and 75% of total peak height can be used to verify the exponential character of the peaks under investigation. Table XIII shows that as the flow rate of the system is increased, the percent deviation in the calculated area increases. For the 51 determinations of peak area for the 100 cm straight tubing, 73% of the peaks were found to fit the EMG model to within 15%. A large majority of the peaks that did not fit the model to within 15% were at the higher flow rates. At flow rates of less than 0.6 mL/min, 90% of the peaks fit the model within 15%, 92% fit the model to within 20%. This apparent aberration from EMG character at high flow rates can be explained by considering two factors: (1) the relatively short manifold length (100 cm) ensures that at high flow rates, less time will be available for diffusional averaging within the sample plug and, most importantly, (2) the straight character of the manifold minimizes mixing within the tube in the radial direction which again results in less averaging of the concentration within the sample plug. It was observed that by coiling

Table XIII. The effect of flow rate upon dispersion (D), area, % deviation of calculated areas (% Dev.), second moment (M_2) and standard deviation of the underlying Gaussian peak (σ_G) in a flow injection system.

Flow Rate (mL/min)	D	Area (mL-μS)	% Dev. (%)	M_2 (μL^2)	σ_G (μL)
0.0576	2.58	287	5.6	746	21.3
0.122	3.45	222	11.9	1371	29.5
0.126	3.58	222	14.3	1557	28.3
0.139	3.60	213	9.7	1640	32.2
0.154	3.76	211	11.6	1860	30.1
0.172	3.93	204	10.1	2112	32.3
0.187	4.11	197	9.4	2184	34.2
0.254	4.84	162	7.1	3053	39.7
0.257	4.63	177	10.2	3105	39.0
0.259	4.64	174	11.4	2782	35.4
0.387	5.44	152	9.3	4443	41.9
0.391	5.54	148	10.6	4395	41.6
0.521	6.10	135	13.1	5554	41.6
0.605	6.59	128	15.6	6776	42.5
0.659	6.71	128	17.0	7658	40.6
0.787	7.17	118	16.7	8657	42.7
1.03	8.22	102	20.9	10385	41.9

Note: Injected sample 0.10 M NaI solution, 20 μL sample volume, 100 cm straight manifold. All results indicate the average value of three trials.

the 100 cm tubing (coiling radius 14 mm), a flow rate of 1.04 mL/min resulted in asymmetric peaks which fit the EMG model to within 10% (an average of 7.80% for 3 trials). Having verified the EMG character of the peaks, equations 4.9 and 4.10 may be applied to examine the dependence of the second moment upon flow rate for this system. Figure 45 shows that there is a linear relationship ($Y = 1.04 \times 10^{4}X + 290$, $r = 0.999$) between M_2 and the flow rate for 20 µL of 0.10 M NaI injected into the 100 cm straight tubing.

We next examined the reproducibility of the second moment and the standard deviation of the underlying Gaussian peak as EMG peak descriptors in a flow injection system. Table XIV shows that for a 20 µL sample of 0.10 M NaI and a flow rate of 1.03 mL/min, the average second moment is 10385±676 μL^2 (RSD = 6.5%). The standard deviation of the parent Gaussian (σ_G) is 41.9±1.9 µL (RSD = 4.5%) for the same 10 trials. Table XV shows that the effect of changing concentration and detector sensitivities on M_2 and σ_G is negligible for the examined system. The contribution of purely Gaussian processes (diffusion related) is minimized as the flow rate is increased in the straight manifold. It is expected, therefore, that as the flow rate is increased, the percent contribution of Gaussian processes to total peak variance would be decreased. The use of equation 4.11 allows us to quantitatively examine the percent contribution of purely Gaussian processes to total peak variance as shown in Figure 46.

Hydrolysis of t-Amyl Iodide

The results of the moment analysis for the response curves monitoring the products of the t-amyl iodide reaction are shown in

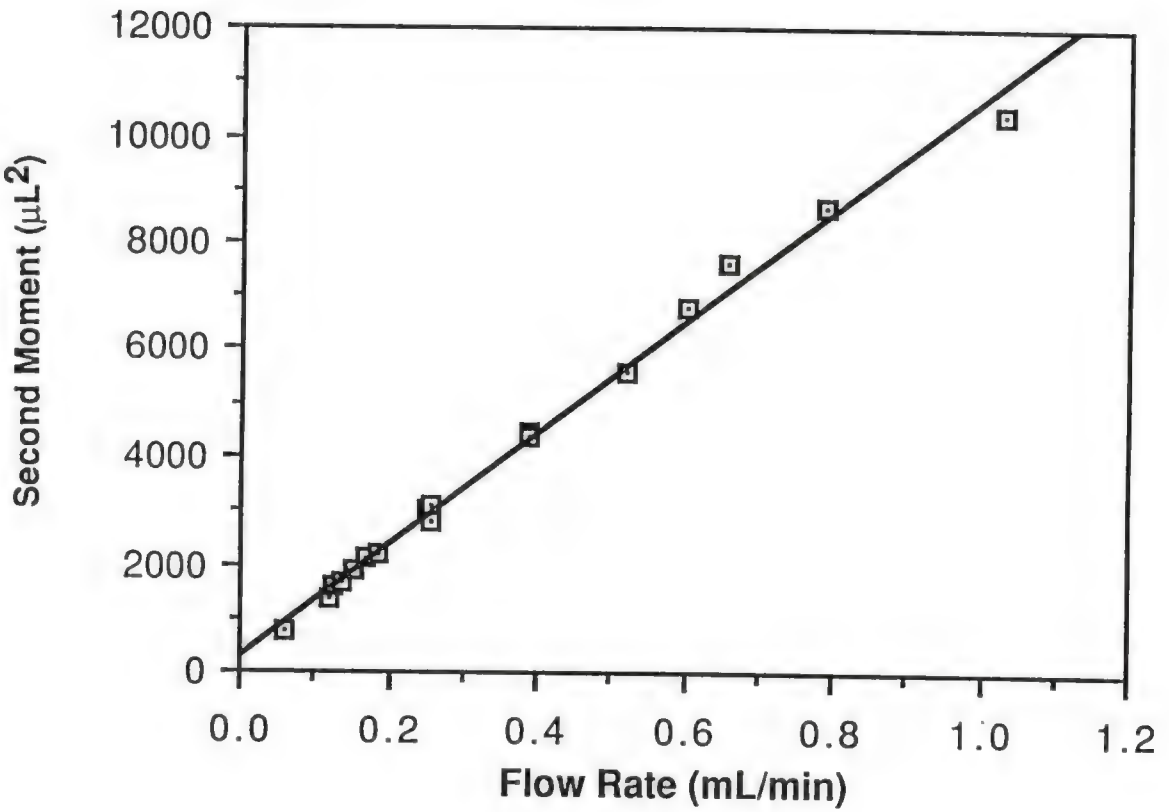

Figure 45. Plot of second moment (as determined by equation 4.9) versus flow rate for a 20 μL sample of 0.10 M NaI injected into a 100 cm straight tubing manifold.

Table XIV. Reproducibility of the second moment determination.

Trial	a,b (cm)	$W_{0.1}$ (cm)	M_2 (μL^2)	σ_G (μL)
1	1.09, 2.31	3.40	9977	43.1
2	1.03, 2.46	3.49	11303	39.9
3	1.06, 2.35	3.41	10323	41.6
4	1.02, 2.44	3.46	11120	39.5
5	1.10, 2.24	3.34	9386	43.8
6	1.10, 2.28	3.38	9721	43.6
7	1.05, 2.40	3.45	10765	41.0
8	1.12, 2.28	3.40	9724	44.6
9	1.08, 2.36	3.44	10411	42.5
10	1.02, 2.44	3.46	11120	39.5
			10385	41.9
		Std. Dev.	676 μL^2	1.9 μL
		RSD	6.5%	4.5%

Note: Injected sample 0.10 M NaI solution, 20 µL sample volume, 100 cm straight manifold, 1.03 mL/min, 100 µS full scale sensitivity setting.

Table XV. Effect of changing concentration and changing sensitivity on the determination of the second moment.

Trial	a,b (cm)	$W_{0.1}$ (cm)	M_2 (μL^2)	σ_G (μL)
0.01 M NaI Solution[a]				
1	1.13, 2.26	3.39	9558	45.1
2	1.10, 2.30	3.40	9892	43.6
3	1.10, 2.30	3.40	9892	43.6
4	1.10, 2.29	3.39	10075	42.0
5	1.09, 2.37	3.46	10500	42.9
			9983	43.4
		Std. Dev.	344 μL^2	1.1 μL
		RSD	3.4%	2.6%
0.004 M NaI Solution[b]				
1	1.08, 2.32	3.40	10062	42.6
2	1.10, 2.29	3.39	10075	42.0
3	1.09, 2.31	3.40	9977	43.1
4	1.08, 2.32	3.40	10062	42.6
			10044	42.6
		Std. Dev.	45.1 μL^2	0.4 μL
		RSD	0.45%	1.0%

[a] Injected sample 0.01 M NaI solution, 20 µL sample volume, 100 cm straight manifold, 1.03 mL/min, 10 µS full scale sensitivity setting.

[b] Injected sample 0.004 M NaI solution, 20 µL sample volume, 100 cm straight manifold, 1.03 mL/min, 10 µS full scale sensitivity setting.

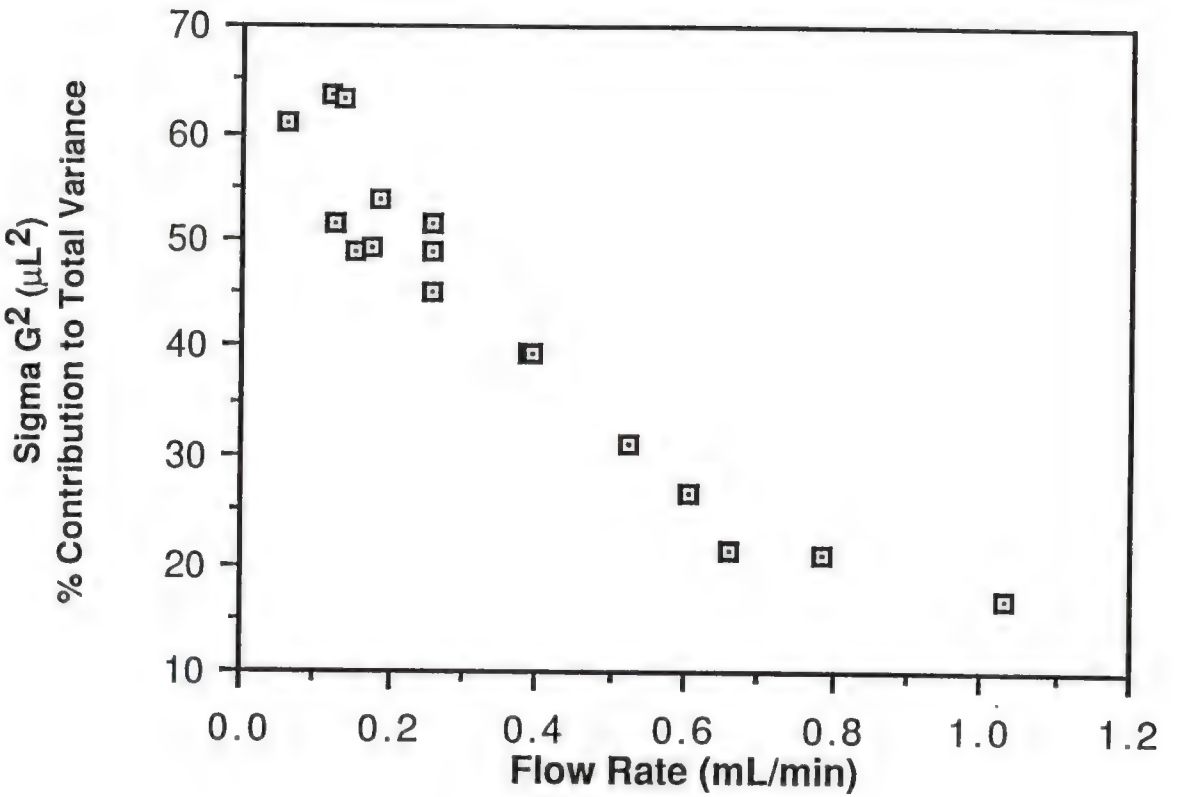

Figure 46. Plot of Gaussian contribution as a percent of the total peak variance (as determined by equations 4.12) versus flow rate for a 20 µL sample of 0.10 M NaI injected into a 100 cm straight tubing manifold.

Figure 47. The carrier stream was 80% by volume ethanol in water and the configuration of the 100 cm manifold was straight. In order to monitor the dispersion of the sample plug without reaction occurring, 300 µL of the t-amyl iodide was reacted in 50 mL of the carrier stream for 24 hours, ensuring completion of the reaction. This prereacted solution (containing the reaction products) was intercalated into the carrier stream at various flow rates to provide a direct measure of the dispersion occurring in the sample plug as a result of purely physical processes. Figure 48 again shows the dependence of the second moment upon flow rate, with and without chemical reaction, in the same experimental system with a coiled manifold (coiling radius, 14 mm).

Examination of the data contained in Figures 47 and 48 yields much information about the dispersion occurring in the sample plug. It is observed that at low flow rates in both the straight and coiled manifolds, the peak variance for injected samples with chemical reaction occurring exceeds the second moment of the sample without chemical reaction. As more time is allowed for the reaction to proceed, the production of product becomes the paramount factor determining the width of the peak, overwhelming longitudinal dispersion due to physical dispersion processes. Using equation 4.4, it is then possible to examine the contribution of the chemical reaction to total peak variance. In both straight and coiled manifolds it is observed that as the flow rate of the system is decreased, the contribution of the chemical reaction becomes increasingly important to the total peak variance. Painton and

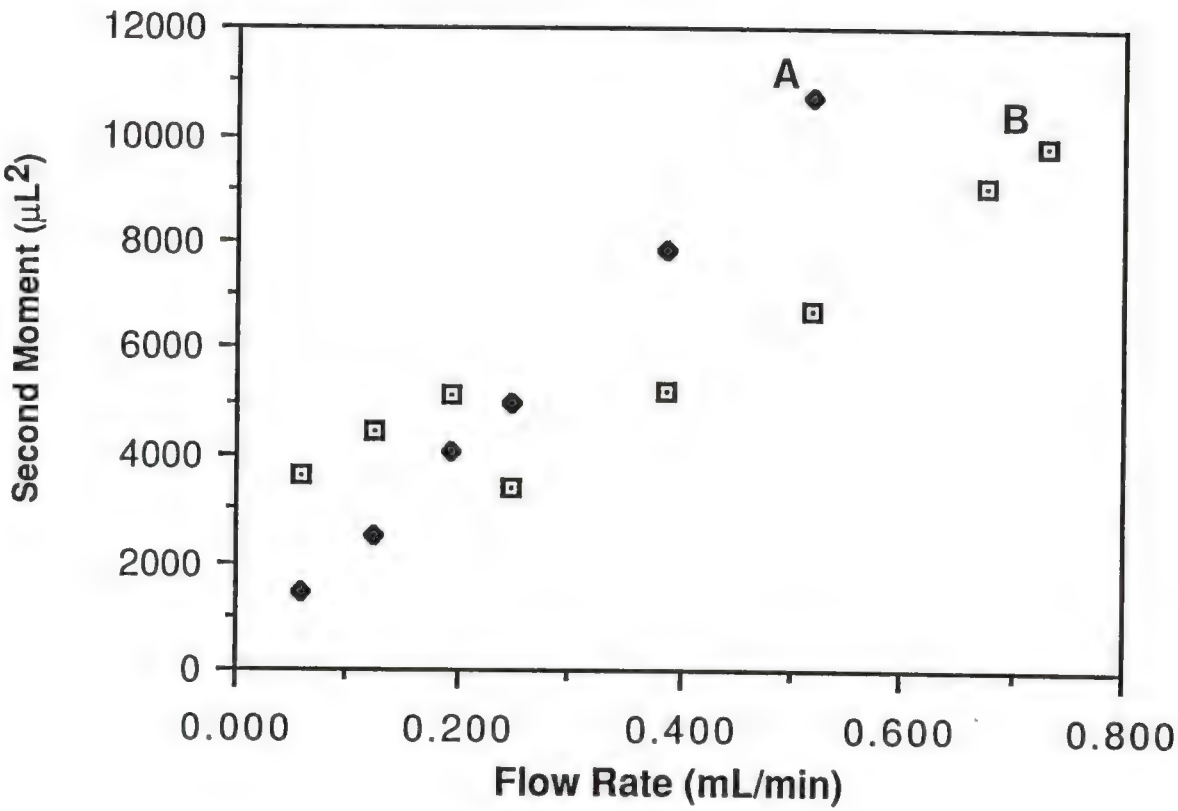

Figure 47. Plot of second moment versus flow rate for the t-amyl iodide hydrolysis (straight manifold). The symbols indicate whether (A) prereacted t-amyl iodide solution (see text for explanation) is introduced into the system or (B) a reaction is occurring in the 100 cm straight tubing manifold (B). The sample volume is 20 μL and the carrier stream is 80:20 ethanol:water (v/v).

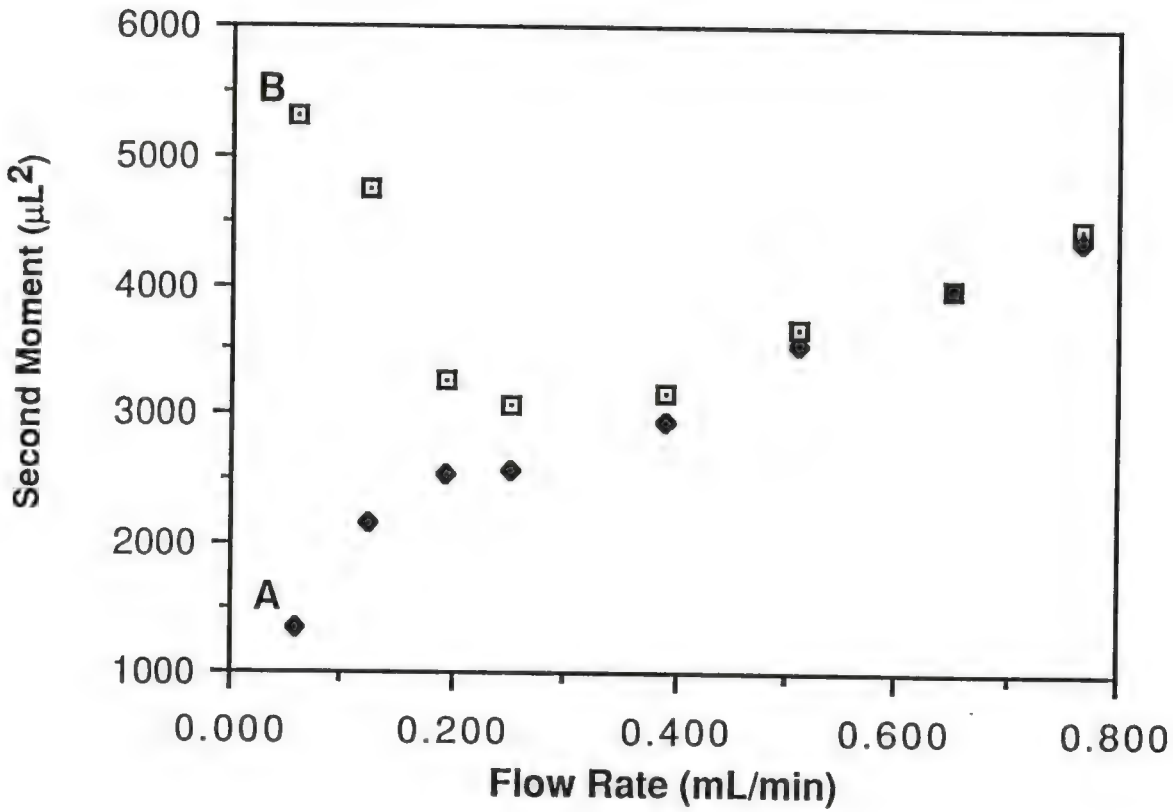

Figure 48. Plot of second moment versus flow rate for the t-amyl iodide hydrolysis (coiled manifold). The symbols indicate whether (A) prereacted t-amyl iodide solution (see text for explanation) is introduced into the system or (B) a reaction is occurring in the 100 cm coiled tubing manifold. The sample volume is 20 μL and the carrier stream is 80:20 ethanol:water (v/v).

Mottola (1981) analogously observed that the dispersion due to chemical reaction increased with decreasing flow rate in a straight manifold. With increased flow rate, however, the effect of the chemical reaction becomes less important in determining the total peak variance.

In Figures 47 and 48 it is apparent that at a flow rate of 0.20-0.30 mL/min, a region of transition occurs where the chemical contribution to dispersion is no longer the dominant factor determining total peak variance. This region of flow corresponds to the flow rates at which the prevailing mechanism of transport within the sample plug changes from purely diffusional (at low flow rates) to convective-diffusional (Valcarcel and Luque de Castro, 1987). They have shown that for single line manifolds, the transition from diffusion controlled to convective-diffusional dispersion occurs at an L to q (L = length of manifold, q = flow rate) ratio between approximately 200 and 550 (q = 0.18-0.50 mL/min for the present system) for a sample of 0.10 M NaI with a diffusion coefficient of 1.52×10^{-5} cm^2/s (CRC Handbook of Chemistry and Physics, 1980b). An 80:20 mixture of ethanol and water has a viscosity approximately twice that of pure water, decreasing the diffusion coefficient of the NaI solution by one half its value in water. For our system, the L/q ratio of 550 (0.18 mL/min) is predicted to be the cutoff for pure diffusion controlled behavior. The transition from diffusional to convective-diffusional transport would then be expected to occur somewhere in the flow rate region of 0.18-0.50 mL/min, in agreement with experimental observations.

As the flow rate of the system is increased and the prevailing mechanism of transport becomes convective-diffusional in nature, the linear relationship between M_2 and the flow rate is again observed. Double hump peaks were observed at relatively high flow rates (>0.50 mL/min) in the straight tube manifold when no chemical reaction was occurring. When, however, the same flow rates and carrier stream were employed with a reaction occurring in the straight manifold, no double hump peaks were observed. This would indicate that the chemical reaction itself increases radial mixing within the sample plug in the straight manifold, and should result in a decrease in M_2 as shown in Figure 47. Double hump peaks were not observed for any examined flow rates in a coiled tube manifold. The shape of the double hump peaks are in agreement with those observed by Atwood and Golay (1979, 1981). They show that for short open tubes, the hyperbolic tail of each peak is truncated by a combination of radial diffusion and velocity shear. These forces combine to sweep the molecules in the trailing portion of the sample at the tubing walls in the form of a hump of concentration which eventually catches up with the average flow in the system. As the flow rate of the system is increased, there is not sufficient time for the hump of concentration to convolute with the main peak. As shown in Figure 49, the sharp front of the peak is eventually destroyed by diffusion as the flow rate is decreased. Increased radial mixing and stronger concentration gradients as a result of chemical reaction eliminate the double hump in our straight tube manifold. The diffusion related nature of the double hump phenomena was verified by the observation that

Figure 49. Plot of response curve shapes as a function of elution time and flow rate in a straight tubing flow injection system with the direction of → indicating direction of increase in parameter. At high flow rates, the peak shape has virtually an instantaneous onset. As the flow rate is decreased and the transition from short-tube peak shapes to Gaussian peak shapes for long tubes occurs. Between these two extremes, the development of a hump is obvious which moves from the tail (high flow rates) to the main peak (at low flow rates) (adapted from Atwood and Golay, 1981).

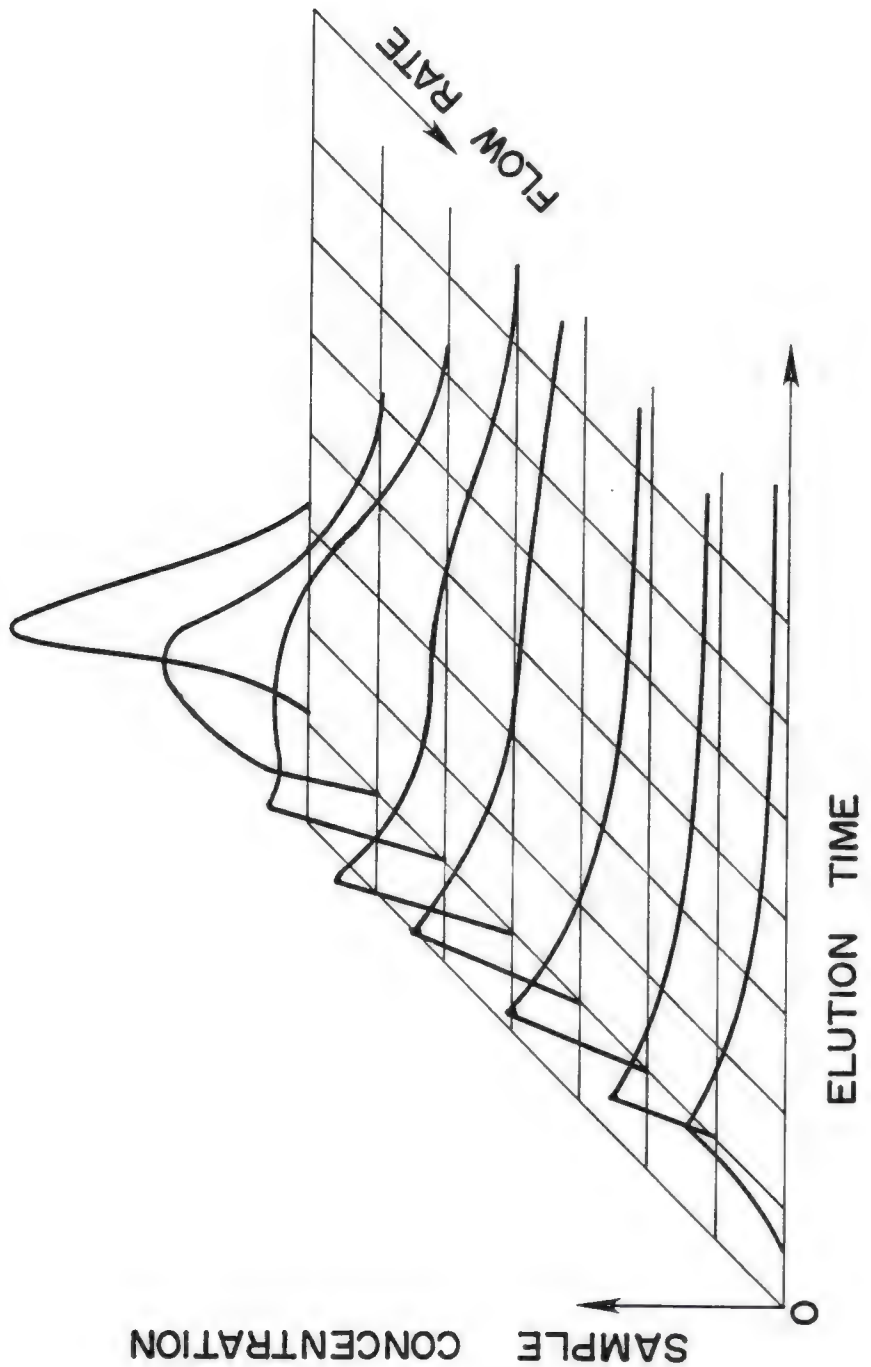
FLOW RATE
ELUTION TIME
SAMPLE CONCENTRATION
0

introduction of the prereacted sample into an aqueous carrier stream (lower viscosity, higher diffusion coefficient) did not result in double hump peaks at the examined flow rates.

Tijssen (1980) has developed a comprehensive theory describing laminar dispersion in coiled tubes and it is well known that secondary flow increases radial mixing in such systems. Painton and Mottola (1981) showed that radial mixing in coiled reactors generates secondary flow which is perpendicular to the centrifugal forces present in the flow channel. This flow is in opposition to dilution of the solute by longitudinal dispersion and in the present system is manifested by the decreased absolute values of the second moment in coiled tubing when compared to straight tubing.

Figure 48 indicates that for coiled tubing, the variance of the response curves with a reaction occurring are identical to those of the nonreacting tracer at equivalent flow rates. The analogous observation was made by Reijn et al. (1984) who found that at high flow rates the variance of an FIA curve was virtually independent of reaction rate for a single bead string reactor manifold. It can be concluded that for typical FIA flow rates, the effect of chemical reaction upon total system dispersion is negligible for this reaction. It is expected that as the rate of reaction is increased, the chemical reaction contribution to total peak variance will persist until greater flow rates.

Effects of Coiling and Carrier Stream Viscosity Upon Total Peak Variance

The straight or coiled nature of the FIA manifold and the viscosity of the carrier stream were important factors determining the

variance of the response curves for this system. Figures 50 and 51 allow for the determination of the effect of manifold coiling upon the variance of the FIA response curves in this system. Figure 50 compares the variance determined for the injection of 20 μL of 0.1 M NaI solution into both a straight and coiled manifold with an aqueous carrier stream. The resultant equations of the two lines are $Y = 10370X + 290$ for the straight manifold and $Y = 2606X + 691$ for the coiled system. One should not attempt to place any physical significance upon the values of the y-intercepts obtained for these plots due to the scarcity of data points for low flow rates. The ratio of the slopes of the two lines is 3.84 and accounts for the presence of coiling in otherwise equivalent manifolds. Figure 51 makes the analogous comparison for the same injected sample into a more viscous (80:20, ethanol:water) carrier stream. The equations of the two lines are $Y = 26970X - 1534$ for the high viscosity, straight manifold and $Y = 7025X + 1536$ for the high viscosity, coiled system. The ratio of the slopes of these two lines is 3.98, which is in agreement with the slope ratio for the aqueous system, showing that the difference in slopes of the variance vs. flow rate plots is a direct result of the coiling of the tubing. Therefore, a fourfold decrease in the second moment and an accompanying increase in the throughput can be achieved by coiling the tubing in this system.

In an analogous fashion, a comparison of the slope ratio for the viscous carrier, straight manifold to the aqueous carrier, straight manifold and the slope ratio for the viscous and aqueous carriers in the coiled system allows for a determination of the effect of

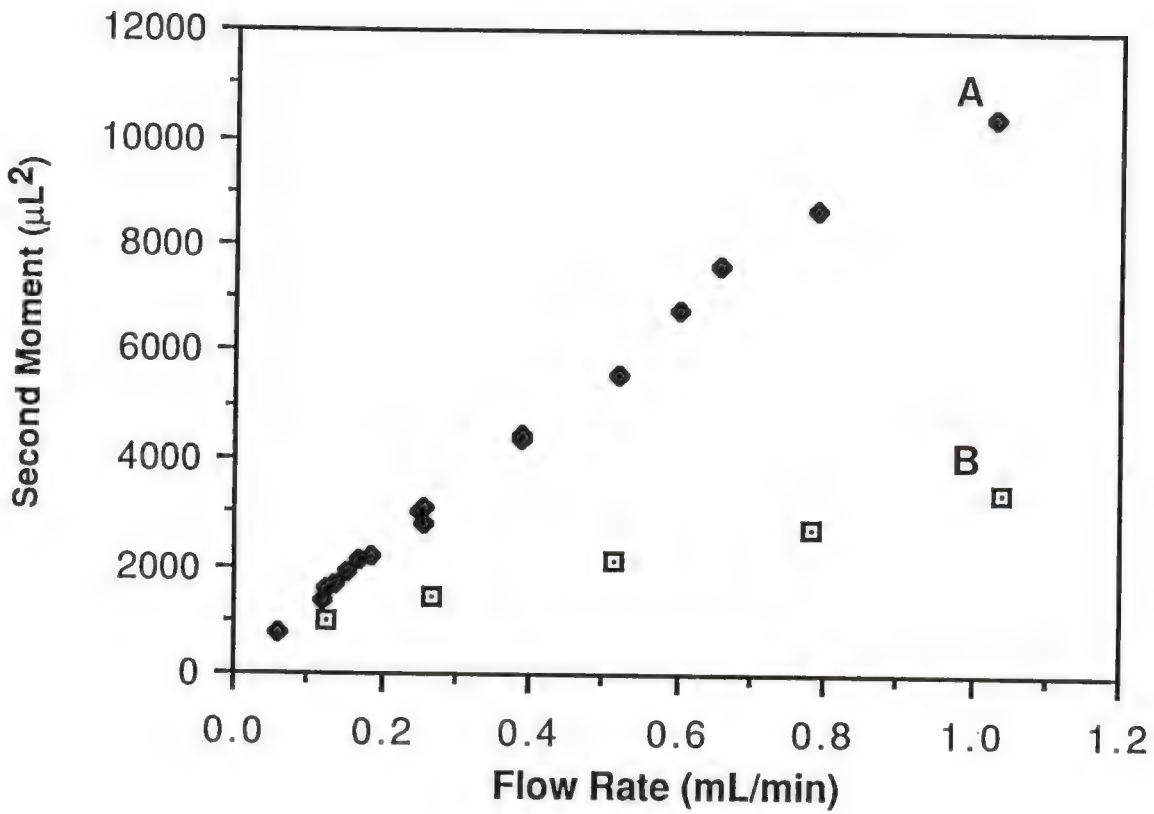

Figure 50. Plot of second moment versus flow rate for a 20 μL sample of 0.10 M NaI injected into an aqueous carrier stream through a 100 cm manifold. The symbols indicate whether the manifold is straight (A) or coiled (B).

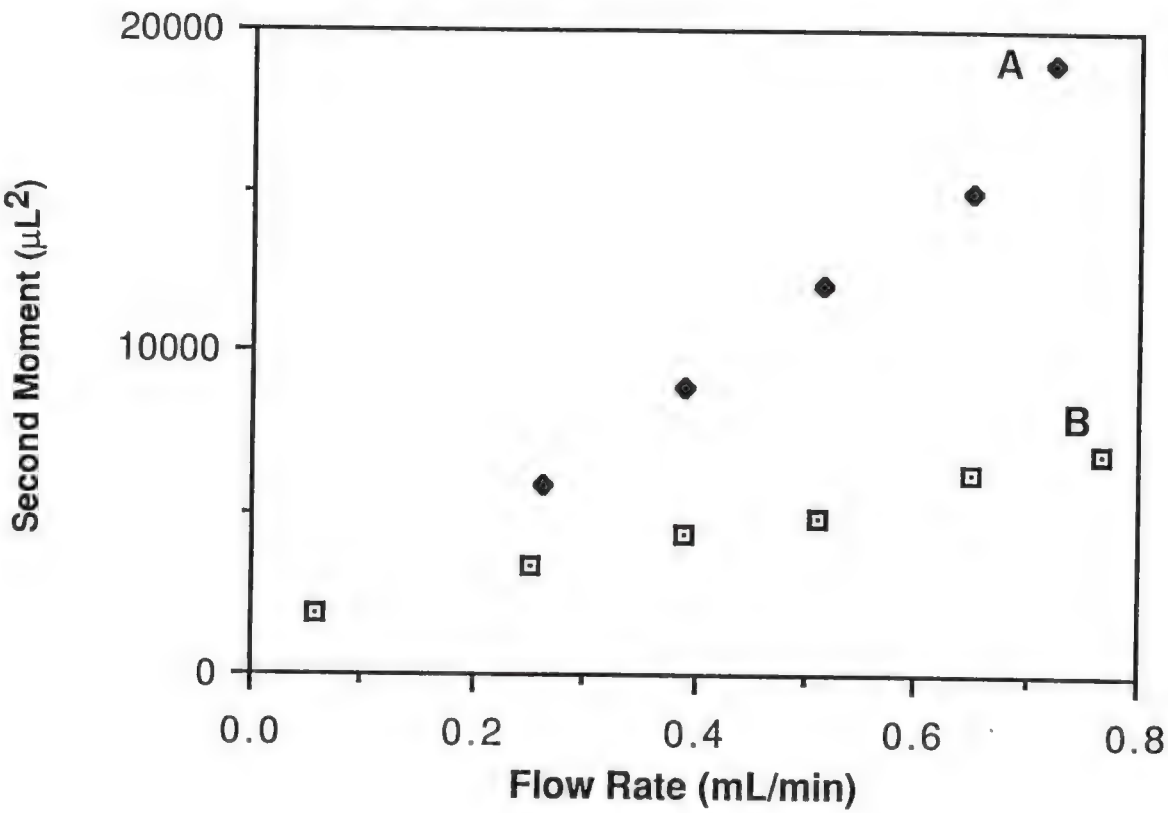

Figure 51. Plot of second moment versus flow rate for a 20 μL sample of 0.10 M NaI injected into a high viscosity 80:20 ethanol:water (v/v) carrier stream through a 100 cm manifold. The symbols indicate whether the manifold is straight (A) or coiled (B).

viscosity differences on the second moment. These slopes ratios are again consistent, 2.60 and 2.70, respectively, and account for the differences in the second moments in the system as a result of viscosity changes. The use of an 80:20 ethanol:water carrier stream increases the variance of the system approximately two and one half times. Therefore, the maximum throughput of the system will be obtained by using a carrier stream of lowest possible viscosity. These conclusions can also be inferred by an analysis of the relative dispersion values of the various configurations; however, moment analysis yields direct information in the time domain.

This work has shown that moment analysis is a valid method for examining response curves from flow injection systems. Much information concerning the behavior of the sample plug within the manifold and a direct comparison of the throughput of various systems can be made. By analyzing the width of the EMG peaks exiting the manifold, it is not necessary for the experimenter to attempt to account for all variations in manifold design and carrier stream constitution to gain valuable information from the response curves. The observation that decreased viscosity decreases variance of injected samples may provide an interesting variation on the classical flow injection theme. The use of a supercritical fluid as the carrier stream would exploit the relatively high solute diffusion coefficients of supercritical fluids (10^{-4} - 10^{-3} cm^2/s compared to 10^{-5} cm^2/s for liquids), increasing sample throughput and lowering LODs in flow injection analysis.

CHAPTER V
EFFICIENCY AND SOLVENT STRENGTH IN MICELLAR LIQUID CHROMATOGRAPHY: EFFECTS OF MEDIUM CHAIN LENGTH NORMAL ALCOHOLS

Introduction

In 1980, Armstrong and Henry first effectively demonstrated the use of aqueous micellar mobile phases for reversed phase liquid chromatography. Since that time, the unique application and potential advantages of the technique over traditional hydro-organic mobile phases have been investigated. Several review articles (Armstrong, 1985; Dorsey, 1987; Khaledi, 1988) and a symposium series volume (Hinze and Armstrong, 1987) have recently appeared on the subject. Two major obstacles to the widespread acceptance of micellar liquid chromatography (MLC) are that the chromatographic efficiency and solvent strength achievable with aqueous micellar mobile phases are much less than those available with traditional hydro-organic mobile phases.

There is much disagreement concerning the reason for the decreased efficiencies evidenced in MLC. Dorsey et al. (1983) were the first to address the problem and through the use of Knox plots (reduced plate height vs. reduced velocity) they were able to show that reduced mass transfer resulted in lower efficiencies in MLC. They attributed the reduced efficiency to poor wetting of the surfactant modified stationary phase and showed that efficiency in MLC

could be improved by the addition of small amounts of n-propanol to the micellar mobile phase. Yarmchuk et al. (1984) attributed the reduced efficiency associated with micellar mobile phases to poor mass transfer between the micelle and the stationary phase, with the micelle exit rate constant being the limiting factor for hydrophobic solutes. Other workers (Borgerding and Hinze, 1985; Armstrong et al., 1986) have attributed the efficiency decreases to poor mass transfer within the stationary phase itself, resulting from adsorption of surfactant onto the stationary phase.

Several investigators have examined the effects of the addition of low concentrations of alcohols as mobile phase modifiers (Graham and Rogers, 1980; Dorsey et al., 1983; Kirkman et al., 1984; Mullins and Kirkbright, 1984; Armstrong et al., 1986; Berthod et al., 1986; Hinze and Armstrong, 1987) in MLC. Foley and May (1987) have shown that the use of low concentrations of n-propanol in secondary chemical equilibria chromatography improves solute mass transfer by improving the wetting of the hydrophobic bonded C_{18} phase, resulting in efficiency enhancement. It has been concluded that the addition of methanol and ethanol does not result in improvement of chromatographic efficiency and that propanol is the shortest-chain alcohol modifier capable of providing efficiency enhancement at low concentrations. Only Hinze (in Hinze and Armstrong, 1987) has considered the effects of the addition of medium chain length normal alcohols to micellar mobile phases and the resultant effects upon efficiency with C_{18} stationary phases.

In this work, we present the results of a comprehensive study of the effects of medium chain length normal alcohols (propanol-hexanol) upon efficiency and solvent strength of SDS micellar mobile phases with a C_{18} stationary phase. Application of the pseudophase retention model (Armstrong and Nome, 1981; Arunyanart and Cline Love, 1984) of MLC yields valuable information about changes in the thermodynamics of solute partitioning as the properties of the micelle are modified by the presence of the alcohols. Additionally, utilization of the random walk model (Giddings, 1965) allows for an examination of the adsorption/desorption kinetics occurring at the stationary phase-mobile phase interface and the changes in these kinetic processes upon the addition of alcohols to the mobile phase. As a result, we are able to unequivocally verify that decreased efficiencies evidenced in MLC when employing C_{18} stationary phases are a direct consequence of inefficient solute mass transfer across the stationary phase-mobile phase interface.

Experimental

Apparatus

The liquid chromatograph was composed of a Spectra-Physics (San Jose, CA) SP8700 solvent delivery system. A 100 × 4.6 mm static mixer column and a 100 × 4.6 mm silica filled precolumn were included before the injector. The silica precolumn was filled with irregularly shaped (25-40 µm particle size) silica gel (Macherey-Nagel & Co., West Germany) and served the dual purpose of saturating the mobile phase with silicates and thermally equilibrating the mobile

phase before the analytical column. Samples were introduced by a Rheodyne (Cotati, CA) 7125 sample injection valve with a 20 µL sample loop. The column used was a 5 µm Zorbax ODS 150 × 4.6 mm (E.I. du Pont de Nemours and Co., Inc., Wilmington, DE). Both the silica precolumn and the analytical column were thermostated to 40±0.2°C using water jackets and an Allied circulator Model 73 (Fisher Scientific Co., Fairlawn, NJ). The detector employed was a Kratos (Ramsey, NJ) Spectroflow 757 variable wavelength detector (254 nm) with an 8 µL flow cell and a time constant of 0.045 s. All signals were recorded on a Fisher Recordall Series 5000 recorder. All least squares calculations were performed by Interactive Microware, Inc. (State College, PA) Curve Fitter program run on an Apple II Plus microcomputer.

The fluorescence spectra were acquired using a Spex Industries, Inc. (Edison, NJ) Fluorolog operated in conjunction with a Spex model DM3000XT personal computer for data acquisition and manipulation. The fluorimeter contains a 450 watt xenon arc lamp source, a monochromator grating consisting of 1200 grooves/mm and the photomultiplier tube was operated at 950 volts. Excitation intensity was centered at 332 nm with a 3.6 nm bandpass. Emission intensity was scanned at a rate of 0.5 nm/s from 365-420 nm with an emission bandpass of 1.8 nm. Figure 52 gives the excitation and emission spectra of pyrene performed in a 60:40 methanol:water solution. Each pyrene spectrum reported is with respect to the emission spectrum of the solvent blank but is uncorrected for instrumental response.

Figure 52. Excitation (a) and emission (b) spectra of pyrene in a 60:40 methanol:water (v/v) solution.

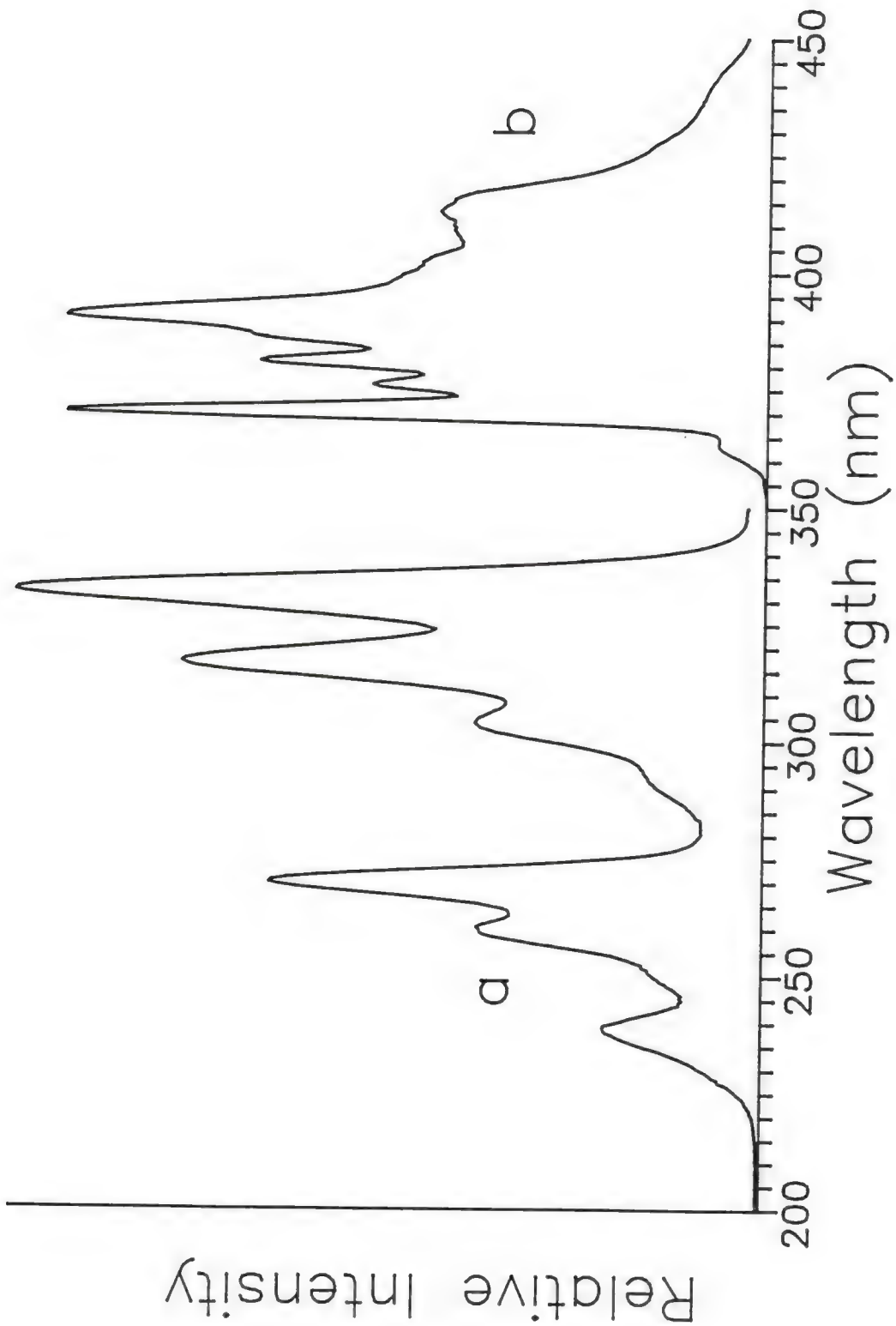
Relative Intensity
200
250
300
350
400
450
Wavelength (nm)
a
b

Chemicals

Sodium dodecyl sulfate (puriss. grade) was obtained from Fluka (Hauppauge, NY) and Aerosol OT (Dioctyl Sodium Sulfosuccinate) was purchased from Fisher Scientific Co. (Fairlawn, NJ). The surfactant solutions were made in deionized, distilled water which was purified with a Barnstead Nanopure System (Sybron Corp., Boston, MA) and irradiated by a Photronix Corp. (Medway, MA) Model 816 HPLC Reservoir. Mobile phase modifiers n-propyl alcohol, n-butyl alcohol (Fisher Scientific Co., Fairlawn, NJ), n-pentyl alcohol (Aldrich Chemical, Milwaukee, WI) and n-hexyl alcohol (Eastman Kodak, Rochester, NY) were all reagent grade and were added in a 3% volume:volume fraction prior to filtering the mobile phase through a 0.45 μm Nylon-66 membrane filter (Rainin Instruments, Woburn, MA). Acetophenone (Fisher), benzene (Mallinkrodt, McGaw Park, IL), naphthalene (Eastman), anthracene (Matheson, Coleman & Bell, Norwood, OH) and pyrene (Chem Service, West Chester, PA) were initially dissolved in HPLC grade methanol (Fisher) and diluted so that injected samples were in 0.05 M SDS for the micellar systems or mobile phase (60:40 methanol:water) for the hydro-organic systems. Hexane was HPLC grade from Fisher. All chemicals were used as received.

Procedure

The void volume of the system was determined by the injection of distilled, deionized, filtered water directly into the system. The time corresponding to the initial baseline disturbance was equated to the void volume of the system. Before introduction of surfactant to the system, the void volume was determined to be 1.34 mL. After

saturating the stationary phase with surfactant the void volume of the system was consistently determined at different surfactant concentrations and different alcohol chain lengths (propanol-pentanol) to be 0.90 mL. Calculation of the stationary phase volume has always been ambiguous. The stationary phase volume of the column is often determined by subtracting the void volume of the column from the total empty-column volume. Here, that volume was found to be 1.59 mL in the surfactant containing system. This measure of stationary phase volume includes the column volume occupied by silica support so is at best a crude estimate.

In determining the stationary phase volume, the pertinent volume should be the volume of the alkyl chains bonded to the silica surface. Sentell and Dorsey (1988) have proposed a novel method which allows for the calculation of the active stationary phase volume and a more accurate estimation of the stationary phase volume:

$$V_s = [(\%C)(M)(W_p)]/[(100)(12.011)(n_c)(\rho)] \qquad \text{(eq. 5.1)}$$

where %C is the percent carbon loading (16% for Zorbax ODS (Antle et al., 1985)) of the stationary phase; M is the molecular weight of the bonded alkyl ligand (311.6 g/mol for monomeric C_{18}); W_p is the weight of the column packing (2.25 g); n_c is the number of carbon atoms in the bonded alkyl ligand (20 for C_{18}); and ρ is the density (0.8607 g/cm^3) of the bonded ligand. These density values for common stationary phases have been determined by Cheng (1985). This method results in a calculated stationary phase volume of 0.54 mL and indicates that the calculated values of stationary phase/water

partition coefficients (P_{sw}) by the pseudophase retention model may be highly inaccurate (due to the direct dependence of P_{sw} on V_s) and, therefore, should not be considered as absolute but rather as relative values. As shown below, a large error in the estimation of the stationary phase volume, however, has a negligible effect upon the value of the solute-micelle binding constant per surfactant monomer. Therefore, inherent inaccuracy in the determination of stationary phase volume has no effect upon the other physicochemical properties (K_2, P_{mw}) determined.

The working concentrations of the injected solutes were acetophenone (0.0048 ppm), benzene (0.4 ppm), naphthalene (68.8 ppm), anthracene (3.75 ppm) and pyrene (31.5 ppm) for the aqueous surfactant mobile phase. For the 3% alcohol-surfactant mobile phases and the hydro-organic mobile phase, the following concentrations were used: acetophenone (0.0012 ppm), benzene (0.2 ppm), naphthalene (34.4 ppm), anthracene (3.75 ppm) and pyrene (31.5 ppm). All results indicate the average of at least duplicate injections.

Theory

Three-Phase Retention Model

Armstrong and Nome (1981) developed the three-phase retention model to describe partitioning behavior of solutes in a micellar chromatographic system. Their equations describe the relationship between measurable chromatographic parameters and the concentration of surfactant in the mobile phase. Armstrong (1985) has recently shown that these equations can be reexpressed in at least 12 related forms

for use in micellar liquid chromatography. The form employed in the present work is given below:

$$V_s/(V_e-V_m) = [V(P_{mw}-1)/P_{sw}][M] + 1/P_{sw} \qquad \text{(eq. 5.2)}$$

where V_s, V_e, V_m are, respectively, the stationary phase volume, elution volume of the solute and the void volume of the system; P_{mw} and P_{sw} are the solute partition coefficients between the micelle and water and the stationary phase and water; [M] represents either the molar concentration of surfactant in the mobile phase or in the micelles; and V is the molar volume of the surfactant in the micelle. If the assumptions of the three-phase model are adhered to for the system under investigation, a plot of V_s/V_e-V_m vs. [M] results in a straight line yielding valuable physicochemical information about the interaction of solute molecules with both the stationary phase and the micelles in the mobile phase. The slope:intercept ratio of this linear plot, $K_2 = V(P_{mw}-1)$, is equal to the solute-micelle binding constant per surfactant monomer in solution. This is related to the solute-micelle binding constant per micelle through the aggregation number of the organized assembly. If the molar volume of the surfactant, V, is known, the micelle/water partition coefficient, P_{mw} may be obtained. Additionally, 1/y-intercept of the linear plot yields the stationary phase/water partition coefficient, P_{sw}.

Arunyanart and Cline Love (1984) have developed an analogous three-phase equilibrium model relating capacity factors to micellar

mobile phase surfactant concentrations in the following manner:

$$1/k = \{K_2/(\phi[L_s]K_1)\}[M] + 1/(\phi[L_s]K_1) \qquad \text{(eq. 5.3)}$$

where k is the capacity factor of the solute; ϕ is the chromatographic phase ratio, the ratio of the volume of the stationary phase, V_s, to the volume of the mobile phase, V_m; $[L_s]$ is the molar concentration of the stationary phase bonding sites; K_1 is the equilibrium constant describing the reversible equilibrium between solute in the bulk mobile phase with the stationary phase binding sites; and K_2 and [M] are defined as above. A plot of 1/k vs. [M] results in a straight line and the value of the solute-micelle binding constant per surfactant monomer, K_2, can again be calculated by taking the ratio of the slope to the y-intercept of the plot. In this work a comparison of the results obtained using both of these treatments will be presented.

Results and Discussion

Adsorption/Desorption Rate Constants

The random walk theory (Giddings, 1965) allows for the examination of quantitative aspects of zone spreading in a chromatographic system. If a large number of molecules start together, such as would be the case for a thin zone of solute injected onto a column, on a random walk of many steps, the standard deviation of the resulting Gaussian profile can be described by

$$\sigma = l\sqrt{n} \qquad \text{(eq. 5.4)}$$

where σ is the standard deviation of the Gaussian profile; l is the fixed step length of the random walk which is equivalent to the average root mean square length of the actual displacement; and n is the number of random walk steps taken. This equation can also be expressed in terms of the variance, σ^2, of the Gaussian profile:

$$\sigma^2 = l^2 n \qquad \text{(eq. 5.5)}$$

The dispersion of a sample zone in a chromatographic system can be described by the random walk model. Due to chromatographic retention, chromatographic zones move along at a velocity which is only a fraction, R, of the mobile phase velocity. In a chromatographic column, n is equal to the number of adsorptions plus the number of desorptions experienced by a solute as it moves through the column. Before a solute can desorb, it must first adsorb to the stationary phase; therefore, for an eluted solute, the number of adsorptions is by definition equivalent to the number of desorptions. If the fixed step length, l, is equivalent throughout the mobile phase, the random walk model (Giddings, 1965) can be applied and

$$H = 2R(1 - R)\nu/k_d \qquad \text{(eq. 5.6)}$$

$$\text{and } H = 2(1 - R)^2\nu/k_a \qquad \text{(eq. 5.7)}$$

where H is the plate height (cm) of the system; ν is the linear

velocity (cm/s) of the solute in the mobile phase; k_d is the desorption rate constant (s^{-1}) of a solute from the stationary phase ($k_d = 1/t_d$, where t_d is the time spent by a solute in the stationary phase prior to desorption to the mobile phase); and k_a is the adsorption rate constant (s^{-1}) of a solute to the stationary phase. It is important to note the dependence of the plate height in equations 5.6 and 5.7 upon the adsorption and desorption rate constants of the solute to and from the stationary phase. Therefore, in practice, when attempting to maximize efficiency, all possible effort should be made to increase the rate of transition (Giddings, 1965) by increasing k_d (and thus k_a). The fraction of the mobile phase velocity, R, at which the chromatographic zone moves is related to the chromatographic capacity factor by

$$R = 1/(1 + k) \qquad \text{(eq. 5.8)}$$

Substitution of the value of R in equation 5.8 into equations 5.6 and 5.7 yields the following definitions for the desorption and adsorption rate constants in relation to the plate height:

$$k_d = 2k\nu/[(1 + k)^2 H] \qquad \text{(eq. 5.9)}$$

$$\text{and } k_a = 2k^2\nu/[(1 + k)^2 H] \qquad \text{(eq. 5.10)}$$

The preceding equations allow for the determination of adsorption and desorption rate constants of a solute to and from the stationary phase using measurable chromatographic parameters. By definition, the

chromatographic capacity factor, $k = k_a/k_d$. Therefore, in order to make direct comparisons between the desorption rate constants of different solutes in a given mobile phase and between equivalent solutes in different mobile phases it is necessary to normalize equation 5.9 for the changes in capacity factor which are a direct result of changes in the defined system. This is accomplished by dividing the result for k_d obtained from equation 5.9 by $k/(1 + k)^2$, resulting in a normalized desorption rate constant, k_d', which allows for direct comparison between different solutes in the same mobile phase and the same solute in different mobile phases:

$$k_d'(s^{-1}) = 2v/H \qquad \text{(eq. 5.11)}$$

Table XVI shows representative calculations for normalized desorption rate constants for the case of no alcohol and 3% C_3-C_6 alcohol present in both a 0.10 M and a 0.25 M SDS mobile phase.

Several trends are observed from an examination of Table XVI. As the hydrophobicity of the arene ring series compound (benzene, naphthalene, anthracene, pyrene) increases, the normalized desorption rate constant decreases, indicating an increase in the time spent in the stationary phase by the more hydrophobic molecules before the desorption step. It is also observed that upon the addition of the different alcohols at 0.10 M SDS, there are marked changes in the k_d' values as the alcohol chain length is varied, indicating that the alcohol itself is the dominating factor determining the normalized rate of desorption. In the case of 0.25 M SDS mobile phase,

Table XVI. Normalized desorption rate constants determined for the investigated solutes in a 0.10 M SDS and a 0.25 M SDS mobile phase in the absence and presence of 3% normal alcohols.

	No Alcohol	Propanol	Butanol	Pentanol	Hexanol
k_d' (s^{-1})(0.10 M SDS + 3% Alcohol)					
Acetophenone	184	244	295	322	294
Benzene	265	330	446	382	427
Naphthalene	210	222	294	260	260
Anthracene	116	162	179	197	156
Pyrene	63	112	113	114	84
k_d' (s^{-1}) (0.25 M SDS + 3% Alcohol)					
Acetophenone	126	252	276	268	245
Benzene	242	380	379	374	382
Naphthalene	175	229	242	222	216
Anthracene	92	128	135	128	114
Pyrene	41	52	69	68	58

the k_d' values for a given solute and a given mobile phase are consistently lower than those obtained in 0.10 M SDS. It is theorized that this phenomenon is a direct result of increased solution viscosity as the surfactant concentration is increased. It is interesting to note that in the case of 0.25 M SDS with 3% alcohol present, for a given solute, there is much less variation in the calculated k_d' values. Additionally, the k_d' values for the alcohol containing micelle mobile phases are significantly larger than the no alcohol case, clearly indicating an increase in mass transfer from the stationary phase with the addition of alcohol.

Application of the random walk model to adsorption-desorption kinetics (Giddings, 1965) allows for an extension of these results to explain solute mass transfer across the stationary phase-mobile phase interface. An average molecule moving through a chromatographic column will remain in the mobile phase for a time, t_a, at which time it becomes adsorbed. Prior to adsorption, this molecule will move at the mean velocity, v, of the mobile phase for a distance vt_a. A solute must then move a total of L/vt_a segments, where L is the length of the column, before it is eluted. For a molecule to be eluted, the total number of adsorptions, n_a, must be equal to the total number of desorptions, n_d; therefore,

$$n_a = n_d = L/vt_a \qquad \text{(eq. 5.12)}$$

where t_a is equal to the time spent by a molecule in the mobile phase before it is adsorbed. Substitution of the definition that $k_a = 1/t_a$

into equation 5.12 yields

$$n_a = n_d = Lk_a/v \qquad \text{(eq. 5.13)}$$

Therefore, an increase in the desorption rate constant in a given system, such as shown in Table XVI, corresponds to an increase in the number of desorptions which must, from equation 5.13, result from an increase in the number of adsorptions. This corresponds to an increase in the rate of solute mass transfer across the stationary phase-mobile phase boundary and should result in higher efficiencies of the chromatographic system. Table XVII lists the adsorption rate constants determined using equation 5.10. Adsorption rate constants are known to be diffusion controlled (Yarmchuk et al., 1984) and this fact is reflected in the results of Table XVII. As both the size of the solute and the viscosity of the solution is increased, there is a decrease in k_a, reflecting the dependence of the adsorption rate constant upon the rate of diffusion.

The diffusion coefficients of the investigated solutes were calculated using the Wilke-Chang equation (Wilke and Chang, 1955) for a pure aqueous solution at 40°C and are listed in Table XVIII:

$$D_m = 7.4 \times 10^{-8} (\Psi_2 M_2)^{0.5} T/\eta_2 (V_1)^{0.6} \qquad \text{(eq. 5.14)}$$

where D_m is the diffusion coefficient (cm^2/s) of the analyte (1) in the mobile phase (2); Ψ_2 is the association factor of the mobile phase, which is 2.6 for water; M_2 is the molecular weight (g/mol) of

Table XVII. Adsorption rate constants determined for the investigated solutes in a 0.10 M SDS and a 0.25 M SDS mobile phase in the absence and presence of 3% normal alcohols.

	No Alcohol	Propanol	Butanol	Pentanol	Hexanol
k_a (s^{-1}) (0.10 M SDS + 3% Alcohol)					
Acetophenone	174	220	250	259	233
Benzene	251	309	410	346	381
Naphthalene	202	215	282	248	242
Anthracene	114	159	178	189	147
Pyrene	63	111	109	109	80
k_a (s^{-1}) (0.25 M SDS + 3% Alcohol)					
Acetophenone	115	206	212	197	177
Benzene	217	331	326	317	323
Naphthalene	164	212	220	199	192
Anthracene	88	121	127	118	104
Pyrene	39	50	65	63	53

Table XVIII. Calculated diffusion coefficients of investigated solutes.

Compound	V_1 (mL/mol)	D_m [a] (cm^2/s)	Relative D_m [b]
Acetophenone	1.028	1.4×10^{-5}	0.85
Benzene	0.879	1.6×10^{-5}	1.00
Naphthalene	1.025	1.3×10^{-5}	0.82
Anthracene	1.283	1.3×10^{-5}	0.77
Pyrene	1.271	1.2×10^{-5}	0.71

[a] $\psi_2 = 2.6$, $M_2 = 18.01$ g/mol, T = 313.15 K, $\eta = 0.653$ cP.

[b] Relative $D_m = D_m$(analyte)/D_m(benzene).

the mobile phase; T is the temperature in K; η_2 is the viscosity of the mobile phase (cP); and V_1 is the molar volume of the analyte (mL) and is calculated by taking the ratio of the molecular weight of the analyte to the density of the analyte.

An examination of the diffusion coefficients qualitatively explains the reason for the observed decrease in efficiencies as the size of the molecule is increased in micellar liquid chromatography. Decreased diffusion results in a decrease in the step lengths, l; therefore, the number of steps, n, must be increased for elution and there exists a greater barrier to mass transfer in the column. It should also be noted that as the concentration of SDS in the mobile phase is increased from 0.10 M to 0.25 M, the absolute values of k_a are decreased, corresponding to an increase in the time spent in the mobile phase, t_a, before the adsorption step. Due to increased viscosity as the surfactant concentration is increased, the solute diffusion coefficients are decreased, again resulting in decreased chromatographic efficiency. In 0.25 M SDS, k_a is approximately constant for all mobile phases with alcohol present and is significantly larger than the no alcohol case. The observed efficiency decreases observed in a micellar mobile phase with no organic modifier present are clearly due to decreased solute mass transfer across the stationary phase-mobile phase boundary and are reflected in the lower k_d' and k_a values in a pure micellar mobile phase.

Efficiency Calculations

In the present work, efficiency calculations were performed using the equation developed by Foley and Dorsey (1983):

$$N = 41.7(t_r/W_{0.1})^2/(b/a + 1.25) \qquad \text{(eq. 5.15)}$$

where t_r is the retention time of the solute at the peak maximum and b/a is the asymmetry ratio measured at 10% peak height. Bidlingmeyer and Warren (1984) have compared many methods for the calculation of column efficiency and have shown that this is the most accurate manual method available. Representative efficiency calculations for a 60:40 methanol:water mobile phase, an aqueous 0.10 M and a 0.25 M SDS mobile phases and for 0.10 M and 0.25 M SDS mobile phases with 3% by volume alcohol present are shown in Table XIX. Several conclusions can be drawn from an examination of the calculated efficiencies. As the chain length of the alcohol added to the micellar mobile phase is increased, a general increase in the chromatographic efficiency of the solutes is observed. Additionally, as the size of the compounds is increased (from benzene to pyrene), the efficiency of the system is decreased. Yarmchuk et al. (1984) have theorized that the decreased efficiencies observed in micellar mobile phases are a direct result of the decreased exit rate constants of aromatic hydrocarbons from SDS micelles as the hydrophobicity of the solute is increased. The exit rate constant from an aqueous SDS micelle (Almgren et al., 1979) for pyrene ($4.1 \times 10^3\ s^{-1}$) is 1000 times smaller than that for benzene

Table XIX. A comparison of chromatographic efficiencies for the investigated solutes in a 0.10 M SDS mobile phase in the absence and presence of 3% normal alcohols and a 60:40 methanol:water mobile phase.

	No Alcohol	Propanol	Butanol	Pentanol	Hexanol	60:40 MeOH:W
N (0.10 M SDS + 3% Alcohol)						
Acetophenone	2500	3300	4000	4400	4000	4100
Benzene	3600	4500	6000	5200	5800	4300
Naphthalene	2800	3000	4000	3500	3500	3300
Anthracene	1600	2200	2500	2600	2100	2200
Pyrene	900	1500	1500	1500	1100	1900
N (0.25 M SDS + 3% Alcohol)						
Acetophenone	1700	3400	3700	3600	3300	4100
Benzene	3300	5100	5100	5100	5200	4300
Naphthalene	2400	3100	3300	3000	2900	3300
Anthracene	1200	1700	1800	1700	1700	2200
Pyrene	600	700	900	900	800	1900

(4.4×10^6 s^{-1}). If the decreased efficiencies in micellar mobile phases were due to decreased exit rate constants for more hydrophobic compounds, one would expect to see a larger relative decrease in efficiency, when moving down a column in Table XIX, in the case of micellar mobile phases when compared to the hydro-organic mobile phase. This is only marginally, if at all observed, indicating that effects other than mass transfer from the micelle are the dominating effects in micellar liquid chromatography. The calculated k_d (0.44 s^{-1}) and k_a (63 s^{-1}) values obtained from equations 5.9 and 5.10 for pyrene in an aqueous 0.10 M SDS mobile phase are 9320 times less and 65 times less than the micelle exit rate constant, respectively. Smaller absolute values of k_d and k_a are then a further indication that the dominating barrier to mass transfer in MLC is across the stationary phase-mobile phase interface.

The efficiency of the solutes in the hydro-organic mobile phase was determined on the new column, before the addition of surfactant which permanently modifies the stationary phase. Dorsey et al. (1983) were the first to show that the addition of small amounts of propanol to a micellar mobile phase resulted in increased efficiencies with a C_{18} stationary phase. The results of the present work indicate that the addition of small amounts of butanol or pentanol to a micellar mobile phase yields markedly improved efficiencies when compared to the propanol case and efficiencies comparable to a hydro-organic mobile phase can be obtained, even for multi-ring hydrophobic compounds. Scott and Simpson (1980) have studied the effects of alcohols upon a reversed phase ODS column and have shown that 5 or

more carbon atoms in the aliphatic alcohol chain could produce complete stationary phase coverage when present in the mobile phase at a level of only a few percent. As a result, the surface of the reversed phase packing can be significantly modified, greatly affecting the solute mass transfer at the stationary phase-mobile phase interface, while the solvent characteristics of the bulk mobile phase are only minimally affected. An examination of the normalized desorption rate constants and the effect of alcohol chain length upon stationary phase adsorption indicates that solute mass transfer across the stationary phase-mobile phase interface is the dominating factor controlling efficiency in micellar liquid chromatography. The addition of 3% butanol or 3% pentanol to a micellar mobile phase is superior as a stationary phase modifier, and thus will result in higher efficiencies when compared to propanol.

Solvent Strength

In reversed phase liquid chromatography, the solvent strength decreases with increasing polarity of the mobile phase. Traditionally, micellar mobile phases are much weaker than their hydro-organic counterparts. Analysis time for micellar mobile phases has been decreased by the use of shorter chain length stationary phases, shorter columns and higher flow rates. In the present work, we examine the effects of alcohol addition upon solvent strength for the investigated solutes.

The equation originally developed by Snyder (1968) to estimate solvent strength (ε^{o}) in normal phase adsorption chromatography has

also been applied to reversed phase chromatography with carbon adsorbents (Colin et al., 1978):

$$\ln (k_1/k_2) = a(\varepsilon_2^{\circ} - \varepsilon_1^{\circ}) \qquad \text{(eq. 5.16)}$$

where k is the capacity factor and a is the molecular area (Snyder, 1968) of the solute with the subscripts 1 and 2 corresponding to the solvents 1 and 2, respectively. By choosing one solvent as a reference mobile phase and setting its $\varepsilon^{\circ} = 0$, equation 5.16 can be used to compare solvent strengths.

In the present work, the reference mobile phase is 60:40 methanol:water. The solvent strengths determined using equation 5.16 are listed in Table XX. Negative ε° values indicate that the micellar mobile phase is weaker than the reference solvent while positive ε° values are obtained when k_1 is greater than k_2. It is seen that the relative solvent strength of the micellar mobile phases when compared to the hydro-organic solvent increases both with increasing chain length of the aliphatic alcohol and as the hydrophobicity of the solute increases. This indicates both an increased mass transfer at the stationary phase-mobile phase interface and a decreased partitioning of the hydrophobic solutes to the micellar aggregates with increasing chain length of the alcohol modifier, yielding a mobile phase of greater strength.

The addition of low concentrations of alcohols to micellar mobile phases has been criticized as negating the desirable qualities of MLC. However, Khaledi et al. (1987) have recently shown that

Table XX. Strength of micellar mobile phases.

	No Alcohol	Propanol	Butanol	Pentanol	Hexanol
ε^o ($\times 10^2$) (0.10 M SDS + 3% Alcohol)[a]					
Acetophenone	-4.73	-3.53	-2.89	-2.45	-2.33
Benzene	-4.26	-3.86	-3.46	-3.12	-2.84
Naphthalene	-2.60	-2.30	-1.91	-1.51	-1.10
Anthracene	-1.26	-0.976	-0.597	-0.174	+0.313
Pyrene	-0.766	-0.486	-0.120	+0.277	+0.735
ε^o ($\times 10^2$) (0.25 M SDS + 3% Alcohol)[a]					
Acetophenone	-3.80	-2.59	-2.15	-1.86	-1.78
Benzene	-2.95	-2.52	-2.27	-2.06	-2.00
Naphthalene	-1.26	-0.952	-0.714	-0.498	-0.381
Anthracene	-0.054	+0.239	+0.484	+0.709	+0.874
Pyrene	+0.344	+0.633	+0.866	+1.07	+1.23

[a] The calculated molecular areas (Snyder, 1968, p. 200) are acetophenone = 63.8 A^2, benzene = 51.0 A^2, naphthalene = 68.9 A^2, anthracene = 82.4 A^2 and pyrene = 91.0 A^2.

methylene selectivity is not affected by the addition of low concentrations of alcohols to micellar mobile phases. The use of low concentrations of alcohols may then provide a useful way of modifying the overall mobile phase strength in MLC.

The Pseudophase Retention Model

There are a number of assumptions which have been made when deriving the pseudophase retention equations (Armstrong and Nome, 1981; Armstrong, 1985). In order to ascertain the validity of the obtained results, these assumptions must be examined for the present system. It is first assumed that compounds which partition to the micelle will show a decrease in retention with an increase in micelle concentration in the mobile phase. Representative retention volumes, V_e (retention time times the flow rate), of solutes eluted in aqueous 0.10 M and 0.25 M SDS mobile phases and for 0.10 M and 0.25 M SDS mobile phases with 3% by volume alcohol present are shown in Table XXI. An examination of the retention volumes indicates that this assumption is valid for all the compounds investigated in all surfactant containing mobile phases.

It is assumed that the binding of the surfactant to the stationary phase does not affect retention. If the retention of the solute is affected, then it is assumed that the binding of the surfactant on the stationary phase has reached a level of saturation. Dorsey et al. (1984) have measured adsorption isotherms for 3% propanol micellar solutions and have shown that at surfactant concentrations above the critical micelle concentration (CMC), the amount of adsorbed surfactant is approximately constant.

Table XXI. A comparison of retention volumes for investigated solutes in 0.10 M and 0.25 M SDS mobile phases in the presence and absence of 3% normal alcohols.

	No Alcohol	Propanol	Butanol	Pentanol	Hexanol
V_e (mL) (0.10 M SDS + 3% Alcohol)					
Acetophenone	34.4	16.5	11.2	8.73	8.15
Benzene	33.0	27.1	22.2	18.7	16.4
Naphthalene	69.0	56.1	43.1	33.0	25.0
Anthracene	114	90.1	66.2	47.0	31.7
Pyrene	128	100	71.9	50.4	33.5
V_e (mL) (0.25 M SDS + 3% Alcohol)					
Acetophenone	19.4	9.49	7.35	6.27	5.98
Benzene	17.4	14.1	12.5	11.3	11.0
Naphthalene	28.0	22.7	19.4	16.9	15.6
Anthracene	42.6	33.7	27.7	23.2	20.3
Pyrene	47.4	36.7	29.8	24.7	21.6

Landy and Dorsey (1984) have also reported a consistent retention time for an early eluting compound immediately after returning to initial conditions (0.2 M SDS) at the completion of a micellar concentration gradient (0.2-0.4 M SDS), indicating that with alcohol present in a micellar system, stationary phase saturation is achieved.

A further assumption of the pseudophase retention model is that the micelle-solute complex is of 1:1 stoichiometry. For a 0.05 M aqueous solution of SDS, a CMC (Mukerjee and Mysels, 1971) of 8.1×10^{-3} M and an aggregation number (Berthod et al., 1986) of 62 has been reported. There are then, at equilibrium, approximately 3.7×10^{17} micelles in the mobile phase volume of 0.90 mL. An examination of Table XXII indicates that at no time does the number of solute molecules in the injected sample volume of 20 µL exceed 3.2×10^{15} molecules. The volumes, at the base of the peak, are for the worst case (fastest eluting compounds) and, therefore, the sample concentration in the eluted peak is at its maximum value. Zana et al. (1981) have shown that for ionic surfactants, the critical micelle concentration decreases upon the addition to solution of low concentrations of medium chain length alcohols. In the above example, presence of 3% pentanol will, therefore, result in the formation of additional micellar aggregates in solution, further decreasing the number of solute molecules per micelle. It is clear that even for this worst case example that the number of micelles far exceeds the number of solute molecules and the assumption of 1:1 stoichiometry is verified.

Table XXII. A comparison of the number of solute molecules and micellar aggregates present in a peak volume for a 0.25 M SDS solution with 3% pentanol.

Solute	Injected Conc. (ppm)	Peak Volume[a] (mL)	# of Molecules[b]	# of Micelles[b]
Acetophenone	0.0012	1.2	1.2×10^{11}	4.9×10^{17}
Benzene	0.2	1.2	3.1×10^{13}	4.9×10^{17}
Naphthalene	34.4	2.5	3.2×10^{15}	1.0×10^{18}
Anthracene	3.75	4.4	2.5×10^{14}	1.8×10^{18}
Pyrene	31.5	6.1	1.9×10^{15}	2.5×10^{18}

[a] Peak volumes calculated for 0.25 M SDS, 3% pentanol mobile phase.

[b] The number of solute molecules and micelles in the peak volume of the solute.

Lastly, it is assumed that the aggregation number and the geometry of the micelle does not change with increasing surfactant concentration. It is well known (Hayase et al., 1984; Leung and Shah, 1986; Rao and Ruckenstein, 1986) that medium chain length alcohols (C_3-C_6) partition between the micelles and the bulk solution resulting in mixed micelles of varying composition, modifying both the structure and properties of the micelles in solution. The most common experimental procedure for studying the effect of alcohols upon micellar solutions is to keep the alcohol concentration constant and vary the concentration of surfactant in solution. The effect of increasing the chain length of the alcohol (at constant alcohol concentration) is to lower the CMC of ionic surfactant solutions. As shown in Table XXIII, as the alcohol chain length increases, so does the micelle/alcohol partition coefficient (K). For ionic surfactants, the effect of added alcohols is most important at low surfactant (C_s):alcohol (C_a) concentration ratios. Therefore, one might first assume that there exists a fundamental drawback in applying the pseudophase retention model to these alcohol containing solutions. The solubilities of the alcohols in water decreases with increasing chain length but until pentanol (27 g/L) there is reasonable solubility (Hayase et al., 1984). The general trend is for an increase in the aggregation number of the micelle with increasing surfactant concentration. This trend, however, is not unique to alcohol containing micellar solutions and is observed in aqueous micellar solutions at high surfactant concentrations. Previous

Table XXIII. Physicochemical properties of SDS solutions in the absence and presence of 3% normal alcohols.

	No Alcohol	1-Propanol	1-Butanol	1-Pentanol
[SDS] (M)[a]	0.14	0.13	0.13	0.13
[Alcohol] (M)	-	0.53	0.43	0.36
$[SDS]_m$ (mM)	136	128	128	128
$[Alcohol]_m$ (mM)	-	114	180	240
N_{SDS}	70	51	41	37
$N_{Alcohol}$	-	46	39	68
Area (A^2)	4120	4080	3690	4033
Radius (A)	18.1	18.1	16.7	17.9
K (25°)	-	103	300	722
K (40°)	-	-	154	659

[a] [X] (M) = the molar concentration of X in solution.
$[X]_m$ (mM) = the millimolar concentration of X in the micellar aggregate
N_x = the number of molecules of X in the micellar aggregate
K = the partition coefficient expressed as the ratio of mole fractions of alcohol in the micelle and aqueous phase

Data adapted from Almgren and Swarup (1983).

applications (Armstrong and Nome, 1981; Arunyanart and Cline Love, 1984; Berthod et al., 1986; Khaledi et al., 1987) of the pseudophase model have also attempted to increase mobile phase strength by using highly concentrated surfactant concentrations as shown in Table XXIV. At large surfactant concentrations, the assumption that micelle geometry and aggregation number do not vary with surfactant concentration is no longer valid (Armstrong and Nome, 1981; Armstrong, 1985). The present work uses equivalent ranges of SDS concentration in all micellar mobile phases and for all solutes investigated. An examination of Table XXIV indicates that surfactant concentrations employed here are well within the range of concentrations which have previously used the pseudophase model. This fact, coupled with the observation of linear plots when employing the pseudophase retention model, indicates that the application of this theory to the current problem is valid.

Almgren and Swarup (1983) have determined the size and composition of SDS micelles upon the addition of medium chain length alcohols to the system. Using these data and extrapolation, we have been able to estimate certain physicochemical properties of the mobile phases as shown in Table XXIII. At approximately 3% alcohol solutions, micelles of a mixed composition are present in solution. This conclusion is in agreement with other findings (Zana et al., 1981) which indicate that micelle formation does occur in ionic surfactant solutions (TTAB) with 3% added propanol, butanol and pentanol. As the chain length of the alcohol is increased, the alcohol partition coefficient (K) increases and the standard free

Table XXIV. Sodium dodecyl sulfate (SDS) concentrations used in previous applications of the pseudophase retention model.

Reference	SDS Concentration Range (M)
Armstrong and Nome, 1981	0.003 - 0.3
Arunyanart and Cline Love, 1984	0.00 - 0.4
Berthod et al., 1986	0.025 - 0.4
Khaledi et al., 1987	0.05 - 0.5

energy of penetration of the alcohol to the micellar phase becomes more favorable, resulting in a decrease in the number of SDS monomers in the micellar aggregate. At a constant surfactant concentration, the size of the micellar aggregate stays approximately constant through the C_3-C_5 alcohol series. For comparison purposes, the physical descriptors of an aqueous 0.14 M SDS micelle are given. The size and area of the micelles are approximately constant in the presence and absence of alcohol for the given surfactant concentration. While the geometry of the micelle appears to remain constant in the presence of alcohols, it is clear that the addition of alcohols does affect the aggregation number of the micelle.

The structure breaking properties of normal alcohols increase with increasing chain length. At higher alcohol content, the degree of micelle ionization increases, resulting in a smaller change of slope of a conductance vs. concentration plot at the CMC. Therefore, it is more difficult to determine the CMCs of solutions with higher alcohol content. In the present work, the addition of 3% hexanol to the surfactant solution is believed to completely labilize the micelle. The micelle/alcohol partition coefficient, K, for hexanol is 2250 at 25°C and 1600 at 40°C (Leung and Shah, 1986). Reference to Table XXIII indicates that this represents more than a twofold increase in the partition coefficient when compared to the pentanol case. Upon the introduction of SDS to 3% hexanol solutions, an increase in the surfactant concentration results in a progressive association of surfactant monomer and hexanol into small species in solution with the size of the aggregate dependent upon the amount of

surfactant in solution (Zana et al., 1981). As discussed below, this finding then explains the deviation of the results obtained using the pseudophase retention model for 3% hexanol in solution.

A comparison of the solute-micelle binding constants per surfactant monomer obtained using equations 5.2 and 5.3 are given in Table XXV. As the retention time of the compound under investigation increases, the slopes of the plot and the y-intercept values decrease, limiting the practical application of the pseudophase model. In this work, it was determined that valid, reproducible results were obtained only for compounds with $1/k \geq 1 \times 10^{-2}$, $V_s/(V_e-V_m) \geq 2 \times 10^{-2}$, and y-intercept values $\geq 1 \times 10^{-3}$.

The volume of the stationary phase, V_s, in the method of Armstrong and Nome (1981) is determined by subtracting the mobile phase volume from the total empty column volume; therefore, V_s includes inert packing support in the active volume of the stationary phase. There is, then, inherent inaccuracy in this determination of V_s. Here we attempt to determine if this inaccuracy will limit the accuracy of the physicochemical properties determined by this method (K_2, P_{mw} and P_{sw}). Examination of $V_s/(V_e-V_m)$ indicates that inaccuracies in V_s will be most pronounced for quickly eluted compounds. For acetophenone in a 3% pentanol mobile phase, the results of V_s changes on K_2, P_{mw} and P_{sw} are shown in Table XXVI. This shows the effect of plus and minus 10% and 25% changes in the volume of the stationary phase upon the physicochemical properties determined using equation 5.2. It is shown that even though the absolute values for the slope and y-intercept determined show a change

Table XXV. Solute-micelle binding constants per surfactant monomer for the investigated solutes determined from the three-phase retention model.

	No Alcohol	Propanol	Butanol	Pentanol	Hexanol
K_2 values determined from equation 5.3[a]					
Acetophenone	13.2	13.8	7.5	5.2	3.8
Benzene	19.2	19.9	13.7	10.1	5.6
Naphthalene	-	-	73.1	25.2	7.5
Anthracene	-	-	-	31.2	6.6
Pyrene	-	-	-	31.7	6.5
K_2 values determined from equation 5.2[a]					
Acetophenone	13.2	13.7	7.5	5.2	3.8
Benzene	19.1	19.9	13.7	10.1	5.5
Naphthalene	-	-	73.5	25.3	7.5
Anthracene	-	-	-	30.9	6.6
Pyrene	-	-	-	31.2	6.4

[a] Coefficients of determination for all plots were greater than 0.997 for all instances except for 3% hexanol in surfactant solution.

Table XXVI. A comparison of the variation of K_2, P_{mw} and P_{sw} for acetophenone in 3% pentanol as a result of changes in the value of stationary phase volume in equation 5.2.

V_s	Slope	Y-Intercept	K_2	P_{mw}	P_{sw}
1.19	0.5074	0.09787	5.2	22.1	10.2
1.43	0.6100	0.1176	5.2	22.1	8.5
1.59	0.6782	0.1308	5.2	22.1	7.6
1.75	0.7464	0.1439	5.2	22.1	6.9
1.99	0.8489	0.1637	5.2	22.1	6.1

with the volume of the stationary phase, the ratio remains constant, yielding consistent values for K_2 and P_{mw}. The changes in the y-intercept values are, however, manifested in the values determined for P_{sw}. Therefore, while the absolute values of P_{sw} will be affected by improper estimation of the stationary phase volume, the agreement between the K_2 values obtained using equations 5.2 and 5.3, the latter of which is not dependent upon V_s, shows that the convention used to calculate the stationary phase volume will not affect P_{mw}. Table XXVII lists the calculated values for P_{mw} and P_{sw} for the solutes under investigation determined from equation 5.2.

An examination of these results indicates that as the chain length of the added alcohol mobile phase modifier is increased, both the micelle/water and stationary phase/water partition coefficients are decreased. The addition of the alcohol to the mobile phase lowers the overall mobile phase polarity, lessening the polarity difference between both the micelle interior and the stationary phase with respect to the bulk mobile phase. This results in a reduction of the driving force for solute partitioning from the bulk mobile phase to both the hydrophobic stationary phase and micelle interior. As expected, for a given mobile phase, an increase in the hydrophobic character of the eluted solute results in an increase in partitioning to the hydrophobic environment.

Measurement of Solvent Polarity

Pyrene has received extensive application as a sensitive probe molecule for monitoring changes in solution polarity in the presence

Table XXVII. A comparison of the micelle/water (P_{mw}) and stationary phase/water (P_{sw}) partition coefficients for investigated solutes in 3% alcohol solutions.

	No Alcohol	Propanol	Butanol	Pentanol	Hexanol
P_{mw} (3% Alcohol)[a]					
Acetophenone	54.5	56.7	31.4	22.1	16.6
Benzene	78.7	81.9	56.7	41.9	23.5
Naphthalene	-	-	299.7	102.9	31.6
Anthracene	-	-	-	126.7	27.8
Pyrene	-	-	-	128.0	27.1
P_{sw} (3% Alcohol)					
Acetophenone	49.4	23.6	11.5	7.6	6.2
Benzene	58.8	49.5	32.2	22.9	15.2
Naphthalene	-	-	224.7	72.8	26.9
Anthracene	-	-	-	120.9	32.7
Pyrene	-	-	-	130.7	34.2

[a] A molar volume of 0.246 L/mol was used for SDS (Berthod et al., 1986).

of micelles (Pownall and Smith, 1973; Kalyanasundaram and Thomas, 1977a, 1977b; Infelta and Grätzel, 1979; Ananthapadmanabhan et al., 1985). The monomer fluorescence spectrum of pyrene shows significant fine structure in solution. Table XXVIII lists the five principal vibronic bands in pyrene monomer fluorescence along with the reported wavelength of maximum emission (Kalyanasundaram and Thomas, 1977). With respect to peak I, peak III exhibits the maximum variation in intensity as a result of changes in solvent polarity. The relative intensity of peak III (I_{III}) to peak I (I_I) (hereafter referred to as the 3/1 ratio) can be used to discuss the environmental effects upon pyrene monomer fluorescence. The concentration of pyrene used in all solutions was 1×10^{-5} M, ensuring that only a single pyrene molecule would occupy each micellar aggregate, minimizing excimer formation. Table XXIX lists the measured wavelengths of maximum emission for peaks I and III, the intensities of these bands and the 3/1 ratios of pyrene in various solvents. The concentration of pyrene and SDS (0.10 M) was constant in all solutions. A concentration of 0.05 M Aerosol OT, well above the reported CMC of 6×10^{-4} M (Cline Love et al., 1984), was used. Literature findings (Kalyanasundaram and Thomas, 1977) indicate that solvents can be divided into three general categories: (a) simple polar solvents with 3/1 ratios in the 0.50-0.80 range (water, 60:40 methanol:water in this work); (b) solvents with some polar character but longer hydrocarbon chain resulting in lower polarity, with 3/1 ratios extending from 0.80-1.20 (SDS solution, SDS with alcohol additives); and (c) hydrocarbon solvents with 3/1 ratios greater than 1.65 (hexane and Aerosol OT with

Table XXVIII. The five principal vibronic bands in pyrene monomer fluorescence.

Peak	η_{max} (nm)
I	372.5
II	379.0
III	383.0
IV	388.6
V	393.1

Data adapted from Kalyanasundaram and Thomas (1977).

Table XXIX. Study of wavelength of maximum emission (λ_{max}) and fluorescence intensity (I) of vibronic bands I and III in various media.

Solvent	λ_{max} (I) (nm)	λ_{max} (III) (nm)	I_I (x 10^4) (counts/s)	(I_{III} (x 10^4) (counts/s)	III/I
Water	370.0	380.5	32.89	20.49	0.623
MeOH:Water[a]	370.0	381.0	334.5	242.6	0.725
SDS[b]	370.5	381.5	148.4	142.2	0.958
SDS, pro[c]	370.5	381.5	135.5	138.4	1.022
SDS, but	370.5	381.5	122.7	132.6	1.080
SDS, pen	370.5	381.5	111.3	126.8	1.139
SDS, hex	370.5	381.5	99.60	117.9	1.183
AOT:Hexane[d]	370.0	381.0	5.607	10.86	1.938
Hexane	370.0	380.5	5.225	10.60	2.030

[a] Methanol:water ratio, 60:40 v/v.

[b] Concentration of SDS = 0.10 M in all SDS containing solutions.

[c] Alcohols present at 3% v/v in all alcohol containing solutions.

[d] Concentration of Aerosol OT = 0.05 M.

hexane). Several trends are evident from an examination of Table XXIX. As the hydrophobicity of the solvent is increased (moving down a column) the 3/1 ratio increases, an indication of decreasing solution polarity. Examination of the absolute intensities of the bands indicates that the 60:40 methanol:water solution yields the greatest signal intensity at the wavelength of maximum emission. Additionally, as the strength of the micellar mobile phase is increased by the addition of 3% normal alcohol, the intensity of the signal decreases. There is then a tradeoff when considering the use of alcohol additives and the limit of detection (LOD) in MLC; as the strength of the mobile phase is increased by the addition of the alcohol (decreasing LODs) the absolute signal decreases (increasing LODs) as shown in Figure 53 and Table XXIX.

At this point, it is necessary to address the reason for deviation from the pseudophase retention model for SDS mobile phases in 3% hexanol. As mentioned earlier, it is believed that 3% hexanol completely labilizes the SDS micelle in solution. Due to the absence of true micelles, the values for K_2 (Table XXV) and P_{mw} (Table XXVII) (the micelle dependent terms) do not show a clear increase with the increase of hydrophobicity of the solute. The coefficients of determination for the linear plots were the lowest for 3% hexanol mobile phases. The trends in k_d' (Table XVI), k_a (Table XVII), N (Table XIX), V_e (Table XXI) and P_{sw} (Table XXVII) (values which are not dependent upon the presence of micelles) are analogous to those observed in the propanol-pentanol/surfactant solutions, another

Figure 53. Emission spectra of pyrene in a 0.10 M SDS solution containing 3% (v/v) propanol (a), butanol (b), pentanol (c) and hexanol (d).

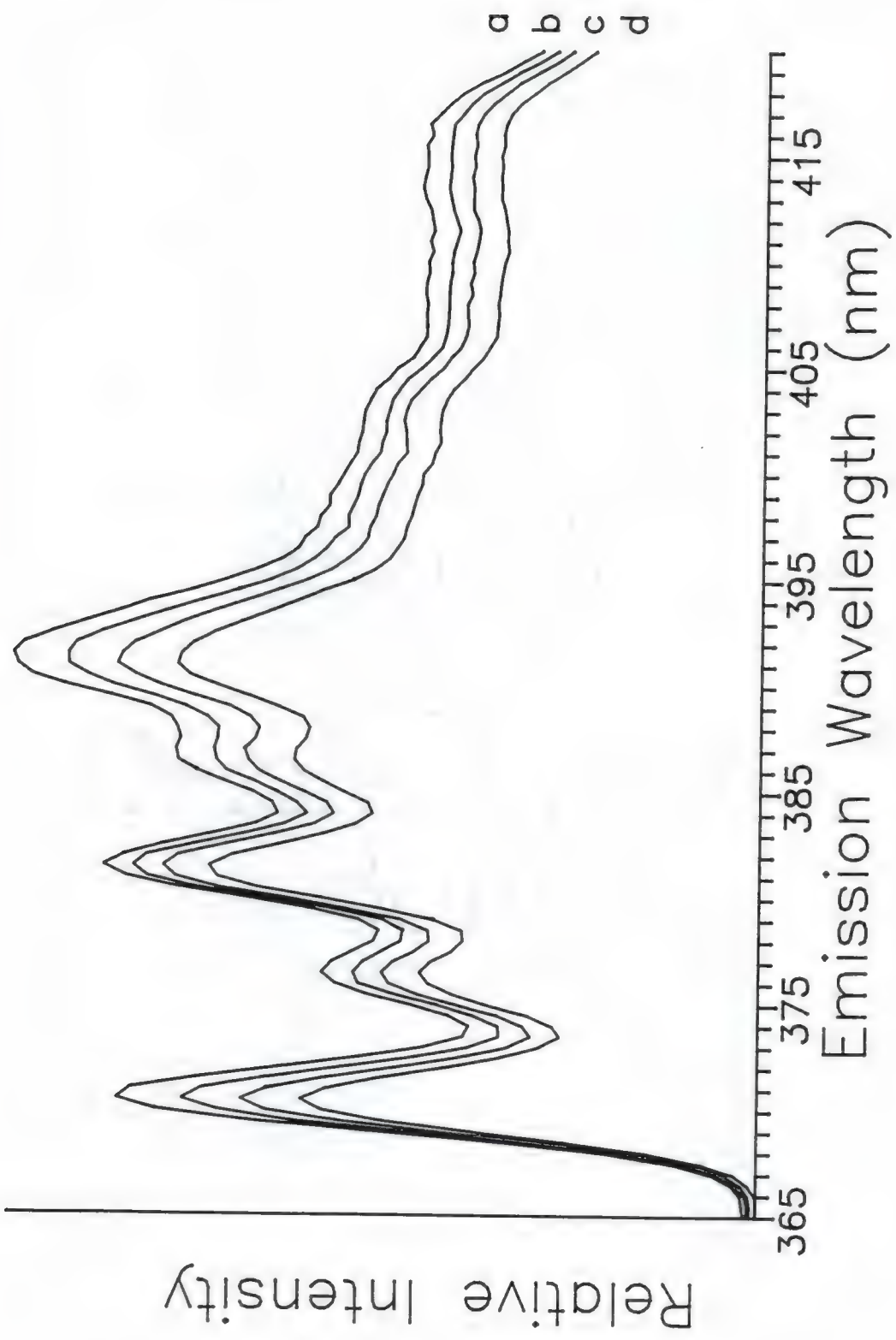
Relative Intensity
365
375
385
395
405
415
Emission Wavelength (nm)
a
b
c
d

indication that a significantly different aggregation structure exists in the 3% hexanol solution.

CHAPTER VI
CONCLUSIONS AND FUTURE WORK

The main focus of our research effort has been to extend the range of applications of organized media in the areas of flow injection analysis (FIA) and high performance liquid chromatography (HPLC). Exploitation of the controlled, reproducible dispersion associated with FIA provides the experimenter with a convenient means to examine the concentration dependence of other surfactant solution properties. Continued development in this area of research should help to free the surfactant using chemist from exhaustive solution preparation and time consuming repetitive measurements which are typical of classical methods for the examination of physicochemical properties of surfactant solutions. Examination of surfactant containing mobile phases in HPLC will continue to provide solutions to problems which cannot be solved using traditional hydro-organic mobile phases and will yield valuable information concerning the structure and properties of micelles in solution.

The introduction of an exponential dilution chamber as the dispersion volume in FIA offers much potential for the determination of the concentration dependence of surfactant solution properties. Flow injection analysis has been shown to be a rapid, accurate, low cost alternative to classical methods for the determination of the critical micelle concentration (CMC) of ionic and nonionic surfactant

solutions. We have shown that the injection of a highly concentrated surfactant solution into an FIA manifold containing a mixing chamber produces an exponential concentration gradient. This concentration gradient consists of two exponential response gradients whose intersection region defines the CMC. This method requires the preparation of only a single standard solution, ensuring minimization of solution preparation and material consumption. The crux of this technique is the formation of an exponential concentration gradient at the output of the chamber. Use of this gradient provides insight for interesting applications which should be considered for future research.

It is well known (Rosen, 1978) that surfactant solution properties are intimately dependent upon the intensive properties of the solution in which the surfactants are found. Changes in temperature and the amount of added electrolyte or organic modifier all effect the value of the CMC. Due to the great variety of solution conditions employed in basic research and applications, accurate literature values for the system which has been defined are often unavailable. The application of FIA yields a rapid and accurate method for the determination of CMCs in many systems and can greatly expand the number and type of literature CMC values available to the experimenter.

Reverse micelles are formed when surfactant is dissolved in nonaqueous media, resulting in an inversion of the micellar structure. These systems are believed to possess a CMC but only limited literature data are available concerning the behavior of

reverse micellar systems. Flow injection analysis will again provide a convenient method for the examination of the behavior of physicochemical properties in the critical region in reverse micellar solutions.

The use of an FIA manifold containing an exponential dilution chamber may provide a novel and rapid method for the examination of the effect of ionic micelles upon the relative rates of kinetically slow reactions. Employing a manifold containing two points of sample introduction, one before and one following the exponential mixing chamber, will provide the experimenter with a convenient method to examine the dependence of the reaction rate upon the surfactant concentration. The injection of a surfactant sample before the dilution chamber will produce an exponential concentration gradient at the output of the chamber. The presence of a T-connector after the mixing chamber will result in identical surfactant concentration gradients in each of two lines of the manifold. It will be necessary to employ two detectors to effectively monitor both the surfactant concentration and the formation of product. The first detector should be placed after the mixing chamber and T-connector in the first line of the manifold at a distance equivalent to the point of the sample injection valve in the second line of the manifold in order to effectively monitor the concentration of surfactant at the time of reactant introduction. The second sample injection valve will allow the experimenter to examine the relative catalytic ability of surfactant solutions over a wide range of concentrations, eliminating

the need for extensive solution preparation and repetitive analysis. A second detector will be present to monitor product formation.

The partition coefficient of a solute between the micellar phase and water in a surfactant solution at a concentration above the CMC is defined as the ratio of the concentration of that solute present in the micellar phase to the concentration present in the aqueous phase. Many hydrophobic solutes exhibit a shift in the wavelength of maximum absorbance upon partitioning into the hydrophobic region of a normal micelle. The use of a surfactant containing carrier stream at a concentration above the CMC, a mixing chamber and a photoiodide array UV-visible detector should allow for the rapid determination of partition coefficients. The presence of surfactant in the carrier stream should allow the experimenter to perform sequential investigations of the partition coefficients of the injected solutes and the diode array spectrophotometer will allow the wavelength of maximum absorbance of the solute in both the micellar and aqueous phases to be monitored. Additionally, an associated data system will allow the experimenter to perform spectral subtraction to remove the absorbance contribution from the solute-surfactant complex, yielding the actual absorbance of the solute in the aqueous phase.

This research has resulted in a greater understanding of the dispersion process in FIA. It has been shown that micellar catalysis observed in a static system may not translate to increased peak height in FIA unless the increase in peak height due to catalysis is sufficient to overcome the loss in sensitivity due to increased second moment resulting from the increased viscosity of the carrier stream.

Agreement of peak areas determined at 10, 25, 50 and 75% of total peak height verified the exponentially modified Gaussian (EMG) character of the FIA response curves. Using previously derived equations and performing simple, manual calculations we were able to show that the second moment of the EMG response curves varied linearly with flow rate. Using the second moment as a fundamental description of dispersion, we were able to learn much about the behavior of the sample plug in an FIA manifold in the presence and absence of a chemical reaction. The contribution of the chemical reaction to the overall peak dispersion is obtainable from these experimental results. The second moment of the response curve also yielded valuable information concerning the effects of carrier stream viscosity and manifold coiling upon the sample plug. The variance as a universal descriptor of dispersion also allows for a direct comparison of different manifolds from different laboratories to be made. It is clear that the application of variance as a descriptor of dispersion shows much promise and much more investigation is required. There are several other problems which come to mind for which FIA appears to be a practical and efficient solution.

The use of FIA for the determination of diffusion coefficients of surfactant containing solutions should eliminate many of the experimental difficulties associated with classical diffusion coefficient determinations. As shown in Chapter IV, FIA response curves resulting from a straight length of tubing are exponentially modified Gaussian (EMG) in character. Measurement of the standard

deviation of the underlying Gaussian peak (σ_G) at several low flow rates should allow for extrapolation to a limiting σ_G value totally eliminating the effects of flow upon σ_G. Substitution of the σ_G into the classical equation derived by Taylor (1953),

$$D = 0.01326\ Q\ V_t^2/L\sigma_G^2 \qquad \text{(eq. 6.1)}$$

where Q is the flow rate, V_t is the retention volume of the peak and L is the length of the manifold, should allow for the accurate and relatively rapid (compared to classical diffusion coefficient determinations) determination of diffusion coefficients of solutes in surfactant containing solutions. Additionally, the use of conventional flow-through detectors will eliminate the need for the addition of added electrolyte (typical of light scattering techniques) which potentially modifies the structure of the micelle.

Another area of interest which should be pursued is the use of supercritical fluids as the carrier stream in FIA. Chapter IV has shown that a decrease in solution viscosity decreases the second moment of a flow injection response curve. The solute diffusion coefficients in supercritical fluids are relatively high (10^{-4}-10^{-3} cm^2/s) when compared to liquids (10^{-5} cm^2/s). Additionally, any enhancement of reaction rates in a supercritical fluid carrier stream will result in larger signals. The use of a supercritical fluid as the carrier in FIA will exploit these diffusion coefficients, narrowed peaks and increased product formation to increase sample throughput and lower limits of detection in flow injection analysis.

Examination of Table XXIX shows that FIA could be used in conjunction with a variable wavelength HPLC fluorescence detector to rapidly measure the relative polarity of surfactant containing solutions. Table XXIX indicates that the wavelength of maximum emission of the 1st and 3rd vibronic bands of pyrene are constant with surfactant. The experimental setup uses the solution under investigation as the carrier stream and injection of a standard pyrene solution. The concentration of the injected pyrene solution should be such that the postdispersion concentration is 10^{-5}-10^{-6} M to avoid the formation of excimers. The wavelength of maximum emission of vibronic peak I is first monitored, followed by peak III. The absolute ratio of the resulting peak heights will allow for the 3/1 ratio to be determined, yielding an accurate measurement of the relative polarity of the surfactant solution.

Much progress was made in this work concerning efficiency and solvent strength in micellar chromatography (MLC) through an examination of the effects of medium chain length normal alcohols upon MLC. The solutes examined (acetophenone, benzene, naphthalene, anthracene and pyrene) show that n-butanol and n-pentanol are far superior as mobile phase additives with respect to both efficiency and solvent strength when compared to n-propanol. The use of the pseudophase retention model of MLC allowed us to directly examine changes in binding constants and partition coefficients with variation of alcohol chain length. Additionally, the validity of the applied model to our and other systems was examined. Application of the random walk model yields solute adsorption/desorption rate constants

across the stationary phase-mobile phase interface and we have confirmed that inefficient mass transfer across this interface is responsible for decreased efficiencies observed in micellar liquid chromatography.

There is great potential for continued examination of the use of surfactant containing mobile phases in liquid chromatography. This work has resulted in increased efficiency and solvent strength of micelle containing mobile phases. An area which needs to receive attention is the gradient capability of these micelle/alcohol mobile phases. As shown in Chapter V, the amount of alcohol partitioning to the micelle is dependent upon the concentration of surfactant in solution. This concentration undergoes a change in gradient MLC as the strength of the mobile phase is increased by increased surfactant concentration. It is believed that over the course of a micellar gradient with constant 3% butanol or pentanol in solution, the amount of alcohol adsorbed on the stationary phase, and thus the stationary phase structure will remain constant. Scott and Simpson (1980) have shown that at low concentrations of butanol and pentanol, the alcohol produces complete stationary phase coverage and, as a result, the stationary phase structure should remain constant as long as the concentration of alcohol in solution remains constant throughout the course of the gradient.

A final topic which should be considered for future investigation concerns the effect of low concentrations of medium chain length alcohols as mobile phase additives in ion-pair chromatography. Ion-pair chromatography allows the separation of solutes which are too

ionizable to be separated by adsorption or partition chromatography and too insoluble in water to be separated by ion-exchange chromatography. Low concentrations of surfactant (below the CMC) are commonly used as mobile phase additives in ion-pair chromatography. The ionic surfactant mobile phase additive allows ionic compounds to be extracted from the aqueous mobile phase into the hydrophobic stationary phase as an ion pair. In Chapter V, we have shown that the addition of medium chain length normal alcohols to a reversed phase system results in an increase in solute mass transfer across the stationary phase-mobile phase interface and an increase in the efficiency of the system. It is believed, therefore, that the addition of low concentrations of medium chain length normal alcohols to a reversed phase ion-pair system should also result in increased chromatographic efficiency and improvements in solvent strength.

APPENDIX A
TABULATION OF CHROMATOGRAPHIC FIGURES OF MERIT
FOR MICELLAR MOBILE PHASES

Concentrations of injected samples: (for aqueous micellar mobile phase)	Acetophenone = 0.0048 ppm Benzene = 0.4 ppm Naphthalene = 68.8 ppm Anthracene = 3.75 ppm Pyrene = 31.5 ppm
Concentrations of injected samples: (for alcoholic micellar and hydro-organic mobile phases)	Acetophenone = 0.0012 ppm Benzene = 0.2 ppm Naphthalene = 34.4 ppm Anthracene = 3.75 ppm Pyrene = 31.5 ppm
Definition of symbols used:	[SDS]M = molar concentration SDS Av. = all reported values represent an average of at least two trials N = number of theoretical plates h = reduced plate height k = chromatographic capacity factor V_s = volume of the stationary phase V_e = elution volume of the solute V_m = void volume of the system NA = due to the limited solubility of hexanol in water, a homogeneous mobile phase was not attainable
Constant parameters in this system:	V_s = 1.59 mL V_m = 0.90 mL

Aqueous Micellar Mobile Phase (No Added Alcohol)

(all values × 10^2)

[SDS]M	Av. V_e	Av. N	Av. h	Av. k	1/k	V_s/V_e-V_m
Acetophenone						
0.05	48.91	3400	8.78	53.34	1.87	3.31
0.10	34.36	2500	12.10	37.18	2.69	4.75
0.15	27.69	2000	14.88	29.77	3.36	5.93
0.20	22.09	1700	17.44	23.54	4.25	7.50
0.25	19.40	1700	17.58	20.55	4.86	8.59
Benzene						
0.05	50.00	4700	6.38	54.56	1.83	3.24
0.10	33.05	3600	8.38	35.73	2.80	4.95
0.15	24.69	4100	7.24	26.43	3.78	6.68
0.20	19.90	3400	8.70	21.11	4.74	8.37
0.25	17.37	3300	9.18	18.30	5.47	9.66
Naphthalene						
0.05	136.83	3200	9.48	151.03	0.662	1.17
0.10	68.99	2800	10.74	75.65	1.32	2.34
0.15	45.25	2400	12.26	49.28	2.03	3.59
0.20	33.68	2200	13.62	36.42	2.75	4.85
0.25	27.95	2400	12.72	30.06	3.33	5.88
Anthracene						
0.05	237.96	1700	17.96	263.40	0.380	0.671
0.10	113.48	1600	19.22	125.09	0.799	1.41
0.15	72.15	1500	20.50	79.17	1.26	2.23
0.20	52.35	1200	24.80	57.17	1.75	3.09
0.25	42.64	1200	24.08	46.38	2.16	3.81
Pyrene						
0.05	272.00	1000	28.44	301.22	0.332	0.586
0.10	128.67	900	35.02	141.97	0.704	1.24
0.15	80.66	700	44.22	88.62	1.13	1.99
0.20	61.09	600	51.90	66.88	1.50	2.64
0.25	47.42	600	53.64	51.69	1.93	3.42

3% Propanol Micellar Mobile Phase

(all values × 10^2)

[SDS]M	Av. V_e	Av. N	Av. h	Av. k	1/k	V_s/V_e-V_m
Acetophenone						
0.05	23.97	4200	7.17	25.63	3.90	6.89
0.10	16.50	3300	9.04	17.33	5.77	10.19
0.15	13.04	3300	9.09	13.49	7.41	13.10
0.20	10.92	3400	8.81	11.13	8.98	15.87
0.25	9.49	3400	8.81	9.51	10.52	18.51
Benzene						
0.05	40.59	6100	4.88	44.10	2.27	4.01
0.10	27.11	4500	6.73	29.12	3.43	6.07
0.15	20.66	4500	6.71	21.96	4.55	8.05
0.20	16.70	5000	6.03	17.56	5.70	10.06
0.25	14.09	5100	5.88	14.66	6.82	12.06
Naphthalene						
0.05	112.88	3500	8.53	124.42	0.804	1.42
0.10	56.07	3000	10.02	61.29	1.63	2.88
0.15	37.63	3000	10.05	40.81	2.45	4.33
0.20	28.28	3200	9.45	30.42	3.29	5.81
0.25	22.71	3100	9.69	24.24	4.12	6.73
Anthracene						
0.05	197.87	2700	11.12	218.85	0.457	0.807
0.10	90.13	2200	13.72	99.15	1.01	1.78
0.15	58.22	1800	16.36	63.69	1.57	2.77
0.20	42.63	1800	16.86	46.36	2.16	3.81
0.25	33.68	1700	17.38	36.42	2.75	4.85
Pyrene						
0.05	223.92	1600	18.74	247.80	0.404	0.713
0.10	99.98	1500	19.71	110.09	0.908	1.60
0.15	63.74	1100	27.31	69.82	1.43	2.53
0.20	46.65	800	36.32	50.84	1.97	3.48
0.25	36.66	700	42.67	39.73	2.52	4.45

3% Butanol Micellar Mobile Phase

(all values × 10^2)

[SDS]M	Av. V_e	Av. N	Av. h	Av. k	1/k	V_s/V_e-V_m
Acetophenone						
0.05	14.62	5400	5.52	15.25	6.56	11.59
0.10	11.25	4000	7.52	11.50	8.70	15.36
0.15	9.37	4300	6.93	9.39	10.65	18.76
0.20	8.21	3500	8.49	8.13	12.30	21.75
0.25	7.35	3700	8.06	7.17	13.95	24.64
Benzene						
0.05	31.93	6900	4.38	34.48	2.90	5.12
0.10	22.25	6000	4.99	23.72	4.22	7.45
0.15	17.46	4600	6.60	18.41	5.43	9.60
0.20	14.60	5500	5.47	15.22	6.57	11.60
0.25	12.51	5100	5.87	12.90	7.75	13.70
Naphthalene						
0.05	79.91	4900	6.17	87.79	1.14	2.01
0.10	43.14	4000	7.56	46.94	2.13	3.76
0.15	30.19	3600	8.39	32.54	3.07	5.43
0.20	23.72	3300	9.01	25.35	3.94	6.97
0.25	19.42	3300	9.19	20.58	4.86	8.58
Anthracene						
0.05	131.96	3300	9.11	145.62	0.687	1.21
0.10	66.19	2500	12.17	72.53	1.33	2.44
0.15	44.68	2300	12.79	48.64	2.06	3.63
0.20	34.42	2100	14.55	37.24	2.68	4.74
0.25	27.70	1800	16.42	29.78	3.36	5.93
Pyrene						
0.05	144.94	1900	15.98	160.04	0.625	1.10
0.10	71.87	1500	19.89	78.86	1.27	2.24
0.15	48.17	1100	28.11	52.52	1.90	3.36
0.20	37.07	1000	28.84	40.19	2.49	4.40
0.25	29.85	900	32.29	32.16	3.11	5.49

3% Pentanol Micellar Mobile Phase

(all values × 10^2)

[SDS]M	Av. V_e	Av. N	Av. h	Av. k	1/k	V_s/V_e-V_m
Acetophenone						
0.05	10.93	5300	5.69	11.14	8.98	15.86
0.10	8.73	4400	6.90	8.70	11.49	20.30
0.15	7.59	3800	8.02	7.44	13.45	23.76
0.20	6.85	3700	8.02	6.61	15.13	26.73
0.25	6.27	3600	8.28	5.97	16.75	29.60
Benzene						
0.05	25.89	6300	4.77	27.77	3.60	6.36
0.10	18.71	5200	5.81	19.79	5.06	8.93
0.15	15.14	5500	5.44	15.83	6.32	11.16
0.20	12.97	5200	5.72	13.41	7.46	13.17
0.25	11.33	5100	5.94	11.59	8.63	15.24
Naphthalene						
0.05	54.62	4200	7.19	59.68	1.68	2.96
0.10	33.02	3500	8.49	35.69	2.80	4.95
0.15	24.52	3300	9.28	26.24	3.81	6.73
0.20	20.00	3100	9.72	21.22	4.71	8.32
0.25	16.86	3000	10.02	17.73	5.64	9.96
Anthracene						
0.05	80.37	3100	9.76	88.30	1.13	2.00
0.10	47.00	2600	11.34	51.22	1.95	3.45
0.15	34.23	2100	14.52	37.03	2.70	4.77
0.20	27.56	2000	15.34	29.62	3.38	5.96
0.25	23.16	1700	17.35	24.73	4.04	7.14
Pyrene						
0.05	86.50	1800	16.27	95.11	1.05	1.86
0.10	50.35	1500	19.60	54.94	1.82	3.22
0.15	36.60	1200	25.50	39.67	2.52	4.45
0.20	29.53	1000	29.25	31.81	3.14	5.55
0.25	24.74	900	32.75	26.49	3.78	6.67

3% Hexanol Micellar Mobile Phase

(all values × 10^2)

[SDS]M	Av. V_e	Av. N	Av. h	Av. k	1/k	V_s/V_e-V_m
Acetophenone						
0.05	NA					
0.10	8.15	4000	7.55	8.05	12.41	21.93
0.15	7.07	3700	8.18	6.86	14.58	25.76
0.20	6.48	3500	8.50	6.20	16.13	28.49
0.25	5.98	3300	9.07	5.65	17.71	31.29
Benzene						
0.05	NA					
0.10	16.45	5800	5.21	17.28	5.79	10.22
0.15	14.11	5300	5.63	14.67	6.81	12.04
0.20	12.45	5000	6.02	12.83	7.79	13.77
0.25	11.02	5200	5.81	11.24	8.90	15.71
Naphthalene						
0.05	NA					
0.10	25.05	3500	8.53	26.84	3.73	6.58
0.15	21.06	3300	9.17	22.40	4.47	7.89
0.20	18.12	3200	9.49	19.13	5.23	9.24
0.25	15.63	2900	10.28	16.36	6.11	10.80
Anthracene						
0.05	NA					
0.10	31.74	2100	14.23	34.27	2.92	5.15
0.15	27.36	2100	14.44	29.40	3.40	6.01
0.20	23.60	1700	17.16	25.22	3.97	7.01
0.25	20.33	1500	19.47	21.59	4.63	8.18
Pyrene						
0.05	NA					
0.10	33.51	1100	26.38	36.23	2.76	4.88
0.15	28.99	900	32.98	31.21	3.20	5.66
0.20	25.09	1000	30.47	26.88	3.72	6.57
0.25	21.55	800	38.64	22.94	4.36	7.70

For comparison purposes hydro-organic mobile phase, 60:40 MeOH:H_2O

	Av. V_e	Av. N	Av. h	Av. k
Acetophenone	3.78	4100	7.26	1.82
Benzene	6.78	4300	7.01	4.06
Naphthalene	18.20	3300	9.12	12.58
Anthracene	60.79	2200	13.48	44.36
Pyrene	96.10	1900	15.55	70.71

V_m = 1.34 mL

APPENDIX B
BINDING CONSTANTS MEASURED FROM EQUATIONS 5.2 AND 5.3
FOR SDS/ALCOHOL MOBILE PHASES WITH A C_{18} COLUMN

Definitions of symbols used:

K_2 =solute-micelle binding constant per surfactant monomer

P_{sw} =partition coefficient of a solute between bulk solvent and the stationary phase

NA =See chapter V, valid results were not obtained because $1/k < 1 \times 10^{-2}$, $V_s/(V_e-V_m) < 2 \times 10^{-2}$ or y-intercept $< 1 \times 10^{-3}$.

Aqueous Micellar Mobile Phase (No Alcohol Added)

	Equation 5.2				Equation 5.3		
Compound	Slope	Intercept	K_2	P_{sw}	K_2	Slope	Intercept
Acetophenone	0.266	2.02×10^{-2}	13.2	49.4	13.2	0.151	1.14×10^{-2}
Benzene	0.325	1.70×10^{-2}	19.1	58.8	19.2	0.184	0.96×10^{-2}
Naphthalene	NA						
Anthracene	NA						
Pyrene	NA						

3% Propanol Micellar Mobile Phase

	Equation 5.2				Equation 5.3		
Compound	Slope	Intercept	K_2	P_{sw}	K_2	Slope	Intercept
Acetophenone	0.578	4.24×10^{-2}	13.7	23.6	13.8	0.329	2.38×10^{-2}
Benzene	0.402	2.02×10^{-2}	19.9	49.5	19.9	0.227	1.14×10^{-2}
Naphthalene	NA						
Anthracene	NA						
Pyrene	NA						

3% Butanol Micellar Mobile Phase

	Equation 5.2				Equation 5.3		
Compound	Slope	Intercept	K_2	P_{sw}	K_2	Slope	Intercept
Acetophenone	0.650	8.67×10^{-2}	7.5	11.5	7.5	0.368	4.92×10^{-2}
Benzene	0.426	3.10×10^{-2}	13.7	32.2	13.7	0.241	1.76×10^{-2}
Naphthalene	0.327	4.45×10^{-3}	73.5	224.7	73.1	0.185	2.53×10^{-3}
Anthracene	NA						
Pyrene	NA						

3% Pentanol Micellar Mobile Phase

	Equation 5.2				Equation 5.3		
Compound	Slope	Intercept	K_2	P_{sw}	K_2	Slope	Intercept
Acetophenone	0.678	0.131	5.2	7.6	5.2	0.384	7.41×10^{-2}
Benzene	0.440	4.37×10^{-2}	10.1	22.9	10.1	0.249	2.48×10^{-2}
Naphthalene	0.347	1.37×10^{-2}	25.3	72.8	25.2	0.200	7.79×10^{-2}
Anthracene	0.259	8.27×10^{-2}	30.9	120.9	31.2	0.145	4.65×10^{-2}
Pyrene	0.239	7.65×19^{-2}	31.2	130.7	31.7	0.136	4.28×10^{-2}

3% Hexanol Micellar Mobile Phase

	Equation 5.2				Equation 5.3		
Compound	Slope	Intercept	K_2	P_{sw}	K_2	Slope	Intercept
Acetophenone	0.616	0.161	3.8	6.2	3.8	0.349	9.10×10^{-2}
Benzene	0.364	6.56×10^{-2}	5.5	15.2	5.6	0.206	3.71×10^{-2}
Naphthalene	0.280	3.72×10^{-2}	7.5	26.9	7.5	0.158	2.12×10^{-2}
Anthracene	0.202	3.06×10^{-2}	6.6	32.7	6.6	0.114	1.74×10^{-2}
Pyrene	0.187	2.92×10^{-2}	6.4	34.2	6.5	0.106	1.65×10^{-2}

REFERENCES

Aihara, M.; Arai, M.; Tomitsugu, T. Anal. Lett., 1986a, 19, 1907.

Aihara, M.; Arai, M.; Tomitsugu, T. Analyst, 1986b, 111, 641.

Almgren, M.; Grieser, F.; Thomas, J.K. J. Amer. Chem. Soc., 1979, 101, 279.

Almgren, M.; Swarup, S. J. Colloid Interface Sci., 1983, 91, 256.

Al-Shabib, W.A.; Dunn, A.S. J. Dispersion Sci. Technol., 1981, 2, 175.

Ananthakrishnan, V.; Gill, W.N.; Barduhn, A.J. Am. Insti. Chem. Eng. J., 1965, 11, 1063.

Ananthapadmanabhan, K.P.; Goddard, E.D.; Turro, N.J.; Kuo, P.L. Langmuir, 1985, 1, 352.

Anderson, D.J.; Walters, R.R. J. Chromatogr. Sci., 1984, 22, 353.

Anderson, R.L. "Practical Statistics for Analytical Chemists"; Van Nostrand Reinhold Co.: New York, 1987, p. 44.

Antle, P.E.; Goldberg, A.P.; Snyder, L.R. J. Chromatogr., 1985, 321, 1.

Armstrong, D.W. Sep. Purif. Methods, 1985, 14, 213.

Armstrong, D.W.; Henry, S.J. J. Liq. Chromatogr., 1980, 3, 657.

Armstrong, D.W.; Nome, F. Anal. Chem., 1981, 53, 1662.

Armstrong, D.W.; Ward, T.J.; Berthod, A. Anal. Chem., 1986, 58, 579.

Arunyanart, M.; Cline Love, L.J. Anal. Chem., 1984, 56, 1557.

Atkins, P.W. "Physical Chemistry"; W.H. Freeman and Company: San Francisco, 1982, p. 825.

Atwood, J.G.; Golay, M.J.E. J. Chromatogr., 1979, 186, 353.

Atwood, J.G.; Golay, M.J.E. J. Chromatogr., 1981, 218, 97.

Bakalyar, S.R.; Spruce, B. Rheodyne Technical Notes 5, Dec. 1983.

Baxter-Hammond, J.; Powley, C.R.; Cook, K.D.; Nieman, T.A. J. Colloid Interface Sci., 1980, 76, 434.

Bazhenov, S.V.; Kazakov, M.V.; Peristyi, V.A. "Pozharotushenie; Baratov, A.N. ed."; Nauchno-Issled. Inst. Proivopozharnoi Oborony: Moscow, U.S.S.R., 1983, p. 108.

Beecher, P. J. Phys. Chem., 1959, 63, 1675.

Berezin, I.V.; Martinek, K.; Yatsimirskii, A.K. Russ. Chem. Rev., 1973, 42, 787.

Berthod, A.; Brooks, S.H.; Dorsey, J.G. J. Colloid Interface Sci., 1988, 122, 514.

Berthod, A.; Georges, J. Nouv. J. Chim., 1985, 9, 101.

Berthod, A.; Girad, I.; Connet, G. Anal. Chem., 1986, 58, 1356.

Betteridge, D. Anal. Chem., 1978, 50, 832A.

Betteridge, D.; Cheng, W.C.; Dagless, E.L.; David, P.; Goad, T.B.; Deans, D.R.; Newton, D.A.; Pierce, T.B. Analyst, 1983, 108, 17.

Betteridge, D.; Dagless, E.L.; Fields, B.; Sweet, P.; Deans, D.R. Anal. Proc., 1981, 18, 26.

Betteridge, D.; Ruzicka, J. Talanta, 1976, 23, 409.

Bidlingmeyer, B.A.; Warren, F.V. Anal. Chem., 1984, 56, 1583A.

Borgerding, M.F.; Hinze, W.L. Anal. Chem., 1985, 57, 2183.

Bradford, M. Anal. Biochem., 1976, 72, 248.

Chem. Eng. News, 1987, 65(4), 39.

Cheng, W. Anal. Chem., 1985, 57, 2409.

Cline Love, L.J.; Habarta, J.G.; Dorsey, J.G. Anal. Chem., 1984, 56, 1133A.

Cline Love, L.J.; Habarta, J.G.; Skrilec, M. Anal. Chem., 1981, 53, 437.

Cline Love, L.J.; Skrilec, M.; Habarta, J.G. Anal. Chem., 1980, 52, 754.

Colin, H.; Diez-Masa, J.C.; Guiochon, G.; Czajkowska, T.; Miedziak, I. J. Chromatogr., 1978, 167, 41.

Corrin, M.L.; Harkins, W.D. J. Amer. Chem. Soc., 1947, 69, 679.

CRC Handbook of Chemistry and Physics, 60th Edition; CRC Press: Boca Raton, FL, 1980a, p. D-237.

CRC Handbook of Chemistry and Physics, 60th Edition; CRC Press: Boca Raton, FL, 1980b, p. F-62.

Danielsson, I.; Lindman, B. Colloids and Surfaces, 1981, 3, 391.

Deinega, Y.F.; Lobastova, A.V.; Lutchenko, V.A.; Demchenko, L.N.; Shilov, V.N. Otkrytiya, Izobret., Prom. Obraztsy, Tovarnye Znaki, 1983, 38, 166.

Diaz Garcia, M.E.; Sanz-Medel, A. Talanta, 1986, 33, 255.

Dill, K.A.; Flory, P.J. Proc. Natl. Acad. Sci. USA, 1981, 78, 676.

Dill, K.A.; Koppel, D.E.; Cantor, R.S.; Dill, J.D.; Bendedouch, D.; Chen, S.H. Nature, 1984, 309, 42.

Dorsey, J.G. Adv. Chromatogr., 1987, 27, 167.

Dorsey, J.G.; DeEchegaray, M.T.; Landy, J.S. Anal. Chem., 1983, 55, 924.

Dorsey, J.G.; Khaledi, M.G.; Landy, J.S.; Lin, J.L. J. Chromatogr., 1984, 316, 183.

Ekwall, P. Acta Acad. Abo., 1927, 4, 1.

Fendler, J.H.; Fendler, E.J. "Catalysis in Micellar and Micromolecular Systems"; Academic Press: New York, 1975.

Fisher, L.R.; Oakenfull, D.G. Chem. Soc. Rev., 1977, 6, 25.

Foley, J.P. Anal. Chem., 1987, 59, 1984.

Foley, J.P.; Dorsey, J.G. Anal. Chem., 1983, 55, 730.

Foley, J.P.; Dorsey, J.G. J. Chromatogr. Sci., 1984, 22, 40.

Foley, J.P.; May, W.E. Anal. Chem., 1987, 59, 110.

Fossey, L.; Cantwell, F.F. Anal. Chem., 1985, 57, 922.

Garrett, H.E. "Surface Active Chemicals"; Pergamon Press: New York, 1972.

Gerhardt, G.; Adams, R.N. Anal. Chem., 1982, 54, 2618.

Gerhardt, G.; Adams, R.N. Anal. Chem., 1983, 55, 816.

Giddings, J.C. "Dynamics of Chromatography" Part 1; Marcel Dekker: New York, 1965.

Gill, W.N.; Ananthakrishnan, V. Am. Insti. Chem. Eng. J., 1967, 13, 801.

Goddard, E.D.; Turro, N.J.; Kuo, P.L. Langmuir, 1985, 1, 352.

Graham, J.A.; Rogers, L.B. J. Chromatogr. Sci., 1980, 18, 614.

Hayase, K.; Hayano, S.; Tsubota, H. J. Colloid Interface Sci., 1984, 101, 336.

Hernandez Torres, M.A.; Khaledi, M.G.; Dorsey, J.G. Anal. Chim. Acta, 1987, 201, 67.

Hinze, W.L. In "Solution Chemistry of Surfactants, Vol. 1" (Mittal, K.L., ed.); Plenum Press: New York, 1975, p. 79.

Hinze, W.L.; Armstrong, D.W. eds. ACS Symp. Ser., 1987, 342.

Hinze, W.L.; Singh, H.N.; Baba, Y.; Harvey, N.G. Trends Anal. Chem., 1984, 3, 193.

Hoar, T.P.; Schulman, J.H. Nature, 1943, 152, 102.

Huber, J.F.K. J. Chromatogr. Sci., 1969, 7, 172.

Hungerford, J.M.; Christian, G.D. Anal. Chim. Acta, 1987, 200, 1.

Hungerford, J.M.; Christian, G.D.; Ruzicka, J.; Giddings, J.C. Anal. Chem., 1985, 57, 1794.

Infelta, P.P.; Grätzel, M. J. Chem. Phys., 1979, 70, 179.

Ishii, M.; Yamada, M.; Suzuki, S. Anal. Lett., 1986, 19, 1591.

Kabachnyi, G.I.; Bashura, G.S.; Lyapunov, N.A.; Solon'ko, V.N.; Mischenko, A.I. Farm Zh. (Kiev), 1982, 5, 45.

Kali, K.M.; Cussler, E.L.; Evans, D.F. J. Phys. Chem., 1980, 84, 593.

Kalyanasundaram, K.; Thomas, J.K. J. Amer. Chem. Soc., 1977a, 99, 2039.

Kalyanasundaram, K.; Thomas, J.K. J. Phys. Chem., 1977b, 81, 2176.

Kapoor, R.C.; Bhardwaj, R.C.; Mishra, V.N. Tenside Deterg., 1982, 19, 224.

Kawashima, N.; Fujimoto, N.; Meguro, K. J. Colloid Interface Sci., 1985, 103, 459.

Kay, R.L.; Lee, K.S. J. Phys. Chem., 1986, 90, 5266.

Khaledi, M.G. Biochromatogr., 1988, 3, 20.

Khaledi, M.G.; Dorsey, J.G. Anal. Chem., 1985, 57, 2190.

Khaledi, M.G.; Peuler, E.; Ngeh-Ngwainbi, J. Anal. Chem., 1987, 59, 2738.

Kirkland, J. J. Chromatogr. Sci., 1977, 15, 303.

Kirkman, C.M.; Zu-Ben, C.; Uden, P.C.; Stratton, W.J.; Henderson, D.E. J. Chromatogr., 1984, 317, 569.

Kretschemer, K.; Koelsch, R.; Bernhardt, M.; Berdichevskii, V.R. Stud. Biophys., 1982, 91, 103.

Lake, M. Makromol. Chem., 1982, 183, 459.

Landy, J.S.; Dorsey, J.G. J. Chromatogr. Sci., 1984, 22, 68.

LeClerc, D.F.; Bloxham, P.A.; Toren, E.C. Anal. Chim. Acta, 1986, 184, 173.

Leung, R.; Shah, D.O. J. Colloid Interface Sci., 1986, 113, 484.

Levenspiel, O. "Chemical Reaction Engineering, 2nd ed."; John Wiley & Sons: New York, 1972.

Levenspiel, O.; Smith, W.H. Chem. Eng. Sci., 1957, 6, 227.

Locascio-Brown, L.; Plant, A.L.; Durst, R.A. Anal. Chem., 1988, 60, 792.

Matthews, G.P. "Experimental Physical Chemistry"; Clarendon Press: Oxford, England, 1985, p. 314.

McIntire, G.L. Amer. Lab., 1986, 18(2), 173.

Memon, M.H.; Worsfold, P.J. Anal. Proc., 1986a, 23, 418.

Memon, M.H.; Worsfold, P.J. Anal. Chim. Acta, 1986b, 183, 179.

Menger, F.M. Acc. Chem. Res., 1979, 12, 111.

Mittal, K.L., ed. "Micellization, Solubilization and Microemulsions, Vol. 1"; Plenum Press: New York, 1977.

Mittal, K.L.; Lindman, B., eds. "Surfactants in Solution, Vol. 3, part VIII"; Plenum Press: New York, 1984.

Monk, C.B. "Electrolytic Dissociation"; Academic Press: London, 1961.

Moore, J.W.; Pearsen, R.G. "Kinetics and Mechanism"; Wiley-Interscience: New York, 1981.

Mukerjee, P.; Mysels, K.J. "Critical Micelle Concentrations of Aqueous Surfactant Systems, NSRDS-NBS 36"; U.S. Government Printing Office: Washington, D.C., 1971.

Mullins, F.G.P.; Kirkbright, G.F. Analyst, 1984, 109, 1217.

Nemoto, Y.; Funahashi, H. J. Colloid Interface Sci., 1981a, 79, 313.

Nemoto, Y.; Funahashi, H. J. Colloid Interface Sci., 1981b, 80, 542.

Nomura, T.; Escabi-Perez, J.R.; Sunamoto, J.; Fendler, J.H. J. Amer. Chem. Soc., 1984, 102, 1980.

Ohyashiki, T.; Mohri, T. Chem. Pharm. Bull., 1983, 31, 1296.

Painton, C.C.; Mottola, H.A. Anal. Chem., 1981, 53, 1713.

Painton, C.C.; Mottola, H.A. Anal. Chim. Acta, 1983, 154, 1.

Painton, C.C.; Mottola, H.A. Anal. Chim. Acta, 1984, 158, 67.

Panda, L.; Behera, G.B. J. Indian Chem. Soc., 1985, 62, 44.

Pardue, H.L.; Fields, B. Anal. Chim. Acta, 1981a, 124, 39.

Pardue, H.L.; Fields, B. Anal. Chim. Acta, 1981b, 124, 65.

Pardue, H.L.; Jager, P. Anal. Chim. Acta, 1986, 179, 169.

Pelizzetti, E.; Pramauro, E. Anal. Chim. Acta, 1985, 169, 1.

Poppe, H. Anal. Chim. Acta, 1980, 114, 59.

Pownall, H.J.; Smith, L.C. J. Amer. Chem. Soc., 1973, 95, 3136.

Prince, L.M. J. Colloid Interface Sci., 1975, 52, 182.

Quarry, M.A.; Grob, R.L.; Snyder, L.R. J. Chromatogr., 1984, 285, 19.

Quarry, M.A.; Grob, R.L.; Snyder, L.R. Anal. Chem., 1986, 58, 907.

Ramsing, A.V.; Ruzicka, J.; Hansen, E.H. Anal. Chim. Acta, 1981, 129, 1.

Rao, I.V.; Ruckenstein, E. J. Colloid Interface Sci., 1986, 113, 375.

Reijn, J.M.; Poppe, H.; Van der Linden, W.E. Anal. Chem., 1984, 56, 943.

Reijn, J.M.; Van der Linden, W.E.; Poppe, H. Anal. Chim. Acta, 1981a, 123, 229.

Reijn, J.M.; Van der Linden, W.E.; Poppe, H. Anal. Chim. Acta, 1981b, 126, 1.

Robinson, B.H.; Loffler, A.; Schwartz, G. J. Chem. Soc. Faraday Trans., 1973, 69, 56.

Rodenas, E.; Vera, S.J. J. Phys. Chem., 1985, 89, 513.

Roe, J.M.; Barry, B.W. J. Colloid Interface Sci., 1983, 94, 580.

Rosen, M.J. "Surfactants and Interfacial Phenomena"; Wiley-Interscience: New York, 1978.

Rosenthal, K.S.; Koussaie, F. Anal. Chem., 1983, 55, 1115.

Ruzicka, J. Anal. Chem., 1983, 55, 1040A.

Ruzicka, J.; Hansen, E.H. Anal. Chim. Acta, 1975, 78, 145.

Ruzicka, J.; Hansen, E.H.; Zagatto, E.A. Anal. Chim. Acta, 1977, 88, 1.

Ruzicka, J.; Hansen, E.H. Anal. Chim. Acta, 1978, 99, 37.

Ruzicka, J.; Hansen, E.H. Chemical Analysis, 1981, 62.

Ruzicka, J.; Hansen, E.H. Anal. Chim. Acta, 1986, 179, 1.

Samsonoff, C.; Daily, J.; Almog, R.; Berns, D.S. J. Colloid Interface Sci., 1985, 109, 325.

Sato, H.; Kawasaki, M.; Kasatani, K. J. Phys. Chem., 1983, 87, 3759.

Scott, R.P.W.; Simpson, C.F. Faraday Symp. Chem. Soc., 1980, 15, 69.

Sentell, K.B.; Dorsey, J.G. Submitted, J. Liq. Chromatogr., April, 1988.

Shinoda, K.; Friberg, S. Adv. Colloid Interface Sci., 1975, 4, 281.

Skeggs, L.T. Anal. Chem., 1966, 38, 31A.

Skrilec, M.; Cline Love, L.J.; Habarta, J.G. Anal. Chem., 1980, 52, 1559.

Smedley, S. "The Interpretation of Ionic Conductivity in Liquids"; Plenum Press: New York, 1980.

Snyder, L.R. In "High Performance Liquid Chromatography: Advances and Perspectives, Vol. 1" (Cs. Horvath, ed.); Academic Press: New York, 1980, Chap. 4.

Snyder, L.R. "Principles of Adsorption Chromatography"; Marcel Dekker: New York, 1968.

Stewart, K.K.; Beecher, G.R.; Hare, P.E. Anal. Biochem., 1976, 70, 167.

Tanford, C. "The Hydrophobic Effect: Formation of Micelles and Biological Membranes"; 2nd ed., Wiley-Interscience: New York, 1980, p. 64.

Taylor, D.W.; Nieman, T.A. Anal. Chem., 1984, 56, 593.

Taylor, G. Proc. Roy. Soc. A., 1953, 219, 186.

Taylor, G. Proc. Roy. Soc. A., 1954, 225, 473.

Tijssen, R. Anal. Chim. Acta, 1980, 114, 71.

Tyson, J.F. Anal. Chim. Acta, 1986, 179, 131.

Ueno, K.; Kina, K. "Introduction to Flow Injection Analysis. Experiments and Applications" (in Japanese); Kodansha Scientific: Tokyo, Japan, 1983.

Valcarcel, M.; Luque de Castro, M.D. "Flow-Injection Analysis: Principles and Applications"; John Wiley & Sons: New York, 1987.

Van den Berg, J.H.M.; Deelder, R.S.; Egberink, H.G.M. Anal. Chim. Acta, 1980, 114, 91.

Vanderslice, J.T.; Beecher, G.R.; Rosenfeld, A.G. Anal. Chem., 1984, 56, 293.

Vanderslice, J.T.; Rosenfeld, A.G.; Beecher, G.R. Anal. Chim. Acta, 1986, 179, 119.

Vanderslice, J.T.; Stewart, K.K.; Rosenfeld, A.G.; Higgs, D.J. Talanta, 1981, 28, 11.

Wilke, C.R.; Chang, P. Am. Insti. Chem. Eng. J., 1955, 1, 264.

Woodhead, J.L.; Lewis, A.; Ralcoru, G.N.; Watson, I.D. J. Colloid Interface Sci., 1981, 82, 307.

Yamada, M.; Suzuki, S. Anal. Lett., 1984, 17, 251.

Yarmchuk, P.; Weinberger, R.; Hirsch, R.F.; Cline Love, L.J. J. Chromatogr., 1984, 283, 47.

Yoza, N.; Miyaji, T.; Hirai, Y.; Ohashi, S. J. Chromatogr., 1984a, 283, 89.

Yoza, N.; Shuto, T.; Baba, Y.; Tanaka, A.; Ohasi, S. J. Chromatogr., 1984b, 298, 419.

Zana, R.; Yiv, S.; Strazielle, C.; Lianos, P. J. Colloid Interface Sci., 1981, 80, 208.

BIOGRAPHICAL SKETCH

Stephen Houghton Brooks was born on November 17, 1961 (Anna Jaques Hospital, Newburyport, Massachusetts). He spent the first 18 years of his life residing in the bedroom community of Cape Elizabeth, Maine. He received his elementary and high school education in the public school system of Cape Elizabeth. He graduated from Cape Elizabeth High School in 1980. He continued his education at Zeta Psi Fraternity and Bowdoin College (Brunswick, Maine), receiving an A.B. in chemistry in the spring of 1984. He entered the University of Florida in August, 1984, and was married to Mariá Avelina Hernández Torres on July 25, 1987. Upon completion of the Doctor of Philosophy degree (August, 1988) he accepted a position as an Analytical Method Development Chemist at I.C.I. Americas (Wilmington, Delaware).

I certify that I have read this study and that in my opinion it conforms to acceptable standards of scholarly presentation and is fully adequate, in scope and quality, as a dissertation for the degree of Doctor of Philosophy.

John G. Dorsey, Chair
Associate Professor of Chemistry

I certify that I have read this study and that in my opinion it conforms to acceptable standards of scholarly presentation and is fully adequate, in scope and quality, as a dissertation for the degree of Doctor of Philosophy.

James D. Winefordner
Graduate Research Professor of Chemistry

I certify that I have read this study and that in my opinion it conforms to acceptable standards of scholarly presentation and is fully adequate, in scope and quality, as a dissertation for the degree of Doctor of Philosophy.

Anna F. Brajter-Toth
Associate Professor of Chemistry

I certify that I have read this study and that in my opinion it conforms to acceptable standards of scholarly presentation and is fully adequate, in scope and quality, as a dissertation for the degree of Doctor of Philosophy.

Gerhard M. Schmid
Associate Professor of Chemistry

I certify that I have read this study and that in my opinion it conforms to acceptable standards of scholarly presentation and is fully adequate, in scope and quality, as a dissertation for the degree of Doctor of Philosophy.

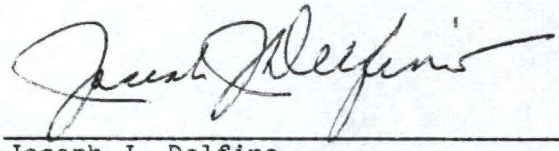

Joseph J. Delfino
Professor of Environmental Engineering Sciences

This dissertation was submitted to the Graduate Faculty of the Department of Chemistry in the College of Liberal Arts and Sciences and to the Graduate School and was accepted as partial fulfillment of the requirements for the degree of Doctor of Philosophy.

August, 1988

Dean, Graduate School